IMAGE: A MAP OF THE STARS OF THE ORION CONSTELLATION

Print ISSN: 2631-8490 Online ISSN: 2631-8504

JournalPreview

London Journal of Research in Science: Natural and Formal
Volume 24 | Issue 4 | Compilation 1.0

Great Britain Journals Press

WWW.JOURNALSPRESS.COM

Journal Content
In this Issue

Great Britain Journals Press

Quantifying Ruin Metrics in a Diffusion-Driven Erlang (2) Risk Model with Dependency Modeled using the Spearman Copula

François Xavier Ouedraogo, Delwendé Abdoul-Kabir Kafando, Frédéric Bere & Pierre Clovis Nitiema

Université Joseph KI ZERBO

ABSTRACT

This paper focuses on the perturbation of an Erlang (2) risk model by a diffusion process, challenging the assumption of independence between claim amounts and inter claim durations. To account for a tail dependency structure, we introduce the Spearman copula, enabling the evaluation of Gerber-Shiu functions and ruin probabilities associated with this model. Our analysis delves into the Laplace transforms of the discounted penalty function and the probability of ruin. Towards the conclusion, explicit expressions are derived, accompanied by numerical examples illustrating ruin probabilities for individual claim sizes with exponential distributions.

Keywords: gerber-shiu functions, dependence, copula, integro-differential equation, laplace transform, ruin probability.

Classification: LCC Code: QA

Language: English

Great Britain Journals Press

LJP Copyright ID: 925641
Print ISSN: 2631-8490
Online ISSN: 2631-8504

London Journal of Research in Science: Natural and Formal

Volume 24 | Issue 4 | Compilation 1.0

Quantifying Ruin Metrics in a Diffusion-Driven Erlang (2) Risk Model with Dependency Modeled using the Spearman Copula

François Xavier Ouedraogo[α], Delwendé Abdoul-Kabir Kafando[σ,*] Frédéric Bere[ρ] & Pierre Clovis Nitiema[ω]

ABSTRACT

This paper focuses on the perturbation of an Erlang (2) risk model by a diffusion process, challenging the assumption of independence between claim amounts and inter claim durations. To account for a tail dependency structure, we introduce the Spearman copula, enabling the evaluation of Gerber-Shiu functions and ruin probabilities associated with this model. Our analysis delves into the Laplace transforms of the discounted penalty function and the probability of ruin. Towards the conclusion, explicit expressions are derived, accompanied by numerical examples illustrating ruin probabilities for individual claim sizes with exponential distributions.

Keywords: gerber-shiu functions, dependence, copula, integro-differential equation, laplace transform, ruin probability.

Author α: Université Joseph KI ZERBO, 03 BP 7021 Ouagadougou, Burkina Faso.
σ: Université Ouaga 3S, Burkina Faso, 06 BP 10347 Ouagadougou 06.
ρ :Ecole Normale Supérieure, 01 BP 1757 Ouagadougou 01, Burkina Faso.
ω : Université Thomas SANKARA, Burkina Faso,04 BP 8938 Ouagadougou 04.

I. INTRODUCTION

A Wiener diffusion has been added to the classic Compound Poisson model by [1] as an ex tension of the classical risk model. Since then many researchers have taken an interest in this model, making their own contributions. For example, [2] for the probability of ruin, [3] for the distributions of maximum surplus before ruin and deficit at ruin. The introduction of the dis counted Gerber-Shiu penalty function [4], has been used in [5] and more recently in [6] to study the model with Brownian perturbation. In addition, it is possible to consider a Sparre Ander sen risk process, also known as a renewal risk process, in which the distribution of interclaim times is not constrained to follow an exponential distribution. These studies include generalised Erlang (n) times as in [7]. All these models assume independence between interclaim times and claim sizes. Although independence simplifies calculations for multiple quantities of interest, it may not be suitable for modelling catastrophic events such as bankruptcies in the banking and insurance sectors. The first attempts to characterise a dependency structure between Poisson interclaim arrival times and claim sizes are presented in [8] with an exponentially weighted mixture dependency and in [9] with a Farlie-Gumbel-Morgenstern (FGM) copula. The authors [10] deal with a dependency structure with an Erlang interclaim times combination and in [11] an Erlang arrival with an FGM copula. But these models do not incorporate diffusion perturbation. Nevertheless, in [12], they deal with a compound Poisson risk model with the two extensions : a diffusion and a dependence structure copula type FGM. However, the FGM copula has one notable limitation as it does not take into account tail dependencies. To remedy this, [14] and [13], based on the classical model of the Compound Poisson model, propose the use of the Spearman copula, which takes account of this tail dependence.

In our paper, we study a the Erlang (2) risk model with two extensions two extensions: the addition of a browian perturbation and a Spearman copula dependence structure. This paper is organized as follows. In Section 2, we describe the dependence structure which is defined by Sperman copula and analyse the roots of a Lundberg-type equation. The Laplace transform of the probability of ruin and some explicit expressions are obtained for the ruin probabilities in section 3. Finally, the conclusion and outlook are developed in section 4.

II. PRELIMINARIES

Consider the Erlang risk model (2) that is perturbed by Brownian motion :

$$U(t) = u + ct + \sigma B(t) - \sum_{i=1}^{N(t)} X_i, \tag{1}$$

where

- $u \geq 0$ is the initial capital and c is the constant rate of premium per unit of time,
- $N(t)$, the number of claim occurrences is described by a renewal process,
- $(X_i)_{i\geq 1}$, sequence of strictly positive random variables, i.i.d., independent of $N(t)$ is the amount of the i-th claim. F_X represents their distribution function, f_X the density function and f_X^* the Laplace transform.
- $B(t)$, standard Brownian motion is independent of $\sum_{i=1}^{N(t)} X_i$, i.e. independent of $N(t)$ and X_i.
- $\sigma > 0$ is the diffusion volatility.

Let $V_i = T_i - T_{i-1}$, be the inter-occurrence times of the claim, that is a sequence of strictly positive random variables and i.i.d. having an Erlang distribution (2) of parameter λ with T_i being the time of occurrence of the ith claim throughout our investigations. F_V represents their distribution function, f_V the density function and f_V^* the Laplace transform such that:

$$f_V(t) = \lambda^2 t e^{-\lambda t}, \tag{2}$$

$$F_V(t) = 1 - e^{-\lambda t} - \lambda t e^{-\lambda t}, \tag{3}$$

$$f_V^*(s) = \mathbb{E}\left[e^{-sV}\right] = \left(\frac{\lambda}{\lambda + s}\right)^2. \tag{4}$$

We also assume that X has an Erlang (2) distribution with parameter β and that the $(X_i, V_i)_{i\geq 1}$ form a sequence of random vectors i.i.d. as the canonical vector (X, V) with the possibility that the components of such a vector are dependent.

Finally, we assume that the claim amounts $X_1, X_2, ...$ are exponentially distributed with a parameter $\beta > 0$, that the random vectors claim amounts and interclaim occurrence times $(X_i, V_i)_{i\geq 1}$ is a sequence of random variables with the same distribution as the random vector (X, V).

We denote $F(x,t)$ the joint cumulative distribution function of the distribution function of claim amounts and interclaim occurrence times (X, V) where $(x,t) \in \mathbb{R}^+ \times \mathbb{R}^+$.

The moment of ruin $U(t)$, which is the first time the risk process $U(t)$ reaches a negative value associated with the risk model (1), is written as follows:

$$\tau = \begin{cases} \inf\{t \geq 0 : U(t) < 0 \mid U(0) = u\} \\ \infty \quad \text{si } U(t) \geq 0,\ \forall t \geq 0. \end{cases} \tag{5}$$

The probability of ruin in finite time t is defined as follows:

$$\psi(u) = \mathbb{P}\left(\tau \in [0,t], U(t) < 0 \mid U(0) = u\right),$$

and the probability of ultimate ruin (infinite-horizon probability) by:

$$\psi(u) = \psi(u,\infty) = \mathbb{P}\left(\tau < \infty, U(t) < 0 \mid U(0) = u\right).$$

We decompose the probability of ruin as in [12] by:

$$\psi(u) = \psi_w(u) + \psi_d(u). \tag{6}$$

This decomposition is justified by the fact that the probability of ruin can be caused either by the claim amounts $\psi_w(u)$, or by the oscillation of the Brownian motion $\psi_d(u)$. To ensure that ruin is not a certain event, we assume that net profit satisfies the following inequality:

$$\mathbb{E}[cV - X] > 0. \tag{7}$$

We can verify by rigorous calculations that (7) is equivalent to:

$$c\beta^2 > \lambda^2.$$

In order to better study ruin measures, we introduce the Gerber-Shiu function defined by:

$$\phi(u) = \mathbb{E}\left[e^{-\delta\tau}\omega\left(U(\tau^-), |U(\tau)|\right) I(\tau < \infty) | U(0) = u\right], \tag{8}$$

where $\delta \geq 0$ is the force of interest; $I(.)$ is the indicator function; $\omega(x_1, x_2)$, the non-negative value of the penalty function is a function of the surplus just before bankruptcy $U(\tau^-)$ and the deficit at bankruptcy $|U(\tau)|$ for $(x_1, x_2) \geq 0$. So is the probability of ruin, the Gerber-Shiu function can be broken down according to whether the ruin is caused by the claim amounts or by the oscillation, i.e:

$$\phi(u) = \phi_w(u) + \phi_d(u), \tag{9}$$

where

$$\phi_w(u) = \mathbb{E}\left[e^{-\delta\tau}\omega\left(U(\tau^-), |U(\tau)|\right) I(\tau < \infty, U(t) < 0) | U(0) = u\right], \tag{10}$$

is the Gerber-Shiu function when ruin is generated by claim amounts, and

$$\begin{aligned}\phi_d(u) &= \mathbb{E}\left[e^{-\delta\tau}\omega\left(U(\tau^-), |U(\tau)|\right) I(\tau < \infty, U(t) = 0) | U(0) = u\right] \\ &= \omega(0,0)\mathbb{E}\left[e^{-\delta\tau} I(\tau < \infty, U(t) = 0) | U(0) = u\right],\end{aligned} \tag{11}$$

is the Gerber-Shiu function when the ruin is generated by the oscillation of Brownian motion. For simplicity, we assume that $\omega(0,0) = 1$. We also note that a particular parameterisation of $\delta = 0$ and $\omega(0,0) \equiv 1$ brings $\phi_w(u)$ and $\phi_d(u)$ to the probabilities of ruin $\psi_w(u)$ and $\psi_d(u)$.

2.1 Dependency structure

The concept of copula was introduced in 1959 by Abe Sklar. The copula are functions that provides a general framework for studying associated structures of random variables and constructing multivariate distribution function using univariate marginal functions and multivariate correlation structure functions. Copulas are used extensively to model the structure of dependence between multiple random variables in finance and insurance ([15],[16],[17],[18])

2.1.1 Tail dependence

Tail dependence is a measure of comovements in the tails of a bivariate distributions . He describes the describe the level of dependence at the extremes of the distribution. Tail dependence represents the limiting proportion that one margin exceeds a certain threshold given that the other mzrgin hzd already exceeded that threshold.This measure is of great importance for extreme events. There are two tail dependence coefficients (upper tail dependence and lower tail dependence) which are defined as follows:

Definition 2.1 *Let X; Y two continuous random variables with respective distribution functions F and G. The lower tail dependence coefficient λ_L is defined by :*

$$\lambda_L(X,Y) = \lim_{\alpha \to 0^+} \mathbb{P}\left(X \leq F^{-1}(\alpha) \middle| Y \leq G^{-1}(\alpha)\right) \tag{12}$$

and the upper tail dependence coefficient λ_U is defined by :

$$\lambda_U(X,Y) = \lim_{\alpha \to 1^-} \mathbb{P}\left(X > F^{-1}(\alpha) \middle| Y > G^{-1}(\alpha)\right)$$

These measurements can be defined in terms of a copula C.

Definition 2.2 (Tail dependence) *Let X; Y be two continuous random variables of copula C, then we have*

$$\lambda_L(X,Y) = \lim_{u\to 0^+} \frac{C(u,u)}{u} \quad and \quad \lambda_U(X,Y) = \lim_{u\to 1^-} \frac{1-2u+C(u,u)}{1-u}.$$

Remark 2.1

- *When $\lambda_L \in]0,1]$; then C has a lower tail dependency.*
- *When $\lambda_L = 0$; then C has no lower tail dependency.*
- *When $\lambda_U \in]0,1]$; then C has an upper tail dependency.*
- *When $\lambda_U = 0$; then C has no upper tail dependency*

Many authors ([11], [12], [9], [19]) have used the Farlie-Gumbel-Morgenstern (FGM) copula to define the dependency structure between the claim sizes and interclaim times. The FGM copula is given by:

$$C_\alpha(u,v) = uv + \alpha uv(1-u)(1-v); 0 \le u,v \le 1. \tag{13}$$

It is not suitable for modelling dependencies on extreme values because $\lambda_L = \lambda_U = 0$.

2.1.2 Dependency model based on Spearman's copula

In this article, the dependency structure of the random vector (X,V) of the amounts of claims and the inter-occurrence times of the claims is described with a copula $C(u_1,u_2)$. In particular, we use the linear Spearman copula studied in [15] then in [14] and defined in [16] by :

$$\forall\, \alpha \in [0,1], \forall\, (u,v) \in [0,1]^2,\ C_\alpha(u,v) = (1-\alpha) C_I(u,v) + \alpha C_M(u,v), \tag{14}$$

where

$$C_I(u,v) = uv \quad \text{and} \quad C_M(u,v) = \min(u,v).$$

The α parameter represents the degree of dependency.

The Spearman copula admits interesting properties in cases with extreme values. Indeed, it suitable for modeling rare events in finance and insurance (earthquakes, hurricanes, floods, etc.) because its upper tail dependence coefficient is equal to its degree of dependence, $\lambda_U = \alpha$.

The bivariate distribution function F of claim amounts and claim inter-occurrence times with margins F_X and F_V can be written as $F(x,t) = C(F_X(x), F_V(t))$ (For the interested reader, see [17]).

The Spearman copula is a convex combination of the independent copula C_I and the comonotone copula C_M (positive dependence between the components of the random vector). This copula also has the ability to capture tail dependence in many situations such as earthquakes and other rare events ([18], [20]).

The Spearman copula is given by $F(x,t) = C_\alpha\left(F_X(x), F_V(t)\right)$, we obtain:

$$\begin{aligned} F(x,t) &= C_\alpha\left(F_X(x), F_V(t)\right) \\ &= (1-\alpha)C_I\left(F_X(x), F_V(t)\right) + \alpha C_M\left(F_X(x), F_V(t)\right) \\ &= (1-\alpha)F_I(x,t) + \alpha F_M(x,t). \end{aligned} \tag{15}$$

The copula $C_M(u,v)$ on $[0,1]^2$, has the set $D = \{(u,v) : u = v\}$ as support. Furthermore, $\frac{\partial^2 C_M}{\partial u \partial v}(u,v) = 0$ on $[0,1]^2 \setminus D$ and C_M is the uniform distribution on D. When the dependent structure of (X,V) is described by the copula C_M, then they are comonotones and there almost certainly exists an increasing function l, such that $X = l(V)$ (See [17]). The distribution function of X then satisfies :

$$F_X(x) = F_V\left(l^{-1}(x)\right) \iff 1 - e^{-\beta x} - \beta t e^{-\beta x} = 1 - e^{-\lambda l^{-1}(x)} - \lambda l^{-1}(x) e^{-\lambda l^{-1}(x)}.$$

First of all, we note by identification that

$$e^{-\beta x}(1+\beta t) = e^{-\lambda l^{-1}(x)}\left(1 + \lambda l^{-1}(x)\right)$$

then by a suitable deduction

$$\beta t = \lambda l^{-1}(x)$$

and last but not least

$$l^{-1}(x) = \frac{\beta t}{\lambda}. \tag{16}$$

This gives us

$$\frac{1}{\beta} = \int_0^\infty e^{-\lambda l^{-1}(x)} dx. \tag{17}$$

From (16), we have $l(t) = \frac{\lambda t}{\beta}$. The joint distribution $F_M(x,t)$ of the random vector (X,V) is singular on the set $D' = \{(x,t) : F_X(x) = F_V(t)\} = \{(x,t); x = l(t)\}$ as support. Similarly, it is the distribution $G(t) = F_M(l(t),t) = 1 - e^{-\lambda t} - \lambda t e^{-\lambda t}$ on $D' = \left\{(x,t) : x = \frac{\lambda t}{\beta}\right\}$.

2.1.2 Dependency model based on Spearman's copula

In this subsection, we analyse the solutions of the Lundberg-type equation associated with the risk model (1) and we determine the Laplace transforms of the Gerber-Shiu functions. The Laplace transform of a function f is denoted $f*$.

By $T_n = \sum_{i=1}^{n} V_i$, we denote the arrival time of the n-th claim with $T_0 = 0$.

Let's assume that $U_0 = u$ and $\forall\ n \in \mathbb{N}$, U_n, the surplus immediately after the n-th claim takes the form :

$$\begin{aligned} U_n = U(T_n) &= u + cT_n + \sigma B(T_n) - \sum_{i=1}^{n} X_i \\ &= u + \sum_{i=1}^{n} [cV_i + \sigma B(V_i) - X_i]. \end{aligned}$$

This last equality can be written as in [12], that is:

$$\begin{aligned} U_n &\overset{D}{=} u + \sum_{i=1}^{n} (cV_i - X_i) + \sigma B\left(\sum_{i=1}^{n} V_i\right) \\ &\overset{D}{=} u + \sum_{i=1}^{n} (cV_i - X_i + \sigma B(V_i)), \end{aligned}$$

where $\overset{D}{=}$ means "equality in distribution".
Consequently, the equation (1) can take the following form:

$$U\left(\sum_{i=1}^{n} V_i\right) = u + \sum_{i=1}^{n} (cV_i - X_i + \sigma B(V_i)).$$

We adopt the "martingale" approach to determine the ruin time of the force of interest δ. Since the claim amounts are distributed exponentially, we have a light-tailed distribution, hence the adjustment coefficient noted s, also known as the Lundberg exponent.

To determine the number s such that the process $\left\{e^{-\delta V_n + sU_n},\ n = 0, 1, ...\right\}$ is a martingale, we :

- first use the Lundberg inequality given in [21], theorem 2.1 on page 63 which guarantees that the probability of utlimate ruin satisfies the inequality $\psi_\delta(u) \leq e^{-su}$ with $s > 0$,
- then increase this probability of failure by introducing an exponential martingale from theorem 2.1 of [22], page 322,
- finally deduce the adjustment coefficient s as in [7] with $\delta \to 0$, which satisfies the following equation in our case

$$\mathbb{E}\left[e^{-s(cV - X + \sigma B(V))}\right] = 1. \tag{18}$$

The equation (18) is called the Lundberg-type equation associated with the (1) risk model. We shall see that it is essential for ruin measures.

We note that with (15), the equation (18) is written in the form (See [13]) :

$$(1 - \alpha)J_I + \alpha J_M, \tag{19}$$

where

$$J_I = \frac{\lambda^2\beta^2}{(\beta+s)^2\left(\lambda+\delta-\frac{\sigma^2}{2}s^2-cs\right)^2} \tag{20}$$

with the real part of the number s denoted $Re(s)$, positive and $Re\left(\frac{\sigma^2}{2}s^2+sc\right) < \lambda+\delta$.

What's more

$$J_M = \frac{\lambda^2\beta^2}{\left(-\frac{\sigma^2}{2}\beta s^2-(c\beta-\lambda)\,s+(\delta+\lambda)\,\beta\right)^2} \tag{21}$$

with the real part $Re(s)$, positive and $Re\left(\frac{\sigma^2}{2}\beta s^2+(c\beta-\lambda)\,s\right) < (\lambda+\delta)\,\beta$.

Lemma 2.1

i. When $\delta > 0$ and $0 < \alpha < 1$, the generalised Lundberg equation (18) has exactly two solutions noted $\rho_1(\delta)$, $\rho_2(\delta)$ with $Re(\rho_j) > 0$, $\forall j = 1, 2$.

ii. When $\delta = 0$, the equation (18) has exactly one solution noted $\rho_1(0)$, with $Re(\rho_1(0)) > 0$ and a second solution $\rho_2(0) = 0$.

Proof. We start with i and end with ii.

f_X^* being the Laplace transform of an exponential distribution exponential with parameter β, we have $f_X^*(s) = \left(\frac{\beta}{s+\beta}\right)^2$. In addition, we have $l(t) = \frac{\lambda}{\beta}t$. While observing the lemma 3.1 in [13], we obtain without difficulty

$$J_I = \frac{\lambda^2\beta^2}{\left(\lambda+\delta-sc-\frac{\sigma^2}{2}s^2\right)^2(s+\beta)^2} \quad \text{and} \quad J_M = \frac{\lambda^2\beta^2}{\left(-\frac{1}{2}\sigma^2\beta s^2+(\lambda-c\beta)\,s+\beta\,(\lambda+\delta)\right)^2} \tag{22}$$

with $Re(s) \geq 0$, $Re\left(sc+\frac{\sigma^2}{2}s^2\right) < \lambda+\delta$ and $Re\left(\frac{\sigma^2}{2}s^2-(\lambda-c\beta)\,s\right) < \beta\,(\lambda+\delta)$.
In this case, the equation (18) can be written as

$$\frac{\lambda^2\beta^2(1-\alpha)}{\left(\lambda+\delta-sc-\frac{\sigma^2}{2}s^2\right)^2(s+\beta)^2}+\frac{\lambda^2\beta^2\alpha}{\left(-\frac{1}{2}\sigma^2\beta s^2+(\lambda-c\beta)\,s+(\beta\lambda+\beta\delta)\right)^2}=1 \tag{23}$$

with $Re(s) \geq 0$ and $Re\left(\frac{\sigma^2}{2}s^2-(\lambda-c\beta)\,s\right) < \beta\,(\lambda+\delta)$.
When $\sigma = 0$, the equation (23) coincides with equation (2.19) in [23] .
For $\sigma > 0$, the equation (23) is equivalent to:

$$h_1(s) = h_2(s), \tag{24}$$

where

$$h_1(s) = (\beta+s)^2\left(\lambda+\delta-\frac{\sigma^2}{2}s^2-cs\right)^2\left(-\frac{\sigma^2}{2}\beta s^2-(c\beta-\lambda)\,s+(\delta+\lambda)\,\beta\right)^2$$

$$h_2(s) = (1-\alpha)\,\lambda^2\beta^2\left(-\frac{\sigma^2}{2}\beta s^2-(c\beta-\lambda)\,s+(\delta+\lambda)\,\beta\right)^2+\alpha\lambda^2\beta^2\,(\beta+s)^2\left(\lambda+\delta-\frac{\sigma^2}{2}s^2-cs\right)^2.$$

By applying Rouche's theorem [24] to the closed contour C as in [13], we have :

$$\lim_{s\to\infty}\left|\frac{\lambda^2\beta^2\,(1-\alpha)}{\left(\lambda+\delta-sc-\frac{\sigma^2}{2}s^2\right)^2(s+\beta)^2}+\frac{\lambda^2\beta^2\alpha}{\left(-\frac{\sigma^2}{2}\beta s^2+(\lambda-c\beta)\,s+\beta\,(\lambda+\delta)\right)^2}\right|=0 \qquad (25)$$

on the contour C where $s\neq 0$.
Furthermore, for $s=0$, we can see that :

$$\frac{(1-\alpha)\,\lambda^2\beta^2}{(\beta+s)^2\left(\lambda+\delta-\frac{\sigma^2}{2}s^2-cs\right)^2}\quad\text{and}\quad\frac{\alpha\lambda^2\beta^2}{\left(-\frac{\sigma^2}{2}\beta s^2-(c\beta-\lambda)\,s+(\delta+\lambda)\,\beta\right)^2}>0. \qquad (26)$$

Also, for $s=0$ and $\delta>0$, we have

$$\frac{\lambda^2\beta^2\,(1-\alpha)}{\beta^2\,(\lambda+\delta)^2}+\frac{\lambda^2\beta^2\alpha}{(\beta\lambda+\beta\delta)^2}=\left(\frac{\lambda\beta}{\beta\,(\lambda+\delta)}\right)^2<1, \qquad (27)$$

because $\lambda^2\beta^2<\beta^2\,(\lambda+\delta)^2$.

Finally, by posing

$$q(s)=\left|\frac{\lambda^2\beta^2\,(1-\alpha)}{\left(\lambda+\delta-sc-\frac{\sigma^2}{2}s^2\right)^2(s+\beta)^2}+\frac{\lambda^2\beta^2\alpha}{\left(-\frac{1}{2}\sigma^2\beta s^2+(\lambda-c\beta)\,s+\beta\,(\lambda+\delta)\right)^2}\right|,$$

we have:

$$\begin{aligned} q(s) &\leq \left|\frac{\lambda^2\beta^2\,(1-\alpha)}{\left(\lambda+\delta-sc-\frac{\sigma^2}{2}s^2\right)^2(s+\beta)^2}\right|+\left|\frac{\lambda^2\beta^2\alpha}{\left(-\frac{1}{2}\sigma^2\beta s^2+(\lambda-c\beta)\,s+\beta\,(\lambda+\delta)\right)^2}\right| \\ &\leq \frac{\lambda^2\beta^2\,(1-\alpha)}{\beta^2\,(\lambda+\delta)^2}+\frac{\lambda^2\beta^2\alpha}{\beta\,(\lambda+\delta)^2} \\ &\leq 1. \end{aligned} \qquad (28)$$

Since $h_1\,(s)$ has exactly two zeros inside the contour C, by application of Rouche's theorem , $h_2\,(s)-h_1\,(s)$ also has two zeros inside the C contour noted $\rho_1\,(\delta)$, $\rho_2\,(\delta)$ with $Re\,(\rho_j)>0$, $\forall j=1,2$.

For $\delta = 0$, the conditions of Rouche's theorem are not satisfied because

$$\left| \frac{\lambda^2\beta^2(1-\alpha)}{\left(\lambda+\delta-sc-\frac{\sigma^2}{2}s^2\right)^2(s+\beta)^2} + \frac{\lambda^2\beta^2\alpha}{\left(-\frac{1}{2}\sigma^2\beta s^2+(\lambda-c\beta)s+(\beta\lambda+\beta\delta)\right)^2} \right| = 1 \qquad (29)$$

for $s = 0$. The proof ii. can be obtained by using an extension of RouchÃ©'s theorem, called Klimenok's theorem in [25].

Remark 2.2 *For $\delta > 0$, the equation (18) has at least one positive real root denoted by $\rho_1(\delta)$.*

$h_1(s)$ is a polynomial with exactly two positive zeros noted :

$$s_1 = -\frac{1}{\sigma^2}\left(c - \sqrt{2(\lambda+\delta)\sigma^2+c^2}\right), \qquad (30)$$

$$s_2 = \frac{1}{\sigma^2\beta}\left(\lambda - c\beta + \sqrt{(\lambda-c\beta)^2+2(\lambda+\delta)\beta^2\sigma^2}\right). \qquad (31)$$

It is immediately clear that $s_1 < s_2$.
Let's calculate $h_2(0)$ and $h_2(s_1)$.

$$h_2(0) = \lambda^2\beta^4(\lambda+\delta)^2 \leq \beta^4(\lambda+\delta)^4 = h_1(0).$$

$$\begin{aligned} h_2(s_1) = {} & (1-\alpha)\lambda^2\beta^2\left(-\frac{\sigma^2}{2}\beta s_1^2-(c\beta-\lambda)s_1+(\delta+\lambda)\beta\right)^2+\alpha\lambda^2\beta^2(\beta+s_1)^2\left(\lambda+\delta-\frac{\sigma^2}{2}s_1^2-cs_1\right)^2 \\ = {} & (1-\alpha)\lambda^2\beta^2\left[\beta\left(-\frac{\sigma^2}{2}s_1^2-cs_1+\delta+\lambda\right)+\lambda s_1\right]^2 \\ = {} & (1-\alpha)\lambda^4\beta^4 s_1^2 \\ > {} & 0 = h_1(s_1). \end{aligned}$$

Since $h_2(0) - h_1(0) < 0$ and $h_2(s_1) - h_1(s_1) > 0$, we deduce by the intermediate value theorem that the equation (18) has a root $\rho_1(\delta)$ satisfying $0 < \rho_1(\delta) < s_1$.

Assume root $s_1 < \rho_2(\delta) < s_2$ is real. We have

$$h_2(s_1) = (1-\alpha)\lambda^4\beta^4 s_1^2 > 0 = h_1(s_1).$$

$$\begin{aligned} h_2(s_2) = {} & \left((1-\alpha)\lambda^2\beta^2\left(-\frac{\sigma^2}{2}\beta s_2^2-(c\beta-\lambda)s_2+(\delta+\lambda)\beta\right)^2+\alpha\lambda^2\beta^2(\beta+s_2)^2\left(\lambda+\delta-\frac{\sigma^2}{2}s_2^2-cs_2\right)^2\right. \\ & \left.\alpha\lambda^2\beta^2(\beta+s_2)^2\left(\lambda+\delta-\frac{\sigma^2}{2}s_2^2-cs_2\right)^2\right. \end{aligned}$$

$$
\begin{aligned}
&= \alpha\lambda^2\beta^2\left(\beta+s_2\right)^2\left[\frac{1}{\beta}\left(-\frac{\sigma^2}{2}\beta s_2^2 - c\beta s_2 + \beta\left(\lambda+\delta\right) + \lambda s_2 - \lambda s_2\right)\right]^2\\
&= \alpha\lambda^2\beta^2\left(\beta+s_2\right)^2\left(\frac{-\lambda}{\beta}s_2\right)^2\\
&= \alpha\lambda^4\left(\beta+s_2\right)^2\\
&> 0 = h_1(s_2).
\end{aligned}
$$

We cannot conclude that ρ_2 is a real root.

III. MAIN RESULTS

In this section, we present the main results of the article.

3.1 Calculation of the ultimate probability of ruin due to claims

In this subsection, we determine the infinite-horizon probability of ruin when it is due to claims

Theorem 3.1 *The ultimate probability of ruin due to a claim $\psi_w(u)$ is given*

$$\psi_w(u) = \frac{2\lambda a}{\beta\left(a^2\sigma^2 - ab\sigma^2\right)}\cdot e^{au} + \frac{2\lambda b}{\beta\left(b^2\sigma^2 - ab\sigma^2\right)}\cdot e^{bu};\ u \geq 0$$

where

$$a = -\frac{1}{2\sigma^2}\left(2c + \sqrt{\sigma^4\beta^2 + 8\sigma^2\lambda + 4c^2 - 4c\sigma^2\beta} + \sigma^2\beta\right) < 0$$

and

$$b = -\frac{1}{\sigma^2}\left(c - \frac{1}{2}\sqrt{\sigma^4\beta^2 + 8\sigma^2\lambda + 4c^2 - 4c\sigma^2\beta} + \frac{1}{2}\sigma^2\beta\right) < 0.$$

To prove the theorem (3.1), we introduce some useful basic results and consider the lemmas (3.1), (3.2) and (3.3),.

Let $W_t = -ct - \sigma(t)$ be an auxiliary function, a Brownian motion starting at 0 with $-c$ drift and σ^2 as variance. We denote $\overline{W}(t) = \sup_{0\leq s\leq t} W(s)$ the supremum of $W(t)$ in the interval $[0,t]$ and $\tau_u = \inf\{t \geq 0 : W(t) = u\}$, the first time of reaching the value $u > 0$. By Borrodin and Salminen's formula [26], we can obtain for $\delta \geq 0$,

$$\mathbb{E}\left[e^{-\delta\tau_u}\right] = e^{-\eta u}, \tag{32}$$

where

$$\eta = \frac{c}{\sigma^2} + \sqrt{\frac{2\delta}{\sigma^2} + \frac{c^2}{\sigma^4}}.$$

For $\delta \geq 0$, we define the following potential measure:

$$\mathcal{P}(u, dx, dy) = \mathbb{E}\left[e^{-\delta V} I\left(\overline{W}(V) < u, W(V) \in dy, X \in dx\right)\right], \quad u, x > 0, \quad y < u. \tag{33}$$

We denote by e_q, an exponential random variable of rate q. We can therefore first calculate the following measure:

$$\mathcal{U}_q\left(u, dy\right) = \Pr\left(\overline{W}(e_q) < u, W(e_q) \in dy, \right), \quad u, > 0, \quad u > y.$$

which can be obtained by the lemma of [27], well known in applied probability.

Finally, we denote by : $\mathcal{D} := \frac{d}{du}(\cdot)$ and $\mathcal{D}^2 := \frac{d}{du^2}(\cdot)$, the differentiation operators and $\mathcal{I}$ the identity operator with the differentiation operator A defined as follows :

$$A\left(\mathcal{D}\right) = \mathcal{D}^2 + \frac{2c}{\sigma^2}\mathcal{D} - \frac{2\left(\lambda+\delta\right)}{\sigma^2}\mathcal{I}. \tag{34}$$

Furthermore, it is easy to notice that :

$$A\left(\mathcal{D}\right) = \left(\mathcal{D} + \eta_1\mathcal{I}\right)\left(\mathcal{D} - \eta_2\mathcal{I}\right). \tag{35}$$

Lemma 3.1 *For $u > 0$, the Gerber-Shiu function $\phi_w(u)$ satisfies the following integro-differential equation*

$$A\left(\mathcal{D}\right)\phi_w(u) = -\frac{2\left(1-\alpha\right)\lambda^2}{\left(\lambda+\delta\right)\sigma^2}\sigma_{w,1}\left(u\right) - \frac{2\alpha\lambda\beta}{\sigma^2}\sigma_{w,2}\left(u\right), \tag{36}$$

with initial conditions of :

$$\phi_w(0) = 0, \tag{37}$$

$$\phi_w''(0) = -\frac{2c}{\sigma^2}\phi_w'(0) - \frac{2\left(1-\alpha\right)\lambda^2}{\left(\lambda+\delta\right)\sigma^2}w_1\left(0\right) - \frac{2\alpha\lambda\beta}{\sigma^2}w_2\left(0\right). \tag{38}$$

Proof. We are inspired by the proof of lemma 3.2 in [13]. We have:

$$\begin{aligned}\phi_w(u) &= \mathbb{E}\left[e^{-V_1\delta}\mathbb{E}\left[\phi(u - W_{V_1} - X_1)\mathbf{1}_{\left\{X_1 < u - W_{V_1}, \overline{W}_{V_1} < u\right\}} \mid (V_1, X_1)\right]\right] \\ &\quad + \mathbb{E}\left[e^{-V_1\delta}\mathbb{E}\left[w(u - W_{V_1}, X_1 - u + W_{V_1})\mathbf{1}_{\left\{X_1 > u - W_{V_1}, \overline{W}_{V_1} < u\right\}} \mid (V_1, X_1)\right]\right],\end{aligned} \tag{39}$$

which gives :

$$\begin{aligned}\phi_w(u) =& \frac{\left(1-\alpha\right)\eta_1\eta_2\lambda^2}{\left(\lambda+\delta\right)^2\left(\eta_1+\eta_2\right)}\left(\int_u^\infty e^{\eta_2(u-s)}\sigma_{w,1}\left(s\right)ds + \int_0^u e^{-\eta_1(u-s)}\sigma_{w,1}\left(s\right)ds - \int_0^\infty e^{-\eta_1 u - \eta_2 s}\sigma_{w,1}\left(s\right)ds\right) \\ &+ \frac{\alpha\lambda\beta\eta_1\eta_2}{\left(\lambda+\delta\right)\left(\eta_1+\eta_2\right)}\left(\int_u^\infty e^{\eta_2(u-s)}\sigma_{w,2}\left(s\right)ds + \int_0^u e^{-\eta_1(u-s)}\sigma_{w,2}\left(s\right)ds - \int_0^\infty e^{-\eta_1 u - \eta_2 s}\sigma_{w,2}\left(s\right)ds\right).\end{aligned} \tag{40}$$

By setting $u = 0$ in the relation (40), we obtain the initial condition $\phi_w(0) = 0$.
With the help of Leibniz's rule for derivation under the integral sign (see [28]) a first time, let's derive the relation (40) with respect to u.

$$\begin{aligned}\phi'_w(u) &= \frac{(1-\alpha)\,\eta_1\eta_2\lambda^2}{(\lambda+\delta)^2(\eta_1+\eta_2)}\left(\eta_2\int_u^\infty e^{\eta_2(u-s)}\sigma_{w,1}(s)\,ds\right.\\ &\quad\left.-\eta_1\int_0^u e^{-\eta_1(u-s)}\sigma_{w,1}(s)\,ds+\eta_1\int_0^\infty e^{-\eta_1 u-\eta_2 s}\sigma_{w,1}(s)\,ds\right)\\ &\quad+\frac{\alpha\lambda\beta\eta_1\eta_2}{(\lambda+\delta)(\eta_1+\eta_2)}\left(\eta_2\int_u^\infty e^{\eta_2(u-s)}\sigma_{w,2}(s)\,ds\right.\\ &\quad\left.-\eta_1\int_0^u e^{-\eta_1(u-s)}\sigma_{w,2}(s)\,ds+\eta_1\int_0^\infty e^{-\eta_1 u-\eta_2 s}\sigma_{w,2}(s)\,ds\right). \qquad (41)\end{aligned}$$

Fixing $u=0$ in the relation (41), we have :

$$\begin{aligned}\phi'_w(0) &= \frac{(1-\alpha)\,\eta_1\eta_2\lambda^2}{(\lambda+\delta)^2(\eta_1+\eta_2)}(\eta_1+\eta_2)\left(\int_0^\infty e^{-\eta_2 s}\sigma_{w,1}(s)\,ds\right)\\ &\quad+\frac{\beta\lambda\eta_1\eta_2}{(\lambda+\delta)(\eta_1+\eta_2)}(\eta_1+\eta_2)\left(\int_0^\infty e^{-\eta_2 s}\sigma_{w,2}(s)\,ds\right)\\ &= \frac{(1-\alpha)\,\eta_1\eta_2\lambda^2}{(\lambda+\delta)^2}\int_0^\infty e^{-\eta_2 s}\sigma_{w,1}(s)\,ds+\frac{\lambda\alpha\beta\eta_1\eta_2}{(\lambda+\delta)}\int_0^\infty e^{-\eta_2 s}\sigma_{w,2}(s)\,ds\\ &= \frac{2(1-\alpha)\,\lambda^2}{(\lambda+\delta)\sigma^2}\int_0^\infty e^{-\eta_2 s}\sigma_{w,1}(s)\,ds+\frac{2\alpha\lambda\beta}{\sigma^2}\int_0^\infty e^{-\eta_2 s}\sigma_{w,2}(s)\,ds. \qquad (42)\end{aligned}$$

Using Leibniz's rule for derivation under the integral sign a second time, let's derive the relation (41) with respect to u, we have :

$$\begin{aligned}\phi''_w(u) &= \frac{(1-\alpha)\,\eta_1\eta_2\lambda^2}{(\lambda+\delta)^2(\eta_1+\eta_2)}\left(\eta_2^2\int_u^\infty e^{\eta_2(u-s)}\sigma_{w,1}(s)\,ds-\eta_2\sigma_{w,1}(u)\right.\\ &\quad+\eta_1^2\int_0^u e^{-\eta_1(u-s)}\sigma_{w,1}(s)\,ds-\eta_1\sigma_{w,1}(u)-\eta_1^2\int_0^\infty e^{-\eta_1 u-\eta_2 s}\sigma_{w,1}(s)\,ds\Big)\\ &\quad+\frac{\alpha\lambda\beta\eta_1\eta_2}{(\lambda+\delta)(\eta_1+\eta_2)}\left(\eta_2^2\int_u^\infty e^{\eta_2(u-s)}\sigma_{w,2}(s)\,ds-\eta_2\sigma_{w,2}(u)\right.\\ &\quad+\eta_1^2\int_0^u e^{-\eta_1(u-s)}\sigma_{w,2}(s)\,ds-\eta_1\sigma_{w,2}(u)-\eta_1^2\int_0^\infty e^{-\eta_1 u-\eta_2 s}\sigma_{w,2}(s)\,ds\Big). \qquad (43)\end{aligned}$$

By setting $u=0$ in the relation (43), we obtain :

$$\begin{aligned}\phi''_w(0) &= \frac{(1-\alpha)\,\eta_1\eta_2\lambda^2}{(\lambda+\delta)^2(\eta_1+\eta_2)}\left(\left(\eta_2^2-\eta_1^2\right)\int_0^\infty e^{-\eta_2 s}\sigma_{w,1}(s)\,ds-(\eta_1+\eta_2)\,\sigma_{w,1}(0)\right)\\ &\quad+\frac{\alpha\lambda\beta\eta_1\eta_2}{(\lambda+\delta)(\eta_1+\eta_2)}\left(\left(\eta_2^2-\eta_1^2\right)\int_u^\infty e^{-\eta_2 s}\sigma_{w,2}(s)\,ds-\eta_2\sigma_{w,2}(u)-(\eta_1+\eta_2)\,\sigma_{w,2}(0)\right)\\ &= \frac{(1-\alpha)\,\eta_1\eta_2(\eta_2-\eta_1)\lambda^2}{(\lambda+\delta)^2}\int_0^\infty e^{-\eta_2 s}\sigma_{w,1}(s)\,ds-\frac{(1-\alpha)\,\eta_1\eta_2\lambda^2}{(\lambda+\delta)^2}\sigma_{w,1}(0)\\ &\quad+\frac{\alpha\lambda^2\eta_1\eta_2(\eta_2-\eta_1)\beta}{(\lambda+\delta)^2}\int_0^\infty e^{-\eta_2 s}\sigma_{w,2}(s)\,ds-\frac{\alpha\beta\eta_1\eta_2\lambda}{(\lambda+\delta)}\sigma_{w,2}(0)\\ &= \frac{-4c\lambda^2(1-\alpha)}{(\lambda+\delta)\sigma^4}\int_0^\infty e^{-\eta_2 s}\sigma_{w,1}(s)\,ds-\frac{2(1-\alpha)\,\lambda^2}{(\lambda+\delta)\sigma^2}w_1(0)\\ &\quad-\frac{4c\beta\lambda\alpha}{\sigma^4}\int_0^\infty e^{-\eta_2 s}\sigma_{w,2}(s)\,ds-\frac{2\alpha\lambda\beta}{\sigma^2}w_2(0). \qquad (44)\end{aligned}$$

From the relations (42) and (44), we have

$$\phi''_w(0) = -\frac{2c}{\sigma^2}\phi'_w(0) - \frac{2(1-\alpha)\lambda^2}{(\lambda+\delta)\sigma^2}w_1(0) - \frac{2\alpha\lambda\beta}{\sigma^2}w_2(0).$$

Now let's demonstrate the relation (36) .
Considering the differentiation, identity and the relations (40) and (41), determine $l(u) = (D - \eta_2 I)\phi_w(u)$.

$$\begin{aligned} l(u) &= \frac{(1-\alpha)\eta_1\eta_2\lambda^2}{(\lambda+\delta)^2(\eta_1+\eta_2)}\left(-(\eta_1+\eta_2)\int_0^u e^{-\eta_1(u-s)}\sigma_{w,1}(s)\,ds + (\eta_1+\eta_2)\int_0^\infty e^{-\eta_1 u-\eta_2 s}\sigma_{w,1}(s)\,ds\right) \\ &+\frac{\alpha\lambda\beta\eta_1\eta_2}{(\lambda+\delta)(\eta_1+\eta_2)}\left(-(\eta_1+\eta_2)\int_0^u e^{-\eta_1(u-s)}\sigma_{w,2}(s)\,ds\right. \\ &\left.+(\eta_1+\eta_2)\int_0^\infty e^{-\eta_1 u-\eta_2 s}\sigma_{w,2}(s)\,ds\right). \end{aligned} \tag{45}$$

With the help of Leibniz's rule for derivation under the integral sign a third time, let's derive $l(u)$ with respect to to u.

$$\begin{aligned} l'(u) &= \frac{(1-\alpha)\eta_1\eta_2\lambda^2}{(\lambda+\delta)^2(\eta_1+\eta_2)}\left((\eta_1+\eta_2)\eta_1\int_0^u e^{-\eta_1(u-s)}\sigma_{w,1}(s)\,ds - (\eta_1+\eta_2)\sigma_{w,1}(u)\right. \\ &\left.-(\eta_1+\eta_2)\eta_1\int_0^\infty e^{-\eta_1 u-\eta_2 s}\sigma_{w,1}(s)\,ds\right) \\ &+\frac{\alpha\lambda\beta\eta_1\eta_2}{(\lambda+\delta)(\eta_1+\eta_2)}\left((\eta_1+\eta_2)\eta_1\int_0^u e^{-\eta_1(u-s)}\sigma_{w,2}(s)\,ds - (\eta_1+\eta_2)\sigma_{w,2}(u)\right. \\ &\left.-(\eta_1+\eta_2)\eta_1\int_0^\infty e^{-\eta_1 u-\eta_2 s}\sigma_{w,2}(s)\,ds\right). \end{aligned} \tag{46}$$

Considering the differentiation and identity operators and the relations (45) and (46), let's find out $z(u) = (D + \eta_1 I)l(u)$.

$$\begin{aligned} z(u) &= -\frac{(1-\alpha)\eta_1\eta_2\lambda^2}{(\lambda+\delta)^2}\sigma_{w,1}(u) - \frac{\lambda\alpha\beta\eta_1\eta_2}{(\lambda+\delta)}\sigma_{w,2}(u) \\ &= -\frac{2(1-\alpha)\lambda^2}{(\lambda+\delta)\sigma^2}\sigma_{w,1}(u) - \frac{2\alpha\lambda\beta}{\sigma^2}\sigma_{w,2}(u), \end{aligned} \tag{47}$$

Hence the result (36).

Lemma 3.2 *The Gerber-Shiu function $\phi_w(u)$ has the following Laplace transforms $\phi^*_w(s)$ defined by :*

$$\phi^*_w(s) = \frac{\phi'_w(0) - \frac{2(1-\alpha)\lambda^2}{(\lambda+\delta)\sigma^2}w^*_1(s) - \frac{2\alpha\lambda\beta}{\sigma^2}w^*_2(s)}{s^2 + \frac{2c}{\sigma^2}s - \frac{2(\lambda+\delta)}{\sigma^2} + \frac{2(1-\alpha)\lambda^2}{(\lambda+\delta)\sigma^2}f^*_X(s) + \frac{2\alpha\lambda\beta}{\sigma^2}h^*(s)}. \tag{48}$$

Proof. In a similar way as the proof of the lemma 3.3 in [13], we get

$$\begin{aligned}\int_0^\infty e^{-su}\frac{2(1-\alpha)\lambda^2}{(\lambda+\delta)\sigma^2}\sigma_{w,1}(u)\,du &= \frac{2(1-\alpha)\lambda^2}{(\delta+\lambda)\sigma^2}\sigma^*_{w,1}(s)\\ &= \frac{2(1-\alpha)\lambda^2}{(\delta+\lambda)\sigma^2}\left(f^*_X(s)\,\phi^*_w(s)+w^*_1(s)\right) \qquad (49)\end{aligned}$$

and

$$\int_0^\infty e^{-su}\frac{2\alpha\lambda\beta}{\sigma^2}\sigma_{w,2}(u) = \frac{2\alpha\lambda\beta}{\sigma^2}\left(h^*(s)\,\phi^*_w(s)+w^*_2(s)\right). \qquad (50)$$

By exploiting the relations (84) and (50) and then extracting $\phi^*_w(s)$, we arrive at the result:

$$\phi^*_w(s)=\frac{\phi'_w(0)-\frac{2(1-\alpha)\lambda^2}{(\lambda+\delta)\sigma^2}w^*_1(s)-\frac{2\alpha\lambda\beta}{\sigma^2}w^*_2(s)}{s^2+\frac{2c}{\sigma^2}s-\frac{2(\lambda+\delta)}{\sigma^2}+\frac{2(1-\alpha)\lambda^2}{(\lambda+\delta)\sigma^2}f^*_X(s)+\frac{2\alpha\lambda\beta}{\sigma^2}h^*(s)}. \qquad (51)$$

For the force of interest $\delta = 0$ and the penalty function $w(x,y) = 1$ with the Laplace transform of the Gerber-Shiu function, $\phi_w(s)$ then characterizes the ultimate probability of ruin $\psi_w(s)$.

Lemma 3.3 *The Laplace transform of the ultimate probability of claims ruin due to claims $\phi^*_w(s)$ is given by :*

$$\psi^*_w(s)=\frac{\psi'_w(0)-\frac{2\lambda}{\sigma^2(s+\beta)}}{s^2+\frac{2c}{\sigma^2}s-\frac{2\lambda}{\sigma^2}+\frac{2\lambda\beta}{\sigma^2(s+\beta)}}, \qquad (52)$$

where

$$\psi'_w(0) = \frac{2(1-\alpha)\lambda}{(\lambda+\delta)\sigma^2}\int_0^\infty e^{-\eta_2 s}\sigma_{w,1}(s)\,ds+\frac{2\alpha\lambda\beta}{\sigma^2}\int_0^\infty e^{-\eta_2 s}\sigma_{w,2}(s)\,ds, \qquad (53)$$

$$\sigma_{w,1}(u) = \int_0^u f_X(x)\,\phi_w(u-x)dx\ +w_1(u), \qquad (54)$$

$$w_1(u) = \int_u^\infty w(u,x-u)\,f_X(x)\,dx, \qquad (55)$$

$$\sigma_{w,2}(u) = \int_0^u h(x)\,\phi_w(u-x)\,dx+w_2(u), \qquad (56)$$

$$w_2(u) = \int_u^\infty h(x)\,w(u,x-u)\,dx, \qquad (57)$$

$$h(x) = e^{-\frac{\beta(\delta+\lambda)x}{\lambda}}, \qquad (58)$$

$$\eta_1 = \frac{c}{\sigma^2} + \sqrt{\frac{2(\lambda+\delta)}{\sigma^2} + \frac{c^2}{\sigma^4}}, \tag{59}$$

$$\eta_2 = \frac{-c}{\sigma^2} + \sqrt{\frac{2(\delta+\lambda)}{\sigma^2} + \frac{c^2}{\sigma^4}}. \tag{60}$$

Proof. From the formula (48),

$$\psi_w^*(s) = \frac{\psi_w'(0) - \frac{2(1-\alpha)\lambda^2}{(\delta+\lambda)\sigma^2} w_1^*(s) - \frac{2\alpha\lambda\beta}{\sigma^2} w_2^*(s)}{s^2 + \frac{2c}{\sigma^2}s - \frac{2(\lambda+\delta)}{\sigma^2} + \frac{2(1-\alpha)\lambda^2}{(\delta+\lambda)\sigma^2} f_X^*(s) + \frac{2\alpha\lambda\beta}{\sigma^2} h^*(s)}, \tag{61}$$

we have :

- $$f_X^*(s) = \frac{\beta}{s+\beta} \qquad \text{and} \qquad h^*(s) = \frac{1}{s+\beta},$$
- $$w_1(u) = \int_u^\infty w(u, x-u) f_X(x)\, dx = \int_u^\infty f_X(x)\, dx = \int_u^\infty \beta e^{-\beta x} dx = e^{-\beta u},$$
- $$w_2(u) = \int_u^\infty w(u, x-u) h(x)\, dx = \int_u^\infty h(x)\, dx = \int_u^\infty e^{-\frac{\beta}{\lambda}\lambda x} dx = \frac{1}{\beta} e^{-\beta u}.$$

It is obvious that

$$w_1^*(s) = \frac{1}{s+\beta} \qquad \text{and} \qquad w_2^*(s) = \frac{1}{\beta(s+\beta)}.$$

The expression (48) then becomes

$$\begin{aligned} \psi_w^*(s) &= \frac{\psi_w'(0) - \frac{2(1-\alpha)\lambda^2}{(\lambda+\delta)\sigma^2(s+\beta)} - \frac{2\alpha\lambda}{\sigma^2(s+\beta)}}{s^2 + \frac{2c}{\sigma^2}s - \frac{2\lambda}{\sigma^2} + \frac{2(1-\alpha)\beta\lambda^2}{(\lambda+\delta)\sigma^2(s+\beta)} + \frac{2\alpha\lambda\beta}{\sigma^2(s+\beta)}} \\ &= \frac{\psi_w'(0) - \frac{2\lambda}{\sigma^2(s+\beta)}}{s^2 + \frac{2c}{\sigma^2}s - \frac{2\lambda}{\sigma^2} + \frac{2\lambda\beta}{\sigma^2(s+\beta)}}. \end{aligned} \tag{62}$$

From the equation (42), we obtain

$$\psi_w'(0) = \frac{2(1-\alpha)\lambda^2}{(\lambda+\delta)\sigma^2} \int_0^\infty e^{-\eta_2 s} \sigma_{w,1}(s)\, ds + \frac{2\alpha\lambda\beta}{\sigma^2} \int_0^\infty e^{-\eta_2 s} \sigma_{w,2}(s)\, ds. \tag{63}$$

We construct the proof of the theorem (3.1).

Proof:
The Laplace transform of the ultimate probability of ruin due to claims $\psi_w^*(s)$ has the expression:

$$\psi_w^*(s) = \frac{\psi_w'(0) - \frac{2(1-\alpha)\lambda}{\sigma^2(s+\beta)} - \frac{2\alpha\lambda}{\sigma^2(s+\beta)}}{s^2 + \frac{2c}{\sigma^2}s - \frac{2\lambda}{\sigma^2} + \frac{2(1-\alpha)\beta\lambda}{\sigma^2(s+\beta)} + \frac{2\alpha\lambda\beta}{\sigma^2(s+\beta)}} = \frac{\psi_w'(0) - \frac{2\lambda}{\sigma^2(s+\beta)}}{s^2 + \frac{2c}{\sigma^2}s - \frac{2\lambda}{\sigma^2} + \frac{2\lambda\beta}{\sigma^2(s+\beta)}}$$

By multiplying the numerator and denominator of $\psi_w^*(s)$ by $\sigma^2(s+\beta)$ then $\psi_w^*(s)$ takes the form :

$$\psi_w^*(s) = \frac{\psi_w'(0)\, s\sigma^2 - 2\lambda + \psi_w'(0)\,\sigma^2\beta}{s\left(\sigma^2 s^2 + (\beta\sigma^2 + 2c)\, s + (2c\beta - 2\lambda)\right)}.$$

Assume that $d(s) = \sigma^2 s^2 + (\beta\sigma^2 + 2c)\, s + (2c\beta - 2\lambda) = 0$. We can then deduce that $d(s) = \sigma^2(s-a)(s-b)$.

Thus we have

$$\psi_w^*(s) = \frac{\psi_w'(0)\, s - \frac{2\lambda}{\sigma^2} + \psi_w'(0)\,\beta}{s(s-a)(s-b)} \tag{64}$$

The simple element decomposition of $\psi_w^*(s)$ is

$$\psi_w^*(s) = \frac{A}{s} + \frac{B}{s-a} + \frac{C}{s-b}. \tag{65}$$

The relation (65) is equivalent to

$$\psi_w^*(s) = \frac{(A+B+C)\, s^2 + (-Aa - Ab - Bb - Ca)\, s + Aab}{s(a-s)(b-s)}. \tag{66}$$

Using relations (65) and (66), we deduce the following system by identification

$$\begin{cases} A + B + C = 0 \\ -Aa - Ab - Bb - Ca = \psi_w'(0) \\ Aab = -\frac{2\lambda}{\sigma^2} + \psi_w'(0)\,\beta \end{cases}$$

We find

$$\begin{aligned} A &= -\frac{1}{ab\sigma^2}\left(2\lambda - \psi_w'(0)\,\sigma^2\beta\right) \\ B &= \frac{1}{a^2\sigma^2 - ab\sigma^2}\left(-2\lambda + \psi_w'(0)\, a\sigma^2 + \psi_w'(0)\,\sigma^2\beta\right) \\ C &= \frac{1}{b^2\sigma^2 - ab\sigma^2}\left(-2\lambda + \psi_w'(0)\, b\sigma^2 + \psi_w'(0)\,\sigma^2\beta\right). \end{aligned}$$

By inversion of the Laplace transform, we have

$$\psi_w(u) = A + B \cdot e^{au} + C \cdot e^{bu},\ u \geq 0.$$

As $\lim_{u\to\infty} \psi_w(u) = 0$, we deduce that $A = 0$ and therefore

$$\begin{aligned} \psi_d'(0) &= \frac{2\lambda}{\sigma^2\beta} \\ B &= \frac{2\lambda}{\beta(a\sigma^2 - b\sigma^2)} \\ C &= \frac{2\lambda}{\beta(b\sigma^2 - a\sigma^2)}. \end{aligned}$$

Finally, by inverting the transform, we obtain

$$\psi_w(u) = \frac{2\lambda}{\beta(a\sigma^2 - b\sigma^2)} \cdot e^{au} + \frac{2\lambda}{\beta(b\sigma^2 - a\sigma^2)} \cdot e^{bu}$$

Example 1:
By setting the parameters $c = 0,5; \lambda = 0,3; \beta = 1; \sigma = 1.5$; and using using MATLAB, we present the curves associated with the probabilities due to claims.

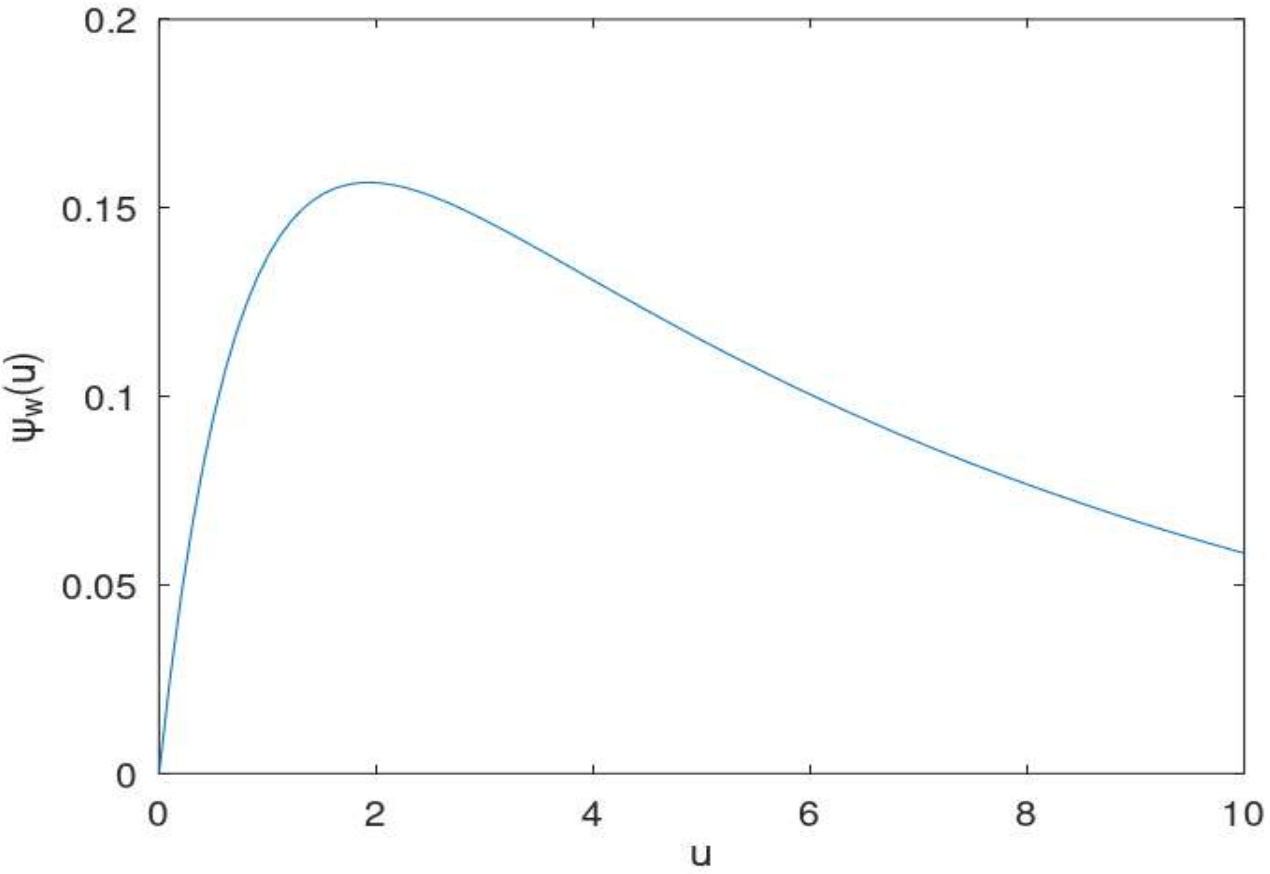

Figure 1: Ruin probability due to claims

3.2 Calculation of the ultimate probability of ruin due to oscillations

In this last subsection, we give the probability of ruin at infinite horizon when this is due to oscillations.

Theorem 3.2 *The ultimate probability of ruin due to a claim $\psi_d(u)$ is given*

$$\psi_d(u) = \frac{a+\beta}{a-b} \cdot e^{au} + \frac{b+\beta}{b-a} \cdot e^{bu},\ u \geq 0$$

where

$$a = -\frac{1}{2\sigma^2}\left(2c + \sqrt{\sigma^4\beta^2 + 8\sigma^2\lambda + 4c^2 - 4c\sigma^2\beta} + \sigma^2\beta\right) < 0$$

and

$$b = -\frac{1}{\sigma^2}\left(c - \frac{1}{2}\sqrt{\sigma^4\beta^2 + 8\sigma^2\lambda + 4c^2 - 4c\sigma^2\beta} + \frac{1}{2}\sigma^2\beta\right) < 0$$

To prove the theorem (3.2) , we use the lemmas (3.4), (3.5) and (3.6).

Lemma 3.4 *For $u > 0$, the Gerber-Shiu function $\phi_d(u)$ satisfies the following integro-differential equation*

$$A(\mathcal{D})\,\phi_d(u) = -\frac{2(1-\alpha)\lambda^2}{(\lambda+\delta)\sigma^2}\sigma_{d,1}(u) - \frac{2\alpha\lambda\beta}{\sigma^2}\sigma_{d,2}(u), \tag{67}$$

with initial conditions of :

$$\phi_d(0) = 1, \tag{68}$$

$$\phi_d'(0) = \frac{2(1-\alpha)\lambda^2}{(\lambda+\delta)\sigma^2}\int_0^\infty e^{-\eta_2 s}\sigma_{w,1}(s)\,ds + \frac{2\alpha\lambda\beta}{\sigma^2}\int_0^\infty e^{-\eta_2 s}\sigma_{w,2}(s)\,ds - \eta_1, \tag{69}$$

$$\phi_d''(0) = -\frac{2c}{\sigma^2}\phi_d'(0) + \frac{2(\lambda+\delta)}{\sigma^2}. \tag{70}$$

Proof. By conditioning and using the fact that ruin does or does not occur due to oscillation before the first claim, we have :

$$\begin{aligned}\phi_d(u) &= \mathbb{E}\left[e^{-V_1\delta}\mathbb{E}\left[\phi_d(u - W_{V_1} - X_1)\mathbf{1}_{\left\{X_1 < u - W_{V_1}, \overline{W}_{V_1} < u\right\}} \mid (V_1, X_1)\right]\right] \\ &\quad + \mathbb{E}\left[e^{-\delta\tau_u}\mathbf{1}_{\{\tau_u < V_1\}}\right] \\ &= \int_{t=0}^{t=\infty}\int_{y=-\infty}^{u}\int_{x=0}^{u-y} e^{-\delta t}\mathbb{P}\left[\overline{W}(t) < u, W(t) \in dy\right] \\ &\quad \times\phi_d(u-y-x)dF(x,t) + \mathbb{E}\left[e^{-\delta\tau_u}\mathbf{1}_{\{\tau_u < V_1\}}\right].\end{aligned} \tag{71}$$

Recall that the variable V_1 independent of the process $\{W_t\}$ follows an Erlang distribution (2) of parameter λ.

From the relation (32), we have :

$$\begin{aligned}\mathbb{E}\left[e^{-\delta\tau_u}\mathbf{1}_{\{\tau_u<V_1\}}\right] &= \mathbb{E}\left[\mathbb{E}\left[e^{-\delta\tau_u}\mathbf{1}_{\{\tau_u<V_1\}} \mid W_t\right]\right] \\ &= \mathbb{E}\left[e^{-(\delta+\lambda)\tau_u}\right] \\ &= e^{-\eta_1 u}. \end{aligned} \tag{72}$$

From (72), the equation (71) can be rewritten as follows :

$$\phi_d(u) = \int_{t=0}^{t=\infty}\int_{y=-\infty}^{u}\int_{x=0}^{u-y} e^{-\delta t}\mathbb{P}\left[\overline{W}(t) < u, W(t) \in dy\right] \times \phi_d(u-y-x)dF(x,t) + e^{-\eta_1 u}.$$

The rest of the proof follows exactly the same reasoning as in the lemme 3.1.

Lemma 3.5 *Laplace transform $\phi_d^*(s)$ defined by :*

$$\phi_d^*(s) = \frac{-s - \phi_d'(0) - \frac{2c}{\sigma^2}}{s^2 + \frac{2c}{\sigma^2}s - \frac{2(\lambda+\delta)}{\sigma^2} + \frac{2(1-\alpha)\lambda^2}{(\lambda+\delta)\sigma^2}f_X^*(s) + \frac{2\alpha\lambda\beta}{\sigma^2}h^*(s)}. \tag{73}$$

Proof. Using the proof of the lemma 3.5 in [13], we have

$$\int_0^\infty e^{-su}\frac{2(1-\alpha)\lambda^2}{(\delta+\lambda)\sigma^2}\sigma_{d,1}(u)\,du = \frac{2(1-\alpha)\lambda^2}{(\delta+\lambda)\sigma^2}\sigma_{d,1}^*(s) = \frac{2(1-\alpha)\lambda^2}{(\delta+\lambda)\sigma^2}f_X^*(s)\,\phi_d^*(s) \tag{74}$$

and

$$\int_0^\infty e^{-su}\frac{2\alpha\lambda\beta}{\sigma^2}\sigma_{d,2}(u) = \frac{2\alpha\lambda\beta}{\sigma^2}h^*(s)\,\phi_d^*(s). \tag{75}$$

By exploiting the relationships (74) and (75) and then extracting $\phi_d^*(s)$, we arrive at the result

$$\phi_d^*(s) = \frac{-s - \phi_d'(0) - \frac{2c}{\sigma^2}}{s^2 + \frac{2c}{\sigma^2}s - \frac{2(\lambda+\delta)}{\sigma^2} + \frac{2(1-\alpha)\lambda^2}{(\delta+\lambda)\sigma^2}f_X^*(s) + \frac{2\alpha\lambda\beta}{\sigma^2}h^*(s)}.$$

For the force of interest $\delta = 0$ and the penalty function $w(x,y) = 1$ and with the Laplace transform of the Gerber-Shiu function, $\phi_d(s)$ then characterizes the ultimate probability of ruin $_d(s)$.

Lemma 3.6 *The Laplace transform of the ultimate probability of ruin due to oscillations $\psi_d^*(s)$ is given by :*

$$\psi_d^*(s) = \frac{s + \psi_d'(0) + \frac{2c}{\sigma^2}}{s^2 + \frac{2c}{\sigma^2}s - \frac{2\lambda}{\sigma^2} + \frac{2\lambda}{\sigma^2(s+\beta)}}, \tag{76}$$

where

$$\psi_d'(0) = \frac{2(1-\alpha)\lambda^2}{(\lambda+\delta)\sigma^2}\int_0^\infty e^{-\eta_2 s}\sigma_{d,1}(s)\,ds + \frac{2\alpha\lambda\beta}{\sigma^2}\int_0^\infty e^{-\eta_2 s}\sigma_{d,2}(s)\,ds - \eta_1, \tag{77}$$

$$\sigma_{d,1}(u) = \int_{0\atop u}^{u} f_X(x)\,\phi_d(u-x)dx, \tag{78}$$

$$\sigma_{d,2}(u) = \int_0^u h(x)\,\phi_w(u-x)\,dx, \tag{79}$$

$$= h(x) = e^{-\frac{\beta(\delta+\lambda)x}{\lambda}}, \tag{80}$$

$$\eta_1 = \frac{c}{\sigma^2} + \sqrt{\frac{2(\lambda+\delta)}{\sigma^2} + \frac{c^2}{\sigma^4}}, \tag{81}$$

$$\eta_2 = \frac{-c}{\sigma^2} + \sqrt{\frac{2(\delta+\lambda)}{\sigma^2} + \frac{c^2}{\sigma^4}}. \tag{82}$$

Proof. We have

$$f_X^*(s) = \frac{\beta}{s+\beta} \qquad \text{and} \qquad h^*(s) = \frac{1}{s+\beta}.$$

The expression (73) then becomes

$$\psi_d^*(s) = \frac{-s - \psi_d'(0) - \frac{2c}{\sigma^2}}{s^2 + \frac{2c}{\sigma^2}s - \frac{2\lambda}{\sigma^2} + \frac{2(1-\alpha)\lambda^2}{(\delta+\lambda)\sigma^2}\left(\frac{\beta}{s+\beta}\right) + \frac{2\alpha\lambda\beta}{\sigma^2}\left(\frac{1}{s+\beta}\right)}$$

$$= \frac{-s - \psi_d'(0) - \frac{2c}{\sigma^2}}{s^2 + \frac{2c}{\sigma^2}s - \frac{2\lambda}{\sigma^2} + \frac{2\lambda}{\sigma^2(s+\beta)}}.$$

From the equation (69), we get

$$\psi_d'(0) = \frac{2(1-\alpha)\lambda^2}{(\delta+\lambda)\sigma^2}\int_0^\infty e^{-\eta_2 s}\sigma_{d,1}(s)\,ds + \frac{2\alpha\lambda\beta}{\sigma^2}\int_0^\infty e^{-\eta_2 s}\sigma_{d,2}(s)\,ds - \eta_1.$$

We construct the proof of the theorem (3.2).

Proof:

The Laplace transform of the ultimate probability of ruin due to claims $\phi_w^*(s)$ has the expression:

$$\psi_d^*(s) = \frac{s + \psi_d'(0) + \frac{2c}{\sigma^2}}{s^2 + \frac{2c}{\sigma^2}s - \frac{2\lambda}{\sigma^2} + \frac{2(1-\alpha)\lambda}{\sigma^2}\left(\frac{\beta}{s+\beta}\right) + \frac{2\alpha\lambda\beta}{\sigma^2}\left(\frac{1}{s+\beta}\right)} = \frac{s + \psi_d'(0) + \frac{2c}{\sigma^2}}{s^2 + \frac{2c}{\sigma^2}s - \frac{2\lambda}{\sigma^2} + \frac{2\lambda\beta}{\sigma^2(s+\beta)}}.$$

By multiplying the numerator and denominator of $\psi_w^*(s)$ by $\sigma^2(s+\beta)$ then $\psi_w^*(s)$ takes the form :

$$\psi_d^*(s) = \frac{\sigma^2 s^2 + (2c + \psi_d'(0)\sigma^2 + \sigma^2\beta)s + (\psi_d'(0)\beta\sigma^2 + 2c\beta)}{sd(s)}. \tag{83}$$

Thus we have

$$\psi_d^*(s) = \frac{s^2 + \left(\frac{2c}{\sigma^2} + \psi_d'(0) + \beta\right)s + \psi_d'(0)\beta + \frac{2c\beta}{\sigma^2}}{s(s-a)(s-b)}.$$

The simple element decomposition of $\psi_d^*(s)$ is

Using relations (65) and (66), we deduce the following system by identification

$$\begin{cases} F+D+E=1 \\ -aD-bD-bE-Fa=\frac{2c}{\sigma^2}+\psi_d'(0)+\beta \\ abD=\psi_d'(0)\,\beta+\frac{2c\beta}{\sigma^2} \end{cases}$$

We find

$$\begin{aligned} D &= \frac{1}{ab\sigma^2}\left(2c\beta+\psi_d'(0)\,\sigma^2\beta\right) \\ E &= \frac{1}{a^2\sigma^2-ab\sigma^2}\left(a^2\sigma^2+2c\beta+2ac+\psi_d'(0)\,a\sigma^2+\psi_d'(0)\,\sigma^2\beta+a\sigma^2\beta\right) \\ F &= \frac{1}{b^2\sigma^2-ab\sigma^2}\left(b^2\sigma^2+2c\beta+2bc+\psi_d'(0)\,b\sigma^2+\psi_d'(0)\,\sigma^2\beta+b\sigma^2\beta\right). \end{aligned}$$

As $\lim_{u\to\infty} {}_d(u)=0$, we deduce that $A=0$ and therefore

$$\begin{aligned} \psi_d'(0) &= \frac{-2c}{\sigma^2} \\ E &= \frac{a+\beta}{a-b} \\ F &= \frac{b+\beta}{b-a} \end{aligned}$$

Finally, by inverting the transform, we obtain

$$\psi_d(u)=\frac{a+\beta}{a-b}\cdot e^{au}+\frac{b+\beta}{b-a}\cdot e^{bu}.$$

Example 2:

By setting the parameters $c=0,5;\lambda=0,3;\beta=1;\sigma=1.5$; and using using MATLAB, we present the curves associated with the probabilities due to oscillations.

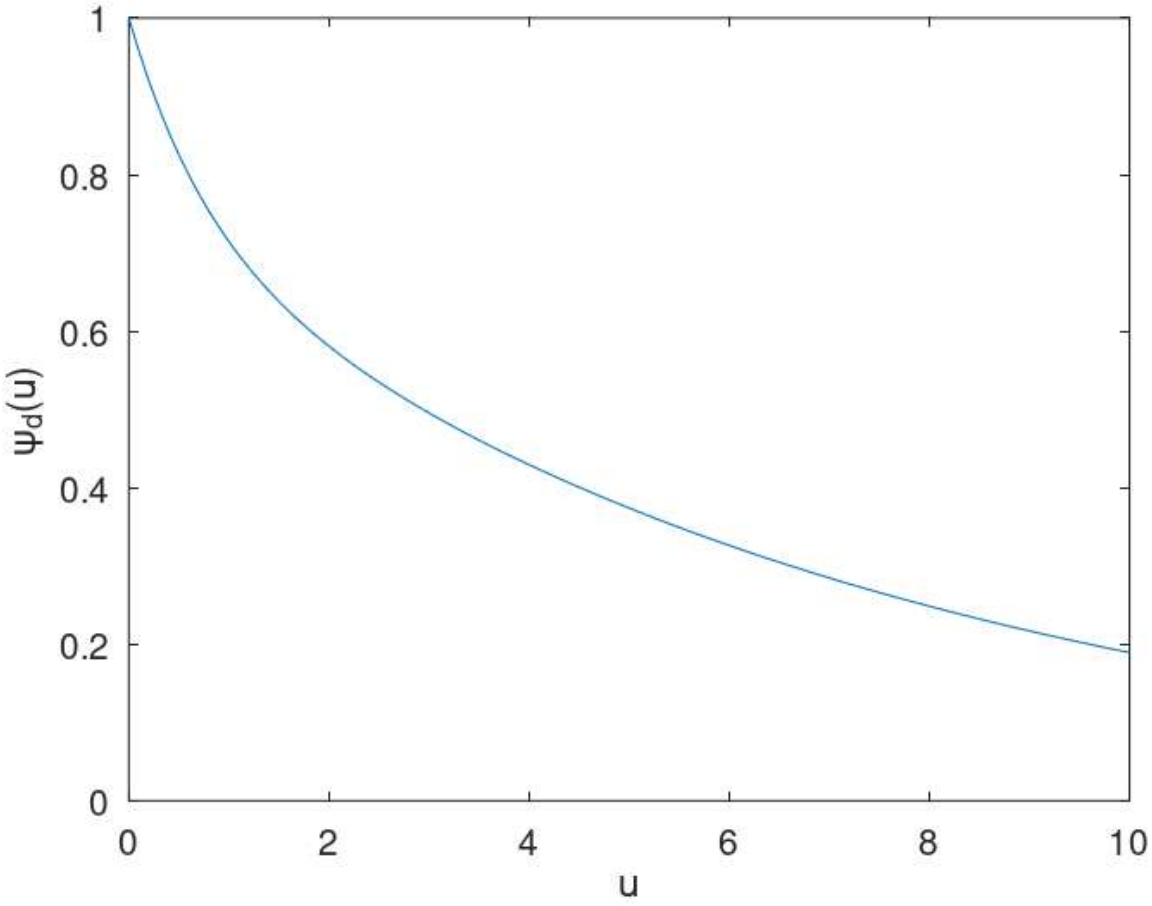

Figure 2: Ruin probability due to oscillations

Remark

In figures 1 and 2 illustrating the ruin probabilities caused by claims and by oscillations of the risk model , we notice that the ruin probabilities (caused by claims and by oscillations) both decrease as the initial capital increases.

IV. CONCLUSION

In this paper, we have determined the transforms of the insurer's loss probabilities and the ruin probabilities in a risk model with dependence perturbed by Brownian motion. To do this, we modelled the dependency structure between claim amounts and inter-claim times using the Spearman copula. The integral-differential equations and the Laplace transforms of the Gerber Shiu functions and the probabilities of ruin have been deduced by assuming that the losses are Erlang (2). In addition, some explicit expressions are obtained and numerical examples for the ruin probabilities for individual claim sizes with exponential distributions. This study can be made more practical by analysing dependency in a framework where policyholders are placed in two groups based on a threshold. This will be the subject of our next article.

5 Conflicts of Interest

The authors declare no conflicts of interest.

REFERENCES

1. H.U. Gerber. An extension of the renewal equation and its application in the collective theory of risk. *Skandinavisk Aktuarietidskrift*, pages 205–210, 1970.
2. F. Dufresne and H.U. Gerber. Risk theory for the compound poisson process that is perturbed by diffusion. *Insurance: Mathematics and Economics*, 10:51–59, 1991.
3. G. Wang and R. Wu. Some distribution for classical risk process that is perturbed by diffusion. *Insurance Mathematics Economics*, 26:15–24, 2000.
4. H.U. Gerber and E.S.W. Shiu. On the time value of ruin. *North American Actuarial Journal*, 2:48–78, 1998.
5. C. C. L. Tsai and G. E. Willmot. A generalized defective renewal equation for the surplus process perturbed by diffusion. *Insurance Mathematics Economics*, 30:51–66, 2002.
6. L. Liu and T. Zhang. Economic policy uncertainty and stock market volatility. *Finance Research Letters*, 15:99–105, 2015.
7. S. Li and J. Garrido. Ruin probabilities for two classes of risk processes. *Astin Bulletin*, 35(1):61–77, 2005.
8. Landriault D. Boudreault M., Cossette H. and Marcean E. On a risk model with dependence between interclaim arrivals and claim sizes. *Scandinavian Actuarial Journal*, pages 301–323, 2006.
9. H. Cossette and E.M.F. Marri. Analysis of ruin measures for the classical compound poisson risk model with dependence. *Scandinavian Actuarial Journal*, pages 221–245, 2010.
10. G.E. Willmot and J.K. Woo. On the analysis of a general class of dependent risk processes. *Insurance: Mathematics and Economics*, 51:134–141, 2012.
11. S. Vrontos Chadjiconstantinidis S. On a renewal risk process with dependence under a farlie-gumbel-morgenstern copula.
12. Z. Zhang and H. Yang. Gerber–shiu analysis in a perturbed risk model with dependence between claim sizes and interclaim times. *Journal of Computational and Applied Mathematics*, 235:1189–1204, 2011.
13. S. Heilpern. Measures for a compound poisson risk model with dependence based on the spearman copula and the exponential claim sizes. *Insurance: Mathematics and Economics*, 59:251–257, 2014.
14. Konane V. Kafando D.A.K, Bere F. and Nitiema P.C. Extension of the compound poisson model via the spearman copula. *Far East Journal of Theoretical Statistics*, 67(2):147–184, 2023.
15. W. Hürlimann. Multivariate frechet copulas and conditional value-at-risk. *International Journal of Mathematics and Mathematical Sciences*, 7:345–364, 2004.
16. H. Joe. *Multivariate Models and Dependence Concepts*. Chapman & Hall / CRC, 1997.
17. R.B. Nelsen. *An Introduction to Copulas, Second Edition*. Springer Series in Statistics. Springer-Verlag, 2006.
18. H. Albrecher and J.L. Teugels. Exponential behavior in the presence of dependence in risk theory. *Journal of Applied Probability*, 43(1):257–273, 2006.
19. Z. Zhang and H. Yang. Ruin probabilities in a perturbed compound poisson risk model with dependence. *Insurance: Mathematics and Economics*, 2009.
20. A.K. Nikoloulopoulos and D. Karlis. Fitting copulas to bivariate earthquake data: the seismic gap hypothesis revisited. *Environmetrics*, 19:251–269, 2008.

21. J. Cai and D.C.M. Dickson. Bounds for ultimate ruin probabilities in the sparre andersen model with interest. *Insurance: Mathematics and Economics*, 32:61–71, 2003.
22. D.J. Yao and R.M. Wang. Exponential bounds for ruin probability in two moving average risk models with constant interest rate. *Acta Mathematica Sinica, English Series*, 24(2):319–328, 2008.
23. Bere F. Kafando D.A.K, Konane V. and Nitiema P.C. Extension of the sparre andersen risk model via the spearman copula. *Advances and Applications in Statistics*, 86(1):79–100, 2023.
24. Ivo Adan. On the application of rouché's theorem in queueing theory. 2017.
25. V. Klimenok. On the modification of rouché's theorem for queuing theory problems. *Queuing Systems*, 38:431–434, 2001.
26. A.N. Borodin and P. Salmi. *Handbook of Brownian Motion-Facts and Formulae*. Birkhäuser-Verlag, 2nd edition, 2002.
27. S. Asmussen. Stationary distributions for fluid flow models with or without brownian noise. *Communications in Statistics - Stochastic Models*, 11:21–49, 1995.
28. Karim Ben Amara. Quelques méthodes pour la résolution des équations intégro-différentielles. 2015. Mémoire de magistère, Université Kasdi Merbah Ouargla.

This page is intentionally left blank

In-Vitro Antibacterial Activity of *Piper Guineense* Extracts and their Silver Nanoparticles Against Bacterial from Gastrointestinal Tract

Bukola Christianah Adebayo-Tayo, Folarin Victor Adeola, Olusola Ademola Olaniyi & Oladeji Aderibigbe Ajani*

University of Ibadan

ABSTRACT

The study investigates the in-vitro antibacterial activity of greenly synthesized silver nanoparticles from Piper guineese leave (PgMLE) and seed (PgMSE) methanol extracts. The greenly synthesized silver nanoparticles from leave (PgMLEAgNPs) and seed (PgMSEAgNPs) extracts were characterized using UV-visible spectroscopy, FTIR, SEM, TEM, XRD, EDX, and TGA, and the in-vitro antibacterial activity of the extracts and nanoparticles against test pathogens from gastrointestinal tracts was evaluated. The PgMLE and PgMSE bio-reduced silver nitrate solution for the biosynthesis of PgMLEAgNPs and PgMSEAgNPs. The nanoparticles had the highest Surface plasmon resonance peaks at 500 nm. Functional groups such as alcohols, phenols, alkenes or alkynes, nitriles, ketones, aldehydes, or esters were identified as indicative of biomolecules present within PgMLEAgNPs, and PgMSEAgNPs. PgMLEAgNPs and PgMSEAgNPs were spherical flakelike and aggregated particles respectively with 15 nm in size, TEM shows the spherical shape nanoparticles. The nanoparticles were crystalline in nature and silver had the highest intensity as shown by XRD and EDX analysis. PgMLEAgNPs and PgMSEAgNPs exhibited varied antibacterial activity against the test pathogens.

Keywords: Piper guineense methanol extracts, antibacterial activity, Silver nanoparticles, Gastrointestinal Tracts, Pathogens.

Classification: FoR Code: 1108

Language: English

Great Britain Journals Press

LJP Copyright ID: 925621
Print ISSN: 2631-8490
Online ISSN: 2631-8504

London Journal of Research in Science: Natural and Formal

Volume 24 | Issue 4 | Compilation 1.0

In-Vitro Antibacterial Activity of *Piper Guineense* Extracts and their Silver Nanoparticles Against Bacterial from Gastrointestinal Tract

Bukola Christianah Adebayo-Tayo[α] *, Folarin Victor Adeola[σ], Olusola Ademola Olaniyi[ρ] & Oladeji Aderibigbe Ajani[ω]

ABSTRACT

The study investigates the in-vitro antibacterial activity of greenly synthesized silver nanoparticles from Piper guineese leave (PgMLE) and seed (PgMSE) methanol extracts. The greenly synthesized silver nanoparticles from leave (PgMLEAgNPs) and seed (PgMSEAgNPs) extracts were characterized using UV-visible spectroscopy, FTIR, SEM, TEM, XRD, EDX, and TGA, and the in-vitro antibacterial activity of the extracts and nanoparticles against test pathogens from gastrointestinal tracts was evaluated. The PgMLE and PgMSE bio-reduced silver nitrate solution for the biosynthesis of PgMLEAgNPs and PgMSEAgNPs. The nanoparticles had the highest Surface plasmon resonance peaks at 500 nm. Functional groups such as alcohols, phenols, alkenes or alkynes, nitriles, ketones, aldehydes, or esters were identified as indicative of biomolecules present within PgMLEAgNPs, and PgMSEAgNPs. PgMLEAgNPs and PgMSEAgNPs were spherical flakelike and aggregated particles respectively with 15 nm in size, TEM shows the spherical shape nanoparticles. The nanoparticles were crystalline in nature and silver had the highest intensity as shown by XRD and EDX analysis. PgMLEAgNPs and PgMSEAgNPs exhibited varied antibacterial activity against the test pathogens. The antibacterial activity ranged from 2.00 to 18.00 mm in which E. coli had the highest susceptibility to PgMSEAgNPs compared to PgMLEAgNPs. The nanoparticles had better antibacterial efficacy against the test pathogens compared to the Piper guineense leaves and seed extracts. In conclusion, Piper guineense leave and seed extract nanoparticles had profound antibacterial activity against bacteria from GIT which makes them a candidate for biomedical application.

Keywords: Piper guineense methanol extracts, antibacterial activity, Silver nanoparticles, Gastrointestinal Tracts, Pathogens.

Author α σ: Department of Microbiology, University of Ibadan, Ibadan, Oyo State, Nigeria.
ρ: Department of Mathematics and Computer Science, University of North Carolina, Pembroke, USA.
ω: Federal Medical Center, Old N. North Carolina HWY 75, Buurner, NC 27509.

I. INTRODUCTION

The gastrointestinal tract is the site of the most well-known infectious diseases. These illnesses are brought on by bacterial infections and have long presented a challenge to the medical research community. Since the majority of people in developing nations live in poverty and infectious diseases are the main cause of morbidity and mortality, the development of new antimicrobials is of paramount importance (Look *et al.*, 2010). Up to date, various threats posed by infectious diseases that cannot be effectively prevented or treated with antibiotics, and antibiotic resistance as a result of numerous factors is of global health concern (Chadwick *et al.*, 2010).

Antimicrobial agent use has occasionally resulted in drops in morbidity and death (Huh and Kwon, 2011). Hydrophobic active plant components are increasingly being nanonized through trapping or encapsulation within inorganic or organic nanocarrier molecules, a technique known as nanotechnology. Nanotechnology is defined as the science of creating, utilizing, and applying nanostructures or nanomaterials, as well as examining the connections between different material qualities and their nanoscale dimensions (Siddiqi and Husen, 2017). It was discovered that nanomedicines created using this method can release active medicinal ingredients continuously from Nano carrier molecules, maintaining the medication's potency for an extended amount of time (Sarmukaddam *et al.*, 2010). Nanoparticles can be defined as small particles ranging in size from 1-100 nm and are undetectable by the human eyes.

As a result of the strong antioxidant action, medicinal plant extracts are employed as nano stabilizers and nanocarriers to decrease metal salts and oxides of Ag, Au, Cu, and Zn to metallic nanoparticles (NPs), which may be produced in a green synthetic form and have antibacterial properties (Dubey *et al.*, 2010; Zamare *et al.*, 2016; Mali *et al.*, 2020; Jayachandran *et al.*, 2021). Modern technologies use metallic nanoparticles because of their distinctive morphologies, surface Plasmon features, and intriguing physicochemical properties, among other things (Agnihotri *et al.,* 2014). According to Jamiu and Bello (2018), silver has long been utilized and recognized for its antibacterial activity. Due to their size, shape, and structure, as well as their huge surface-to-volume ratio, silver nanoparticles (AgNPs) have unique and more effective antibacterial properties when reduced to their nano-form (Rafique *et al.*, 2017). AgNPs are among the most widely used nanoparticles that show a broad spectrum of antibacterial activity (Ghodsieh *et al.,* 2016). The development of new bioactive antimicrobial compounds from plant extracts and the formulation of novel antimicrobial nanoparticles (NPs) using plant extracts as a bio-reducing agent can be considered as an adjuvant treatment or an alternative to antibiotics that can be used as therapeutics against gastrointestinal pathogens.

Piper guineense from the family Piperaceae is grown in Nigeria and is commonly known as Iyere in Yoruba and Uziza in Igbo. This plant yields fruit that is used as black pepper, Benin pepper, Ashanti pepper, or West African pepper (Faluyi, 2020). Iyere is regarded as the "king of all spices," and because of the presence of various bioactive compounds such as piperine, phenolic acids, and antioxidants, it has been employed in Ayurvedic medicine for thousands of years (Faluyi, 2020). It is used as a seasoning agent, for cosmetic, therapeutic, and insecticidal uses (Anyanwu and Nwosu, 2014 and Ogbunugafor *et al.,* 2017). The plant possesses antioxidant, anticonvulsant, anti-inflammatory, and neuropharmacological activities (Oyemitan *et al.,* 2015 and Salehi *et al.,* 2019).

To develop novel therapeutic antimicrobials using plant extracts as a nanocarrier to combat antibiotic resistance and gastroenteritis, hence a need for the use of *Piper guineense* extracts for the green synthesis of a novel drug. The study aimed at the biosynthesis of silver nanoparticles using methanol extract of *Piper guineense* seed and leaf as a bio-reducing and nanocarrier, characterization of the nanoparticles, and in-vitro determination of the antibacterial potential of the extracts and their nanoparticles against clinical isolates from gastrointestinal tracts.

II. MATERIALS AND METHODS

2.1 Collection of Plant Material and Cultures

Uziza (*Piper guineense*) seed and leaf used for this study were obtained from Gbogan market, Osun state, Nigeria. The plants were identified and authenticated at the Herbarium unit, Department of Botany, University of Ibadan. Clinical cultures (*E.coli, Klebsiella pneumoniae, and Shigella* sp.)

previously isolated from Gastrointestinal Tracts were collected from Microbiology Unit, University Teaching Hospital, University of Ibadan, Ibadan, Oyo state, Nigeria.

2.2 Sample Preparation and Extraction for Seed and Leave samples

Piper guineense seeds were thoroughly rinsed with distilled water, dried, and ground into fine powder. Five grams of powdered seed samples were weighed into an Erlenmeyer flask containing 50 mL of methanol. The mixture was heated for 15–20 min at 80 °C in a water bath. After boiling, the extract was filtered through Whatman's filter paper (No. 1) to remove any coarse material. A rotary evaporator operating at low temperatures and reduced pressure was used to concentrate the filtrate. The extract was then stored in an airtight container at 4°C in the refrigerator before use (Rautela *et al.,* 2019).

The leaves were cleaned with sterile water, dried, and then chopped into little pieces with a blender to prepare the plant crude extract. Then 50 g of each leaf sample was heated at 80°C in 250 ml of sterile water in a 500 mL Erlenmeyer flask for 30 min. After that, Whatman No. 1 was used to filter the crude leaf extracts, and they were kept at 4°C (Velu *et al.*, 2017).

2.3 Green Synthesis of Silver Nanoparticles Using Piper guineense Methanol Extracts

The production of silver nanoparticles was done according to the method of Rizwana *et al.* (2022). The crude extract from seeds and leaves was used for the biosynthesis of silver nanoparticles. 100 mL of 1 mM of the aqueous solution of silver nitrate ($AgNO_3$) was prepared in 250 mL Erlenmeyer flasks. The extracts were dissolved in Dimethyl Sulphur oxide (DMSO) at a concentration of 20 mg/mL. From the dissolved extracts, 10 mL each was mixed with 40 mL of silver nitrate ($AgNO_3$) solution in different 250 mL Erlenmeyer flasks for bio-reduction of the silver nitrate ($AgNO_3$) to silver (Ag^+) ions. The mixtures were then exposed to sunlight for bio-reduction of the $AgNO_3$ by the extracts to Ag^o ions. This formation of ions will form a deep brown color.

2.4 Characterization of Biosynthesized Nanoparticles

2.4.1 UV–Visible Spectroscopy of the Biosynthesized Ag Nanoparticles

This was carried out to ascertain the biosynthesized silver nanoparticles' optical characteristics. The biosynthesized nanoparticles were diluted with 2mL of deionized water and measured for spectrum at regular intervals. To blank all spectra for background correction, deionized water was used. All samples were loaded into a 1cm path-length quartz cuvette for UV-Vis spectrometric readings and scanned between 200 and 800nm wavelength, having a resolution of 1 nm. The UV-visible spectra were recorded at different intervals of 24-72 hours (Sanchooli *et al.*, 2018).

2.5 Fourier Transform Infrared Spectroscopy (FT-IR) of the Biosynthesized Ag Nanoparticles

The biosynthesized nanoparticles were further characterized using FTIR (spectrometer model 8400, Shimadzu) to detect the various functional groups responsible for the reduction, capping, and stabilizing of silver nitrate to form silver ions. For the FTIR analysis, the dried biosynthesized AgNPs were added to FTIR-grade potassium bromide (KBr) in 1: 30 ratios, and in transmittance mode, the spectrum was recorded at a resolution of 4 cm^{-1} and the spectrum was observed in the wave number range of 350-4,000 cm^{-1} (Mondal *et al.,* 2020).

2.6 Scanning Electron Microscopy (SEM) of the Biosynthesized Ag Nanoparticles

Scanning electron microscopy was employed to evaluate the Ag nanoparticles' surface structure. After 72 hours of reaction, the colloidal sample AgNPs was centrifuged at 4,000 x g for 15 minutes. The supernatant was discarded while the precipitate was dispersed in sterile water, followed by

centrifugation. This process was repeated thrice following a 30 minutes sonication to create a suspension, a drop of the nanoparticle solution was applied to a copper grid coated with carbon. The sample was kept under a lamp until completely dried and subjected to SEM analysis using a Phenom ProX Scanning Electron Microscope (Alkammash, 2017).

2.7 Transmission Electron Microscopy (TEM) of the Biosynthesized Ag Nanoparticles

TEM is used to study the sizes of the biosynthesized AgNPs from Uziza methanolic leaf and seed extracts. The biosynthesized nanoparticles were centrifuged at 4,000 x g for 15 minutes after 72 hrs of reaction. The sediments were dispersed in sterile water and centrifuged after the supernatant was discarded. A tiny droplet of the pellets was spread out on a copper grid coated in carbon and let to dry. TEM analysis was performed by using JOEL JCM-7000 instrument operated at an accelerating voltage of 15kV with a resolution of 0.23 nm (Gericke and Pinches, 2006).

2.8 X-ray diffraction (XRD) of the Biosynthesized Ag Nanoparticles

XRD was used to determine the crystalline nature of the greenly synthesized nanoparticles. The XRD pattern obtained from Rigaku D/Max-IIIC PW 1800 X-ray diffractometer at 2θ ranges from 4 to 70°. The sample for XRD measurement was prepared by casting the powder of silver nanoparticles on a glass slide and subsequently airdrying it under ambient conditions. The pattern was recorded by CuKα radiation with λ of 0.15 Å at a voltage of 40 kV and current of 20 mA with a scan rate of 10°/min (Adebayo-Tayo *et al.,* 2019 and Rautela *et al.,* 2019).

2.9 Energy Dispersive X-ray (EDX) of the Biosynthesized Ag Nanoparticles

EDX was used to determine the elemental composition of nanoparticles. The biosynthesized nanoparticles were centrifuged at 4,000 x g to obtain the pellet. The pellet was allowed to dry. A 100 nm thick section of the pellet was placed on the grid and analyzed using the Rigaku instrument model NEXCG. A pure selenium standard was used for calibration, and then a working curve was selected according to the sample. The sample was then tested and the result was outputted (Nayak *et al.*, 2014).

2.10 Thermogravimetric Analysis (TGA)

TGA was used to examine the thermal-induced degradation of the biosynthesized silver nanoparticles and this was conducted using Perkin-Elmer Thermogravimetry Analyzer Pyris 2. The analysis was carried out on approximately 25mg of samples at the temperature range of 35-1000 °C at a constant heating rate of 5 °C/min in a static air atmosphere.

2.11 Antibacterial Activities of the plant extracts and the biosynthesized Silver Nanoparticles (SNPS) against some GIT pathogens.

The test pathogens were maintained on an agar slant and stored at 4°C until use. The antibacterial activity of the extracts, and nanoparticles were determined using the agar well diffusion method. The extracts were dissolved in DMSO to form a concentration of 20 mg/mL. $AgNO_3$, DMSO, and Streptomycin were used as controls. The turbidity standard of each of the typed strains was prepared and compared to the McFarland standard. With sterile swab sticks, lawns of the standard were made on Nutrient Agar (NA) and a sterile cork-borer of diameter 6 mm was used to make holes in the plates. A micropipette machine was used to dispense 200 µL of the crude extracts and their SNPs into respective labeled wells. The plates were incubated at 37°C for 24 hours and the zones of inhibition (ZOI) (mm) were measured and recorded.

III. RESULTS

Silver nanoparticles were biosynthesized from the methanolic extract of *Piper guineense* seed and leaf. Figure 1 shows the visual observation of the biosynthesized nanoparticles. Color changes from green to brown after exposure to sunlight for bio-reduction of the $AgNO_3$ indicating the formation of AgNPs.

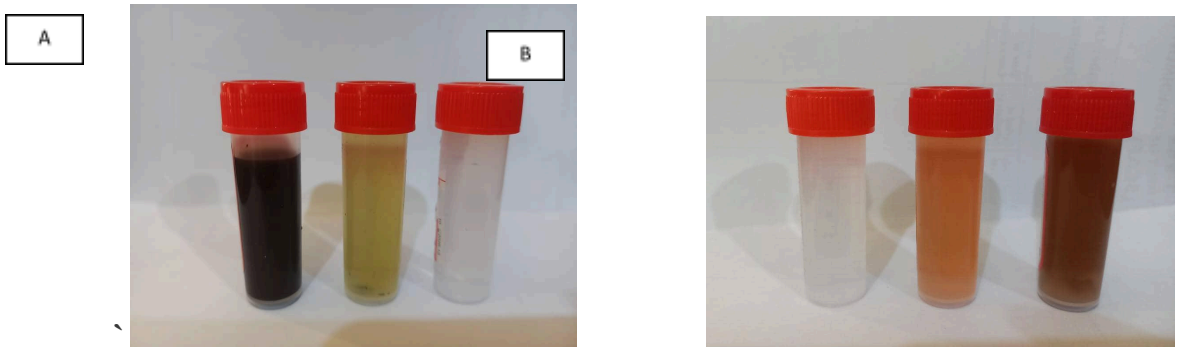

Key: A: 1- PgMSEAgNPs; 2-$AgNO_3$ + PgMSE and 3 - $AgNO_3$: B: 1 - $AgNO_3$, 2-$AgNO_3$ + PgMLE, **3-** PgMLEAgNPs

Figure 1a and b: Visual Observation of a) PgMSEAgNPs and b) PgMLEAgNPs

The biosynthesized AgNPs were monitored by measuring the metal ion reduction by periodically measuring their absorbance at different wavelengths ranging from 200 nm to 900 nm using a UV-Vis spectrophotometer. UV-vis spectra of the biosynthesized AgNPs are shown in Figures 2a and b. The PgMSEAgNPs had an absorption maximum within 400 nm to 500 nm with the highest surface Plasmon Resonance (SPR) peak absorbance of 1.889, 2.211, and 2.102 OD observed after 24, 48, and 72 hrs respectively at 500 nm wavelength which indicates the production of AgNPs. The PgMLEAgNPs had an absorption maximum within 400 nm to 500 nm with the highest surface Plasmon Resonance (SPR) peak absorbance of 1.970, 2.369, and 2.223 OD observed after 24, 48, and 72 hrs respectively at 500 nm wavelength which indicates the production of AgNPs.

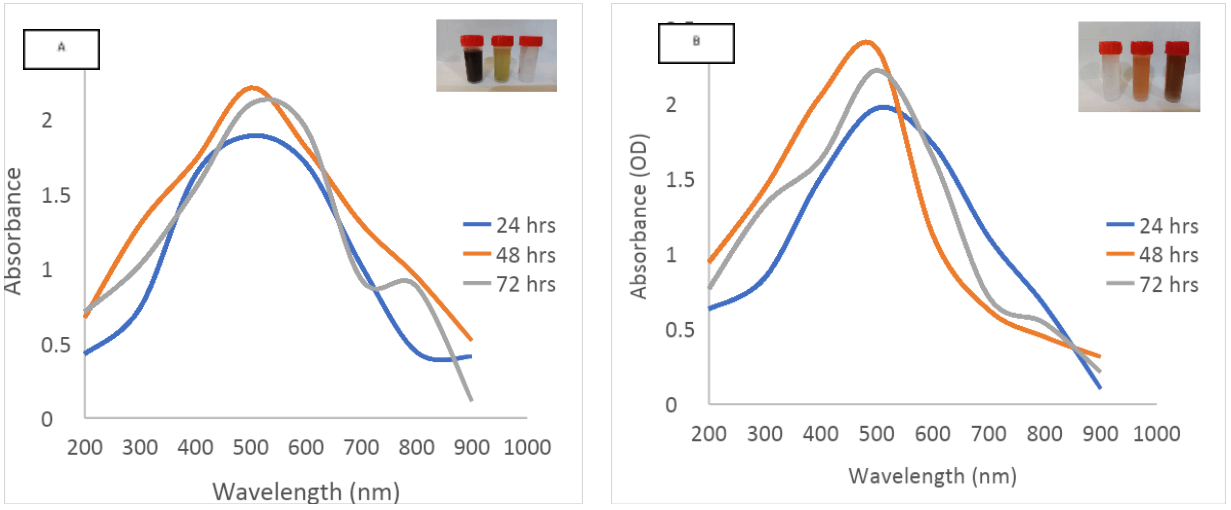

Figure 2a and b: UV-Visible Spectra of a) PgMSEAgNPs and b) PgMLEAgNPs

The FTIR analysis was performed to identify the potential biomolecules in PgMSEAgNPs and PgMLEAgNPs which are responsible for the bio-reduction and capping of the biosynthesized nanoparticles by characterizing the functional groups present on the surface of the nanoparticles. Figure 3a and b shows the FTIR spectrum of the biosynthesized nanoparticles and the spectra were measured at wave number 4000 – 350 cm^{-1}. The spectra for PgMSEAgNPs showed 12 major absorption peaks which indicates the presence of the different functional groups. The peak observed in the higher

energy region of intense absorption is 3757.00 and 3436.00 cm^{-1} which is characteristic of the stretching vibrations of O-H bonds in hydrogen-bonded hydroxyl (OH) groups, such as in alcohols or phenols. The peak at 2926.54, and 2859.80 corresponds to the asymmetric stretching vibrations of C-H bonds in aliphatic hydrocarbons. It is typical of alkanes and similar compounds. The peak at 2374.66 suggests the presence of a highly polarized bond, such as a triple bond (e.g., C≡N or C≡C) or nitriles. The peak at 2000.00 indicates the presence of carbon-carbon multiple bonds, like C=C double bonds in alkenes or alkynes. The peak at 1878.21 is often associated with carbon-carbon multiple bonds or possibly nitriles (C≡N) while the peak at 1630.66 indicates the presence of carbonyl groups (C=O) in compounds, such as ketones, aldehydes, or esters. The peak at 1054.09 is often related to C-O stretching vibrations in alcohols, ethers, or esters. The peak at 778.34 and 683.13 indicates the out-of-plane bending vibrations of aromatic (benzene-like) C-H bonds. The peak at 451.36 is in the fingerprint region, and this indicates the existence of metal oxide. These functional groups identified are indicative of biomolecules present within PgMSEAgNPs.

The spectra for PgMLEAgNPs showed 13 major absorption peaks which indicates the presence of the different functional groups. The peak observed in the higher energy region of intense absorption is 3868.00, 3752.23, and 3445.00 which is characteristic of the stretching vibrations of O-H bonds in hydrogen-bonded hydroxyl (OH) groups, such as in alcohols or phenols. The peak at 2927.76 corresponds to the asymmetric stretching vibrations of C-H bonds in aliphatic hydrocarbons. It is typical of alkanes and similar compounds. The peak at 2375.83 suggests the presence of a highly polarized bond, such as a triple bond (e.g., C≡N or C≡C) or nitriles. The peak at 1997.76 indicates the presence of carbon-carbon multiple bonds, like C=C double bonds in alkenes or alkynes. The peak at 1877.00 is often associated with carbon-carbon multiple bonds or possibly nitriles (C≡N) while the peak at 1631.73 indicates the presence of carbonyl groups (C=O) in compounds, such as ketones, aldehydes, or esters. The peak at 1056.00 is often related to C-O stretching vibrations in alcohols, ethers, or esters. The peak at 780.48 and 685.36 indicates the out-of-plane bending vibrations of aromatic (benzene-like) C-H bonds. The peak at 451.65 is in the fingerprint region, and this indicates the existence of metal oxide, and the peak at 373.47 is associated with the bending vibrations of strong covalent bonds or lattice vibrations in inorganic compounds. These functional groups identified are indicative of biomolecules present within PgMLEAgNPs.

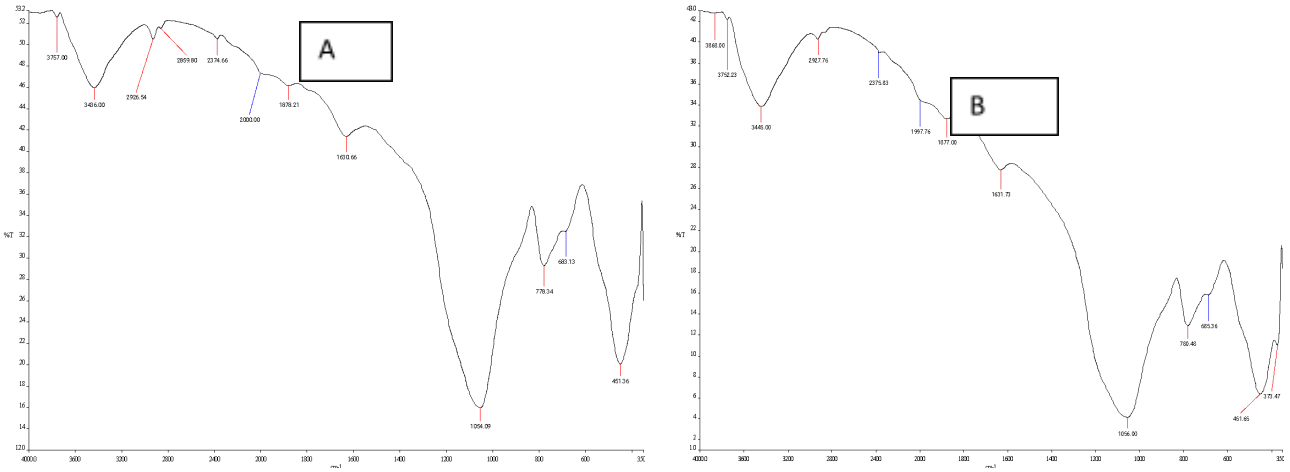

Figure 3a and b: Fourier Transform Infrared Spectroscopy (FTIR) of a) PgMSEAgNPs and b) PgMLEAgNPs

Scanning Electron Microscope (SEM) was used to observe the shape and surface characteristics of the biosynthesized nanoparticles. Figure 4a and b shows the scanning electron micrograph of the biosynthesized PgMSEAgNPs and PgMLEAgNPs. PgMSEAgNPs had an aggregated surface however there were variations in their morphology which is not unusual for biosynthesized nanoparticles shape while PgMLEAgNPs were spherical and flakelike in shape. Figure 4c and d shows the 3D image of PgMSEAgNPs and PgMLEAgNPs. Both 3D SEM images of the biosynthesized AgNPs revealed the particles to have nano-sized 15 nm.

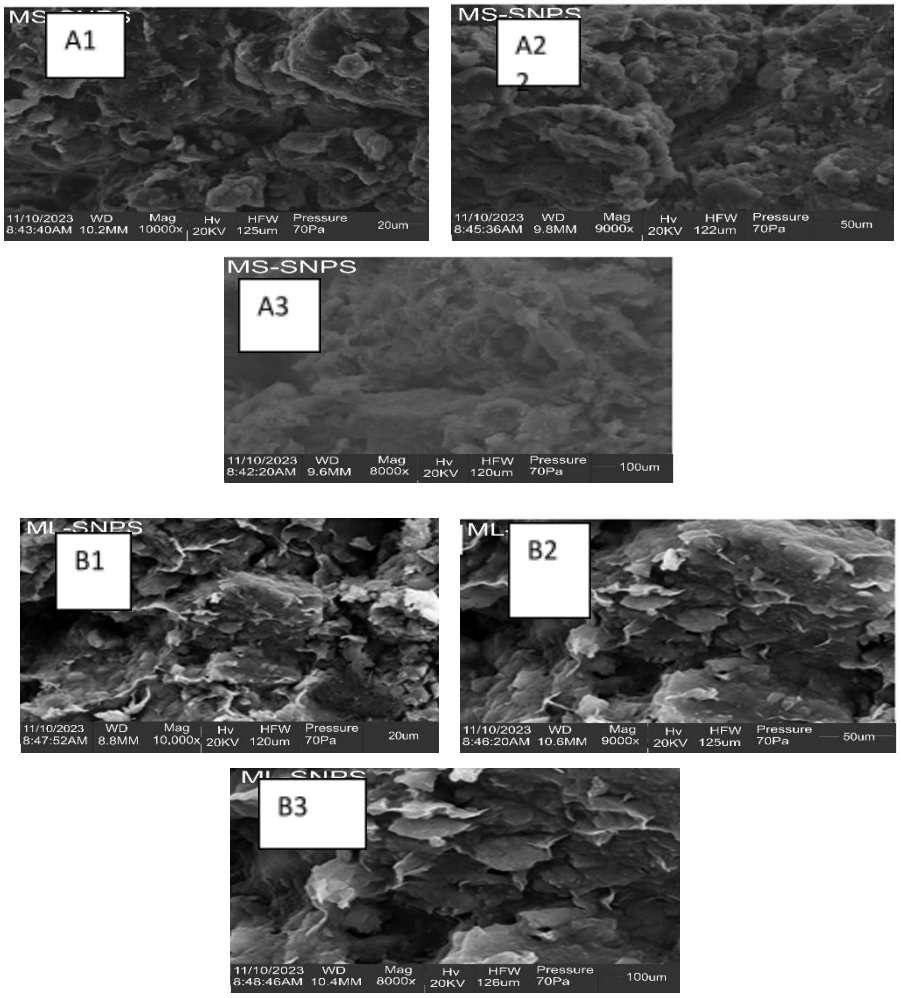

Figure 4a and b: Scanning Electron Microscopy (SEM) of a) PgMSEAgNPs and b) PgMLEAgNPs

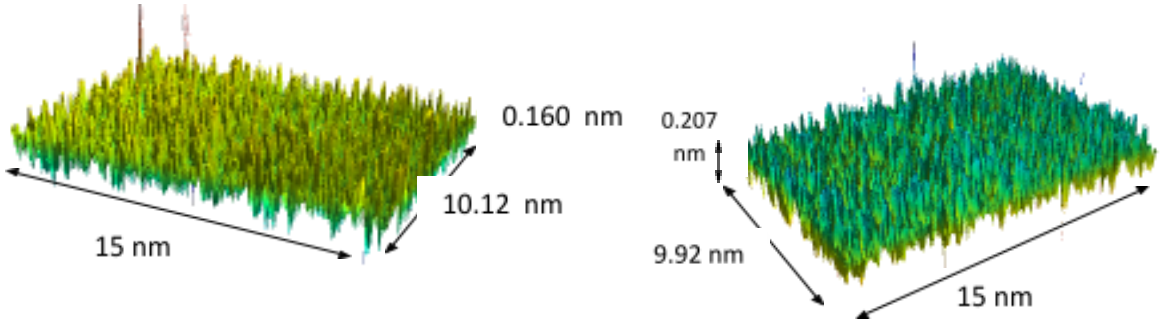

Figure 4c and d: 3D image of a) PgMSEAgNPs and b) PgMLEAgNPs.

Transmission Electron Microscope (TEM) was used to observe the shape and size of the biosynthesized nanoparticles. Figure 5a and b shows the Transmission electron micrograph of the biosynthesized PgMSEAgNPs and PgMLEAgNPs and that the particles are both nanoscale and uniform. PgMSEAgNPs and PgMLEAgNPs had spherical forms and the size ranged from 1.32 to 5.32 nm.

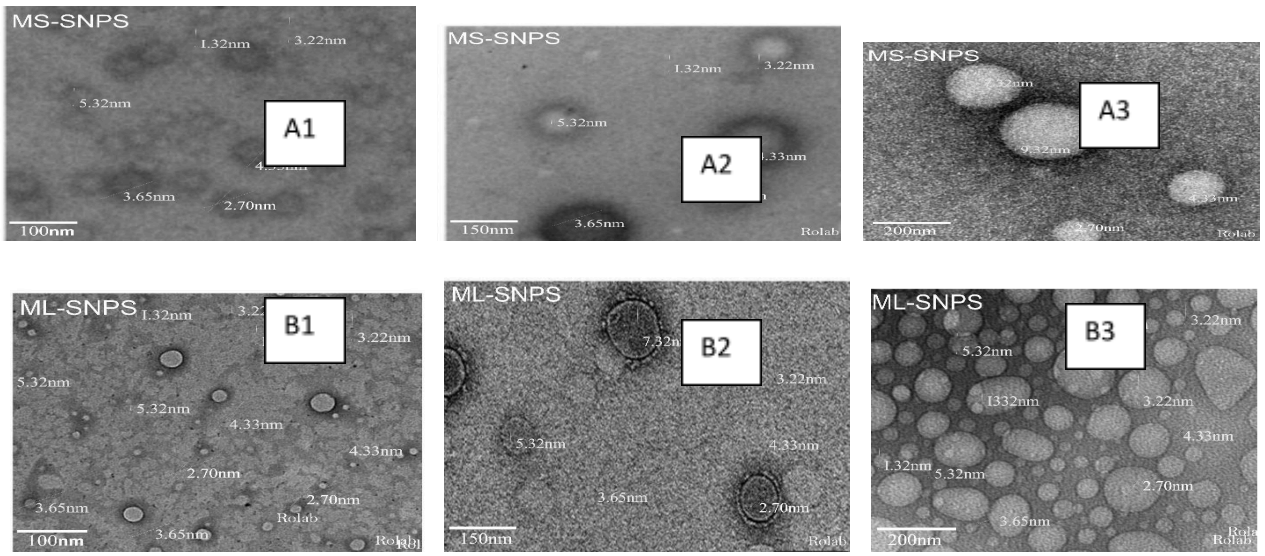

Figure 5a and b: Transmission Electron Microscopy (TEM) of a) PgMSEAgNPs and b) PgMLEAgNPs

X-ray diffraction was used to examine the size, crystalline makeup, purity, and quality of the nanoparticle. Figure 6a and b shows the X-ray diffractogram (XRD) pattern for PgMSEAgNPs and PgMLEAgNPs. The diffraction highs 2θ = 26.5, 32.4, 35.6, 36.4, 47.4, 56.3, 63.4, 67.2, and 67.3 are related to 005, 100, 002, 101, 102, 110, 103, 112, and 201 respectively for PgMSEAgNPs while the diffraction highs 2θ were 30.3, 34.5, 35.8, 46.5, 55.5, 63.2, 66.3, 68.6, 70.2, and 73.3 are related to 100, 002, 101, 102, 110, 103, 200, 112, 201, and 202 respectively for PgMLEAgNPs. The biosynthesized nanoparticles were crystalline in nature.

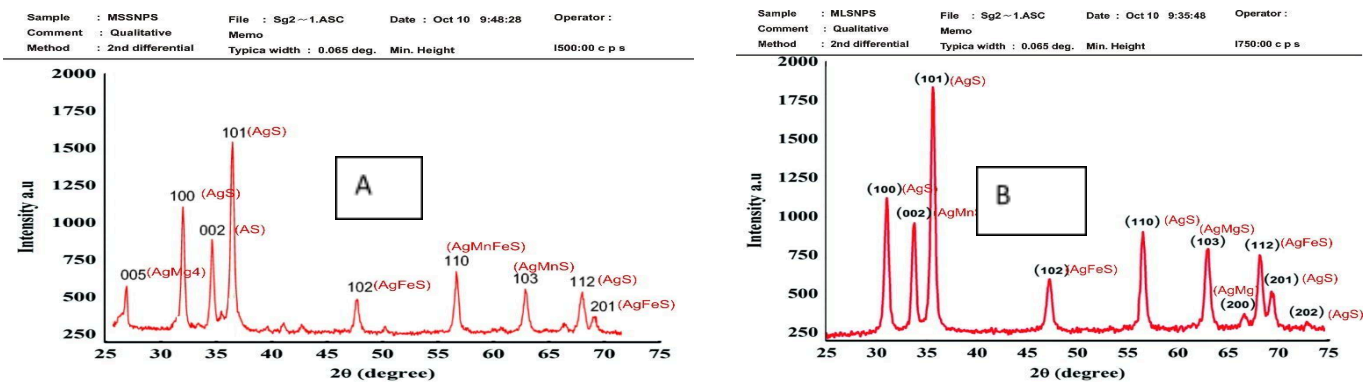

Figure 6a and b: X-ray Diffraction of PgMSEAgNPs and PgMLEAgNPs

The elemental analysis of PgMSEAgNPs and PgMLEAgNPs was revealed using the Energy X-ray Spectroscopy (EDX) which is shown in Figure 7a and b. The findings of EDX show that the Silver (Ag) atoms present have a significant signal. Further peaks that were seen include C, O, K, S, and Si for PgMSEAgNPs while C, O, Na, S, and Si for PgMLEAgNPs. From the result, silver (Ag) has the highest intensity of 65.20 % and 64.50 % for PgMSEAgNPs and PgMLEAgNPs respectively.

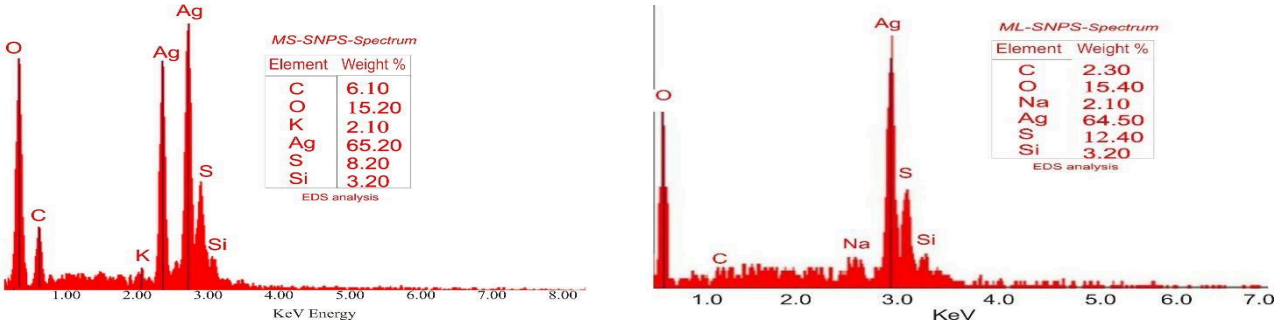

Figure 7a and b: EDX analysis of a) PgMSEAgNPs and b) PgMLEAgNPs

The thermal stability of PgMSEAgNPs and PgMLEAgNPs about its weight was evaluated using Thermogravimetry (TGA). Figure 8a and b shows the TGA curve of weight loss that occurred in temperature region between 160 °C and 250 °C for PgMSEAgNPs and 200 °C and 300 °C for PgMLEAgNPs. There was little weight loss below 160 °C and above 250 °C for PgMSEAgNPs and little weight loss below 200 °C and above 300 °C for PgMLEAgNPs.

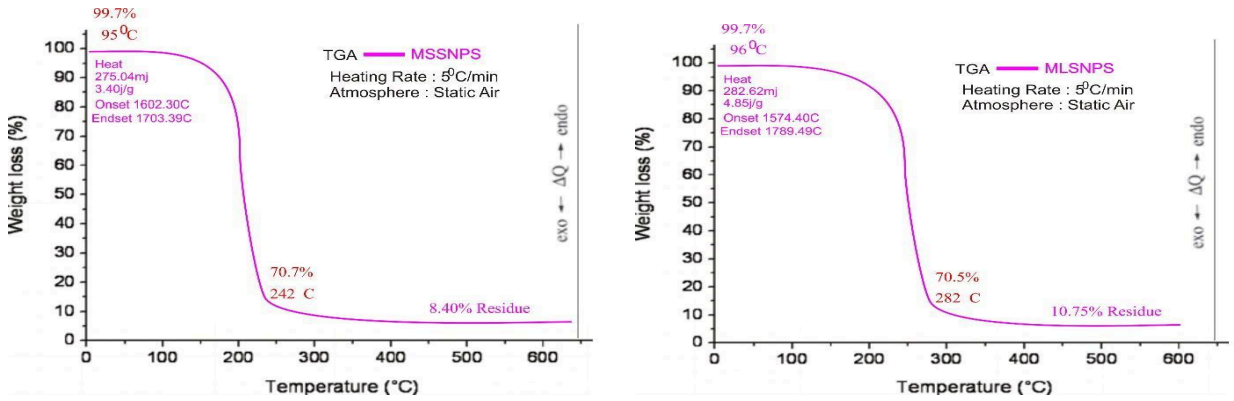

Figure 8a and b: TGA analysis of a) PgMSEAgNPs and b) PgMLEAgNPs

The antibacterial activity of the *P. guineense* methanol leaf and seed extract and its biosynthesized silver nanoparticle against test strains using the agar well diffusion method is shown in Table 1. The extracts and their nanoparticles have varied antibacterial activity against the test strains. The antibacterial activity ranged from 2.0 - 6.0 mm, 2.0 – 18.0 mm, 2.0 – 12.0 mm and 6.0 – 18.0 mm for Methanol leaf (ML), PgMLEAgNPs, Methanol Seed (MS) and PgMSEAgNPs respectively in which *E. coli* had the highest susceptibility (18mm) to PgMLEAgNPs. EC1 and U99 had the highest susceptibility (12mm) to MS and both UP_1 and EC11 had the highest susceptibility (18mm) to PgMSEAgNPs. It was observed that all extracts were 91.6% effective against the test pathogens except for PgMSEAgNPs which were 100% effective against all test strains. The result indicated that EC14 was resistant to both ML and PgMSEAgNPs, while EC21 was resistant to MS.

Table 1: Antimicrobial Activity of the methanol Piper *guineense* Extract and their Methanolic Silver Nanoparticle

Sample Code			Antibacterial Activity (mm) / Test pathogens									
	EC14	EC53	EC21	KLEB	EC114	EC1	SHI P45	UP1	EC104	EC11	U32	U99
ML	0	6	6	2	6	6	4	6	6	6	6	4
ML SNPs	0	8	14	6	2	8	8	8	8	12	0	18
MS	6	2	0	6	4	12	8	10	10	8	8	12
MS SNPs	12	10	12	6	14	12	12	18	6	20	0	8
Streptomycin	10	4	8	6	5	6	0	2	2	0	8	2
DMSO	0	0	0	0	0	0	0	0	0	0	0	0

KEY:

EC14	*Escherichia coli* Ec14		EC104	*Escherichia coli* EC104		EC1	*Escherichia coli* Ec1
EC53	*Escherichia coli* Ec53		EC11	*Escherichia coli* EC11		UP1	*Esxherichia coli* UP1
EC21	*Escherichia coli* Ec21		U32	*Escherichia coli* U32		KLEB	*Klebsiella pneumoniae*
EC114	*Esherichia coli* Ec114		U99	*Escherichia coli* U99		SHIP 45	*Shigella* sp P45

IV. DISCUSSION

The *P. guinesse* methanol leaves and seed extracts were able to bio-reduce silver nitrate for the biosynthesis of silver nanoparticles. Maxima absorbance peaks within 400 nm to 500 nm with increasing Surface Plasmon Resonance (SPR) peak as incubation time increased from 24 hrs to 48 hrs after which a decline set in at 72 hrs. A similar observation was reported by Cherian *et al.* (2018) in their study on "synthesis of biocompatible silver nanoparticles using leaf extract of *Piper nigrum*" which reported an absorbance peak at 420 nm specific for the AgNPs. Furthermore, it has been reported that absorption spectra of larger metallic colloidal dispersions can exhibit wide or additional bands in the UV–visible range due to the excitation of plasmon resonances or higher multipole plasmon excitations. The results from this study are consistent with previous studies reported by Jacob *et al.* (2012) and Otunola and Afolayan, (2018) on silver nanoparticles from *Piper longum* leaf extracts and aqueous extract of a spice blend formulation respectively. Also, according to Hemlata *et al.,* (2020) reported the presence of an absorbance peak at about 420 nm indicating the formation of AgNPs in the solution which may be as a results of surface plasmon resonance (SPR) electrons on the nanoparticle surface. The size, shape, and other individual metal particle characteristics, as well as the medium's dielectric qualities, all affect the SPR pattern and the inter-nanoparticle coupling interactions. The intensity of the SPR band increased with reaction time, indicating the synthesis of the AgNPs (Sikdar, 2023).

The FTIR analyses were to characterize AgNPs and to examine the possible bio-reducing functional groups present in PgMSEAgNPs and PgMLEAgNPs. The spectrum was captured from 350 cm^{-1} to 4000

cm^{-1}. The FTIR result of this study was in agreement with the report of Krishnan *et al.* (2016) on silver nanoparticles from *Piper nigrum* concoction. Similar peaks which indicated the same functional groups as indicated in this study were reported. However, the c=c stretch indicating the presence of alkenes was not recorded by Krishnan *et al.,* (2016). Complete suppression of iodo compounds OH group out of plane bending (521 and 565) may be due to the addition of silver nitrate, which means the complete reduction and stabilization of the silver nanoparticles. This is in agreement with this study at 451.65 and 373.47 for PgMLEAgNPs while 451.36 for PgMSEAgNPs. The modulated transmittance percentage of ketone, fluoro compounds, and amine groups was confirmed as they play a vital role in the bio-reduction of silver nitrate to silver nanoparticles. The presence of these peaks demonstrated that plant secondary metabolites, including terpenoids, flavonoids, glycosides, phenols, and tannins, as well as functional groups like aldehyde, carboxylic acid, and others, coated the nanoparticles. The presence of these groups is due to the stability of the nanoparticles (Bagherzade *et al.,* 2017).

The SEM analysis identified the nano-size and shape of PgMSEAgNPs and PgMLEAgNPs. The shape of the PgMSEAgNPs was not clear because they are aggregated. Due to the drying process, the aggregation may be observed. Adebayo-Tayo *et al.* (2019) observed a similar situation in their work on the rapid synthesis and characterization of gold and silver nanoparticles using exopolysaccharides and metabolites of *Wesiella confusa*. They concluded that sample preparation including drying can affect the shape and size of SNPs (Adebayo-Tayo *et al.,* 2019). The flake-like shape of PgMLEAgNPs was similar to the report Guo *et al.* (2021) on "Shape-controlled synthesis of flake-like $FeNi_3$ nanoparticles based on sodium lignosulfonate". Endah *et al.* (2022) reported a mixture of spherical and flake-like shapes for ZnO nanoparticles.

Using the XRD pattern the size of crystals was investigated and the crystallite size of silver nanoparticles for PgMSEAgNPs and PgMLEAgNPs was about 54 nm and 38 nm respectively. The XRD pattern thus clearly indicated that the AgNPs organized by the reduction of Ag+ ions by the aqueous extract of *Piper guineense* were crystalline in nature. Presence of these peaks was due to seed and leave extract which contains organic compounds and is responsible for the reduction of silver ions and stabilization of resultant nanoparticles. This result is similar to Giri *et al.,* (2022) as they report the average crystalline size of silver nanoparticle synthesized to be approximately 35 The elemental composition of the biosynthesized nanoparticles was analyzed using EDX spectroscopy. EDX analysis of the PgMSEAgNPs and PgMLEAgNPs shows that silver had the highest peak at 3 keV which indicates that Silver (Ag) is the main element present. The presence of other elements may be as a result of the residual phytoconstituents of *Piper guineense* acting as a capping agent on the surface of the nanoparticles or contaminants introduced into the sample during handling. The results of EDX spectroscopy support the results of UV-visible spectrophotometric analysis, confirming the formation of AgNPs by methanol extract of *P. guineense*. The EDX result in this study is similar to the findings of Adeleye *et al.* (2023) for *Ehretia cymosa* silver nanoparticles. When compared to SNPs from aqueous extract, SNPs had a greater absorption peak and element concentration by weight. This also agrees with the results of Maloma *et al.* (2023) on *T. polyzona* Laccase-Mediated Silver Nanoparticles. The silver nanoparticles show a characteristic strong signal peak at 3 keV as a result of the surface plasmon resonance. Additionally, other signals although weak, indicate the presence of C, O, S, and Si and these elements may have played a vital role in the stability and reduction of the nanoparticles. This agrees with the report of Adebayo-Tayo *et al.* (2022).

The Thermogravimetric analysis (TGA) of the synthesized nanoparticles revealed the thermal stability of the AgNPs synthesized. According to the TGA curve, the study weight loss was consistent and occurred in the temperature range of 160 °C and 250 °C (70.7%) for PgMSEAgNPs and 200 °C and 300 °C (70.5%) for PgMLEAgNPs. The loss was due to the decomposition and evaporation of phytochemicals/biomolecules on the surfaces of the silver nanoparticles as surface stabilizing/capping

agents for both AgNPs synthesized. A closely similar result was reported by Zahoor *et al.* (2022) on *Rhynchosia capitata* leaf extract silver nanoparticles. A single weight loss between the temperature range 40 to 80 °C was observed which was due to the elimination of moisture contents from the NPs caused the sample's weight to decrease and the capping agent being organically decomposed rapidly with the increase in temperature and resulted in abrupt mass loss. Also, Hemali and Sumitra (2020) had a similar report on silver nanoparticles using *Ziziphus nummularia* leaf extract. They reported similar weight loss of AgNPs 100 °C to 800 °C which was due to thermal decomposition of plant bioorganic compounds absorbed on the surface of nanoparticles.

The result indicated that silver nanoparticles have considerably more antibacterial effects compared to leaf and seed extract of the plant. This observation conforms to the finding of Ghodsieh *et al.* (2017) on silver nanoparticles from aqueous extract of saffron (*Crocus sativus* L.) wastages. They reported a significant antibacterial effect of the nanoparticles against *some test pathogens* and concluded that it can be used in biomedical applications. This also agreed with the work of Loo *et al.* (2018) who reported that the AgNPs showed antibacterial activity against Gram-negative foodborne pathogens.

V. CONCLUSION

In this study, methanol extract of *Piper guineense* leaf and seed bio-reduced silver nitrate for nanoparticles biosynthesis and act as a nanocarrier for the *P. guineense* seed and leave bioactive chemicals with varied antibacterial activity against the test pathogens from gastrointestinal tract. The biosynthesized silver nanoparticles from methanol leaf and seed *Piper guineense* extract have more potent antimicrobial activity compare to the extracts. Therefore, further studies are needed to fully characterize the toxicity and the modes and mechanisms of antimicrobial action and antioxidant activity of these biomolecules and the particles.

Data Availability

The data that support the findings of this study are available on request.

Conflicts of Interest

The authors have no competing interests to declare regarding this article.

Authors' Contributions

The conception, design, and execution of the study were a collaborative effort by all authors. Bukola Christianah Adebayo-Tayo, Folarin Victor Adeola, Olusola Ademola Olaniyi and Oladeji Aderibigbe Ajani performed material preparation, data collection, and analysis. The initial manuscript draft was written by Folarin Victor Adeola, and all authors provided feedback on previous versions. The final manuscript was read and approved by all authors.

Acknowledgments - Not applicable

Funding

The research was self-funded by the authors.

REFERENCES

1. Adebayo-Tayo, B.C., A. Salaam, A. Ajibade (2019). Green synthesis of silver nanoparticle using *Oscillatoria* sp. extract, its antibacterial, antibiofilm potential and cytotoxicity activity. *Journal of Heliyon*. **5**: 10-25.

2. Adebayo-Tayo, B. C., S. O. Borode, S. O. Alao (2022). *In–Vitro* Antibacterial and Antifungal Efficacy of Greenly Fabricated *Senna alata* Leaf Extract Silver Nanoparticles and Silver Nanoparticle-Cream Blend. *Period. Polytech. Chem. Eng*. **66**: 248–260.
3. Adeleye, O.A., K. O. Aremu, H. Iqbal, M. O. Adedokun, O. A. Bamiro, O. L. Okunye, M. N. Femi-Oyewo, K. O. Sodeinde, S. Z. Yahaya, A. O. Awolesi (2023). Green Synthesis of Silver Nanoparticles Using Extracts of *Ehretia cymosa* and Evaluation of Its Antibacterial Activity in Cream and Ointment Drug Delivery Systems. *J. Nanotechnol.* https://doi.org/10.1155/2023/2808015.
4. Agnihotri, S., S. Mukherji, S. Mukherji (2014). Size-controlled silver nanoparticles synthesized over the range 5 – 100 nm using the same protocol and their antibacterial efficacy. *Adv. Res*. 3974-3983
5. Ajileye, O.O., M. A. Aderogba, E. M. Obuotor, E. O. Akinkunmi (2015). Isolation and characterization of antioxidant and antimicrobial compounds from *Acacardium occidentale* L. (Anacardiaceae) leaf extract. *J. King Saud Univ. Sci.* **27**: 244-252
6. Alkammash, N. M. (2017). Synthesis of Silver Nanoparticles from Artemisia Sieberi and Calotropis Procera Medical Plant Extracts and Their Characterization using SEM Analysis. *Biosci. Biotechnol. Res. Asia*. **14(**2).
7. Anyanwu, C.U., G. C. Nwosu (2014). Assessment of the antimicrobial activity of aqueous and ethanolic extracts of *Piper guineense* leaves. *J. Med. P. Res*. **8**: 436–40.
8. Bagherzade, G., M. M. Tavakoli, M. H. Namaei (2017). Green synthesis of silver nanoparticles using aqueous extract of saffron (*Crocus sativus* L.) wastages and its antibacterial activity against six bacteria. *Asian Pac. J. Trop. Biomed*. **7**: 227–233.
9. Chadwick, S., C. Kriegel, M. Amiji (2010). Nanotechnology solutions for mucosal immunization. *Adv. Drug Deliv. Rev*. **62**: 394-407.
10. Cherian, T., T. Jamal, S. K. Yalla, R. Mohanraju (2018). One-pot green synthesis of biocompatible silver nanoparticles using leaf extract of *Piper nigrum*. *IJPBS*. **8**: 1082-1088.
11. Dubey, S. P., M. Lahtinen, H. Sarkka, M. Silanpaa (2010). Bioprospective of *Sorbus aucuparia* leaf extract in development of silver and gold nanocolloids. *Colloids Surf. B*. **80**: 26–33.
12. Endah, E.S., V. Saraswaty, D. Ratnaningrum, W. Kosasih, A. Ardiansyah, C. Risdian, P. Nugroho, S. E. Aji, H. Setiyanto (2022). Phyto-assisted synthesis of zinc oxide nanoparticles using mango (Mangifera indica) fruit peel extract and their antibacterial activity. *Environ. Earth Sci.* **1201:** 012081.
13. Faluyi, O. (2020). Take advantage of the health benefits of iyere (*Piper guineense*). https://punchng.com/take-advantage-of-the-health-benefits-of-iyere-piper-guineense/
14. Gericke, M., A. Pinches (2006). Biological Synthesis of Metal Nanoparticles. *Hydrometallurgy*. **83:** 132-140.
15. Ghodsieh, B., M. T. Maryam, H. N. Mohmmad (2016). Green synthesis of silver nanoparticles using aqueous extract of saffron (*Crocus sativus* L.) wastages and its antibacterial activity against six bacteria. *Asian Pac. J. Trop. Biomed*. **7**: 227-233.
16. Hemali, P., C. Sumitra (2020). Synthesis of silver nanoparticles using *Ziziphus nummularia* leaf extract and evaluation of their antimicrobial, antioxidant, cytotoxic and genotoxic potential (4-in-1 system). *Artif Cells Nanomed Biotechnol*. **49**: 354-366.
17. Hemlata, P. R. Meena, P. A. Singh, K. K. Tejavath (2020). Biosynthesis of Silver Nanoparticles Using *Cucumis prophetarum* Aqueous Leaf Extract and Their Antibacterial and Antiproliferative Activity Against Cancer Cell Lines. *ACS omega*. **5**: 5520–5528
18. Huh, A. J., Y. J. Kwon (2011). "Nanoantibiotics": a new paradigm for treating infectious diseases using nanomaterials in the antibiotics resistant era. *JCR*. **156**: 128-145.
19. Jacob, J.P.S., J. S. Finub, A. Narayanan (2012). Synthesis of silver nanoparticles using *Piper longum* leaf extracts and its cytotoxic activity against Hep-2 cell line. *Colloids Surf. B*. **91**: 212– 214

20. Jamiu, A.T., S. Bello (2018). Biosynthesis of Silver Nanoparticles using *Azadirachta indica* Leaf Extract and Assessment of its Antibacterial Activity on some Pathogenic Enteric Bacteria. *IJRDPL*. **5**: 25-31.
21. Jayachandran, A., T. R. Aswathy, A. S. Nair (2021). Green synthesis and characterization of zinc oxide nanoparticles using Cayratia pedata leaf extract. *Biochem. Biophys. Rep*. **26:** 100995.
22. Krishnan, V.l., G. Bupesh, E. Manikandan, A. K. Thanigai, S. Magesh, R. Kalyanaraman, M. Maaza (2016). Green Synthesis of Silver Nanoparticles Using Piper nigrum Concoction and its Anticancer Activity against MCF-7 and Hep-2 Cell Lines. *J. Antimicrob. Agents*. **2**: 1000123
23. Loo, Y.Y., Y. Rukayadi, M. Nor-Khaizura, C. H. Kuan, B. W. Chieng, M. Nishibuchi, S. Radu (2018). In Vitro Antimicrobial Activity of Green Synthesized Silver Nanoparticles Against Selected Gram-negative Foodborne Pathogens. *Front. microbiol*. **16**: 9
24. Look, M., A. Bandyopadhyay, J. S. Blum, T. M. Fahmy (2010). Application of nanotechnologies for improved immune response against infectious diseases in the developing world. *Adv. Drug Deliv. Rev*. **62:** 378-393.
25. Mali, S.C., A. Dhaka, C. K. Githala, R. Trivedi (2020). Green synthesis of copper nanoparticles using *Celastrus paniculatus* Wild leaf extract and their photocatalytic and antifungal properties. *Biotechnol. Rep*. **27:** e00518.
26. Maloma, R.M., B. C. Adebayo-Tayo, Y. A. Alli, P. O. Oladoye (2023). Synthesis and Characterization of *T. polyzona* and Laccase-Mediated Silver Nanoparticles: Antimicrobial and Printing Press Wastewater Treatment Efficiency. *Chem. Afr*. **6:** 2509–2521.
27. Mondal, A.H., D. Yadav, S. Mitra, K. Mukhopadhyay (2020). Biosynthesis of Silver Nanoparticles Using Culture Supernatant of *Shewanella* sp. ARYI and their Antibacterial Activity. *Int J Nanomed*. **15:** 8295-8307.
28. Nayak, B.K., N. Chitra, A. Nanda (2014). Efficacy of biosynthesized AgNPs from *Alternaria chlamydospore* isolated from indoor air of vegetable market. *Int. J. Pharm. Technol*. **6:** 1309-1314.
29. Ogbunugafor, H.A., C. G. Ugochukwu, A. E. Kyrian-Ogbonna (2017). The role of spices in nutrition and health: A review of three popular spices used in Southern Nigeria. *Food Qual. Saf*. **1**:171–85.
30. Otunola, G.A., A. J. Afolayan (2018). In vitro antibacterial, antioxidant and toxicity profile of silver nanoparticles green synthesized and characterized from aqueous extract of a spice blend formulation. *Biotechnol. Biotechnol. Equip*. **32:** 1-10.
31. Oyemitan, I. A., O. A. Olayera, A. Alabi, L. A. Abass, C. A. Elusiyan, A. O. Oyedeji, M. A. Akanmu (2015). Psychoneuropharmacological activities and chemical composition of essential oil of fresh fruits of *Piper guineense* (Piperaceae) in mice. *J. Ethnopharmacol*. **166:** 240–9.
32. Rafique, M., I. Sadaf, M. S. Rafique, M. B. Tahir (2017). A review on green synthesis of silver nanoparticles and their applications. *Artif Cells Nanomed Biotechnol*. **45:** 1272-1291.
33. Rautela, A., J. Rani, M. Debnath (2019). Green synthesis of silver nanoparticles from Tectona grandis seeds extract: characterization and mechanism of antimicrobial action on different microorganisms. *JAST*. **10:** 5.
34. Rizwana, H., M. S. Alwhibi, R. A. Al-Judaie, H. A. Aldehaish, N. S. Alsaggabi (2022). Sunlight-Mediated Green Synthesis of Silver Nanoparticles Using the Berries of *Ribes rubrum* (Red Currants): Characterisation and Evaluation of Their Antifungal and Antibacterial Activities. *Molecules*. **27**: 2186.
35. Salehi, B., Z. A. Zakaria, R. Gyawali, S. A. Ibrahim, J. Rajkovic, Z. K. Shinwari, T. Khan, J. Sharifi-Rad, A. Ozleyen, E. Turkdonmez (2019). *Piper* species: A comprehensive review on their phytochemistry, biological activities and applications. *Molecules*. **24**: 1364.
36. Sanchooli, N., S. Saeidi, H. K. Barani, E. Sanchooli (2018). In vitro antibacterial effects of silver nanoparticles synthesized using *Verbena officinalis* leaf extract on *Yersinia ruckeri*, *Vibrio cholera* and *Listeria monocytogenes*. *IJM*. **10:** 400-408.

37. Sarmukaddam, S., A. Chopra, G. Tillu (2010). Efficacy and safety of Ayurvedic medicines: recommending equivalence trial design and proposing safety index. *Int. J. Ayurveda Res.* **1:** 175–180.
38. Siddiqi, S.K., A. Husen (2017). Plant Response to Engineered Metal Oxide Nanoparticles. *Nanoscale Res. Lett.* **12**.
39. Sikdar, M (2023). Green synthesis, optimization and analyzing of silver nanoparticles encapsulated with *Syzygium aromaticum* extract: Evaluating antibacterial and photocatalytic properties. *Bioresour. Technol. Rep.* ***24:*** 101669.
40. Velu, M., J. H. Lee, W. S. Chang, N. Lovanh, Y. J. Park, P. Jayanthi, V. Palanivel, B. T. Oh (2017). Fabrication, optimization, and characterization of noble silver nanoparticles from sugarcane leaf (*Saccharum officinarum*) extract for antifungal application. *Biotech.* **7:** 1-9.
41. Zahoor, M., M. Nisar, I. S. Haq, M. Ikram, N. U. Islam, M. Naeem, A. Alotaibi (2022). Green synthesis, characterization of silver nanoparticles using *Rhynchosia capitata* leaf extract and their biological activities. *Open Chem.* **21**: 20220318
42. Zamare, M.S., S. S. Vutukuru, R. Babu (2016). Biosynthesis of nanoparticles from agro-waste: a sustainable approach. *Int. j. appl. Sci.* **1:** 85–92.

This page is intentionally left blank

Preparation of FeCoNiWMoCr High-Entropy Alloy Coatings Via Double Glow Plasma Surface Alloying Technology

Chong Liu, Chenglei Wang,, Chaojie Liang, Xin Li, Hu Chen, Zhujiang Tan,Jingya Zhang, Mei Huang & Yatao Zhu*

ABSTRACT

In this work, the FeCoNiWMoCr high-entropy alloy (HEA) gradient coatings metallurgically bonded to the substrate was successfully prepared using double glow plasma surface alloying technology (DGPSAT) under vacuum conditions. The HEA coating was then aged at 900 ℃ for 2 h. The microstructure, elemental distribution, mechanical properties, and tribology properties of the HEA coatings was systematically studied. The results showed that the coatings consists of the σ phase, hexagonal closed-packed phase, and face-centered cubic phase, with gradient distribution and uniform elemental composition. The properties of the HEA coating after aging treatment are greatly improved compared with those before aging treatment. The HEA coating after aging treatment exhibits good bonding strength with the substrate with a bonding force of 51.4 N. The microhardness is 802 HV, which is nearly 7.5 times higher than that of the substrate. The wear amount is 2×10^{-3} mm^3, almost 6.5 times higher than that of the substrate. The wear mechanism of the HEA coatings is abrasive wear with oxidation wear and adhesive wear. DGPSAT is a practical and useful method for preparing HEA coatings with high hardness and good wear resistance.

Keywords: HEA coating; DGPSAT; aging treatment; hardness; tribology properties.

Classification: FoR Code: 0913

Language: English

Great Britain Journals Press

LJP Copyright ID: 925621
Print ISSN: 2631-8490
Online ISSN: 2631-8504

London Journal of Research in Science: Natural and Formal

Volume 24 | Issue 4 | Compilation 1.0

Preparation of FeCoNiWMoCr High-Entropy Alloy Coatings Via Double Glow Plasma Surface Alloying Technology

Chong Liu[α], Chenglei Wang[σ, *], Chaojie Liang[ρ], Xin Li[ↀ], Hu Chen[¥], Zhujiang Tan [§], Jingya Zhang [χ], Mei Huang [ν] & Yatao Zhu[Θ]

ABSTRACT

In this work, the FeCoNiWMoCr high-entropy alloy (HEA) gradient coatings metallurgically bonded to the substrate was successfully prepared using double glow plasma surface alloying technology (DGPSAT) under vacuum conditions. The HEA coating was then aged at 900 ℃ for 2 h. The microstructure, elemental distribution, mechanical properties, and tribology properties of the HEA coatings was systematically studied. The results showed that the coatings consists of the σ phase, hexagonal closed-packed phase, and face-centered cubic phase, with gradient distribution and uniform elemental composition. The properties of the HEA coating after aging treatment are greatly improved compared with those before aging treatment. The HEA coating after aging treatment exhibits good bonding strength with the substrate with a bonding force of 51.4 N. The microhardness is 802 HV, which is nearly 7.5 times higher than that of the substrate. The wear amount is 2×10^{-3} mm^3, almost 6.5 times higher than that of the substrate. The wear mechanism of the HEA coatings is abrasive wear with oxidation wear and adhesive wear. DGPSAT is a practical and useful method for preparing HEA coatings with high hardness and good wear resistance.

Keywords: HEA coating; DGPSAT; aging treatment; hardness; tribology properties.

Author α σ ↀ ¥ § χ ν,Θ: School of Materials Science and Engineering, and Guangxi Key Laboratory of Information Materials, and Engineering Research Center of Electronic Information Materials and Devices, Ministry of Education, Guilin University of Electronic Technology, Guilin 541004, P.R. China.
ρ: School of Materials Science and Engineering, Central South University, Hunan, Changsha 410083, P.R. China.

I. INTRODUCTION

Fe and steel materials are important resources that are essential for national construction. They are characterized by high strength, good plasticity and toughness, and easy processing. However, their use has resulted in a large amount of economic losses due to the effects of fracture, corrosion, wear and deformation, and premature failure of materials. Material failure frequently starts on the surface [1-2], and modifying the surface of materials can considerably improve the performance and lifetime of materials, while simultaneously reducing the amount of alloys used and economic costs. Accordingly, material surface modification technologies are widely used at present [3-5].

Double glow plasma surface alloying technology (DGPSAT) is a surface modification technology that has been extensively used in aerospace, biomedicine, and many other fields in recent years and has attracted widespread attention [6-9]. This technology uses low- temperature plasma generated by glow or arc discharge to form alloy coatings on a material surface under vacuum conditions [10-11]. It can be used to prepare high-performance surface-modified coatings on the surface of workpieces with various

London Journal of Research in Science: Natural and Formal

complex shapes, and the coating is metallurgically bonded to the substrate, achieving controlled composition and good structural characteristics [12-13].

DGPSAT can allow the combination of Ni, W, Co, Mo, Cr, and other metal elements to infiltrate into steel materials and various metal surfaces to form alloy coatings with excellent properties. Huang et al. [14] prepared a Cr–Ni alloy coating on the surface of Q235 low-C steel via DGPSAT, and the highest protection efficiency of this alloy coating in 3.5% NaCl corrosion solution reached 99.23%, effectively improving the corrosion resistance of Q235. Qiu et al. [15] prepared a dense W–Mo layer on gear steel by using DGPSAT, and the specific wear rates of the coating were 11.2×10^{-5} $mm^3\cdot N^{-1}\cdot m^{-1}$ and 8.1×10^{-5} $mm^3\cdot N^{-1}\cdot m^{-1}$ at high temperature and room temperature, respectively, which was 19% of that of the substrate, significantly improving the wear resistance of the gear steel. Liu et al. [16] prepared a multi-alloy layer that contained Cr, Co, Mo, and Ni on the surface of pure Fe via DGPSAT and then aged this layer. The results showed that the alloy layer formed using the appropriate aging treatment exhibited better wear resistance than stainless steel. Numerous studies have shown that the metal elements Co, Ni, W, Mo, and Cr can form a good solid solution in steel materials and penetrate well into the substrate, improving the properties of the material surface. At present, however, surface-modified alloy coatings prepared via DGPSAT are mostly based on traditional alloys, and research on the preparation of new high-entropy alloy (HEA) coatings is minimal. In recent years, HEAs have become a research hotspot because of their better performance than traditional alloys. He et al. [17] prepared $(FeCoNiCr)_{94}Ti_2Al_4$ HEA with tensile strength up to 900 MPa and ductility up to 40% under aging treatment at 800 ℃. Tong et al. [18] prepared FeCoNiCrTi0.2 HEA and strengthened it with precipitation. Their results showed that the yield strength of the precipitation-strengthened HEA increased from 700 MPa to 860 MPa compared with that before strengthening. Varun et al. [19] studied the influence of different Cu contents on the magnetic properties of FeCoNiCrCu(x) HEA, and their results indicated that saturation magnetization intensity increased from 30.7 emu/g to 32.7 emu/g when Cu content was increased from 0 to 0.5. Numerous studies have demonstrated that the FeCoNiWMoCr system of HEAs has excellent mechanical properties, a wide range of applications, and good prospects for application. Compared with bulk HEA, HEA coatings have fewer organizational defects and can significantly improve the performance of the material surface, reduce the amount of alloy used, and decrease economic costs. HEA coating exhibits the same four effects of block HEA, but is better than block HEA in terms of performance [20-22].

Notably, in conventional DGPSAT, the surface alloy coatings prepared on steel materials are solid solution diffusion layers with the base element as the primary element. Simultaneously, solid solution diffusion layers cannot form HEA coatings with multiple dominant elements. Therefore, this study is designed to prepare a gradient HEA coating with a deposited layer + diffusion layer via DGPSAT.

In this study, we will break the idea of preparing traditional alloy-modified coatings on steel materials via DGPSAT and prepare a new gradient FeCoNiWMoCr HEA coating that is metallurgically bonded to the substrate via Co–Ni–W–Mo–Cr five-element co-diffusion on pure Fe surface and then perform aging treatment on it. The structure and elemental composition distribution of the HEA coating before and after aging treatment were analyzed. Bond strength, hardness, and wear resistance were systematically studied to provide a reference for the study of HEA coating preparation via DGPSAT.

II. EXPERIMENTAL METHOD

2.1 Preparation of FeCoNiWMoCr HEA coatings

In this work, the DGLT-15F multifunctional ion chemical heat treatment furnace was used to carry out Co-Ni-W-Mo-Cr five elements co-infiltration on the surface of pure iron under vacuum conditions to obtain FeCoNiWMoCr HEA coating. The base material is pure iron (purity >99.9%, size: 100 mm×15

mm×2 mm), the target material is pure Co, Ni, W, Mo, Cr bar target (purity ≥99.9%, size: ⌀4 mm×40 mm), the quantity ratio is Co: Ni: W: Mo: Cr = 35:65:11:11:65. The source level bar target is uniformly inserted into a hollow circular barrel (size: ⌀130 mm×180 mm) prepared from carbon steel, and the workpiece is suspended in the center of the circular barrel with a hook, and at the same time, the workpiece is connected to the source power supply through the hook, so as to achieve the effect of controlling the voltage of the source level and the voltage of the workpiece with a single power supply at the same time, and to form an equipotential effect between the source level and the workpiece. The process parameters of the test are as follows: pole spacing, 30mm, workpiece gas pressure 30Pa (at Ar atmosphere, purity ≥99.99%), voltage 850V, holding temperature 1300°C, holding time 2h. Holding at high temperatures, after the end of the holding time with the furnace slowly cooled down to room temperature, to obtain the HEA coatings (hereinafter referred to as C1), the use of high temperature chamber muffle furnaces SGM-M6/14 to the obtained HEA double glow plasma surface gold treatment. The SGM-M6/14 high-temperature chamber muffle furnace was used to carry out aging treatment on the obtained high-entropy alloy double-glow plasma surface treatment layer to obtain the HEA coating after aging treatment (hereinafter referred to as C2), and the aging treatment was carried out under the following process conditions: temperature of 900°C and time of 2h.

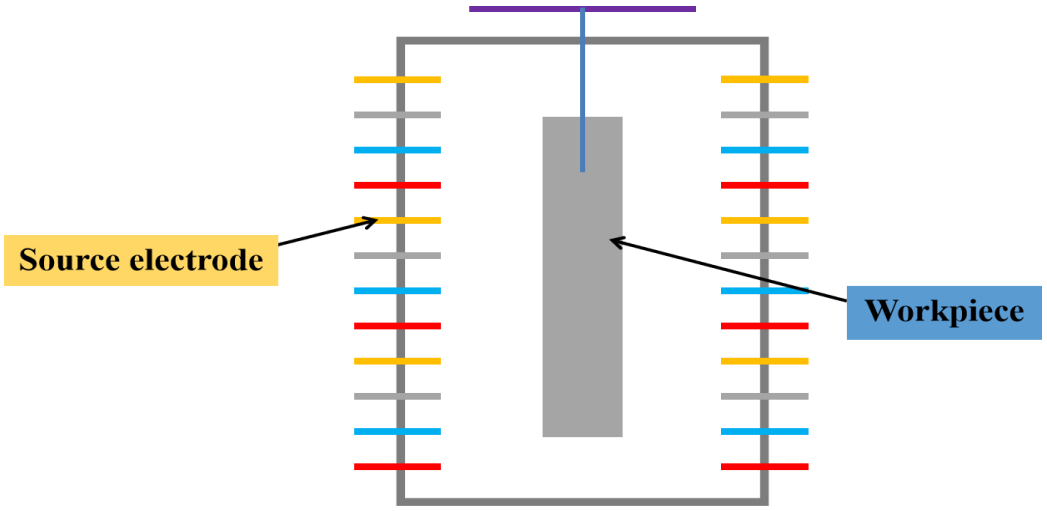

Fig.1: Schematic diagram of the spatial structure of the workpiece and source electrode.

2.2 Testing and analysis of FeCoNiWMoCr HEA coatings

The topography and composition of the surface and cross section of FeCoNiWMoCr HEA coatings were analyzed via scanning electron microscopy (SEM, JSM-IT800, JEOL Ltd.). The physical phase structure of the HEA coatings was analyzed via X-ray diffraction (XRD, Bruker D8 ADVANCE X). The hardness testing of the HEA coatings was performed using a microhardness tester (HV-1000, Shenzhen Haoxinda Instrument Co., Ltd.). The hardness values of the HEA coatings were measured at 10 locations and then averaged. A coating adhesion automatic scratch tester (WS-2005, Lanzhou Zhongke Kaihua Technology development Co., Ltd.) was utilized to test the coating bond strength of the HEA coatings by using acoustic emission signals, dynamic loading of up to 100 N, a loading rate of 100 N/min, and a scratch length of 5 mm. A 3D laser microscope (OLS4100 3D, OLYMPUS Ltd.) and a high-temperature reciprocating friction and wear tester (MGG-02, Jinan Yihua Tribology Testing Technology Co., Ltd.) were used to examine the friction and wear properties of the HEA coatings. The friction substrate was a 6 mm-diameter Si_3N_4 ball, the load was 600 g, the back-and-forth distance was 5 mm, the frequency was 300 r/min, and test time was 60 min.

III. RESULTS AND DISCUSSION

3.1 Surface appearance and element distribution of FeCoNiWMoCr HEA coatings

The surface morphology of FeCoNiWMoCr HEA coatings before and after aging treatment is shown in Fig. 2. It can be seen that surface of the HEA coatings is flat and dense, without apparent holes and cracks, and the surface denseness of C2 is better. The composition content (at.%) of the energy-dispersive X-ray spectroscopy (EDS) at the marker points of the HEA coatings and the calculated mixed entropy values are provided in Table 1. In accordance with the results, on the one hand, the composition of the HEA coatings is uniform without major differences and elemental contents are all between 5 at.% and 35 at.%. On the other hand, the molar mixed entropy of HEA with the isoatomic ratio alloy in solid-solution state is calculated as

$$\Delta S_{conf} = R \ln ln\, n \tag{1}$$

where ΔS_{conf} is the mixed entropy value ($J \cdot K^{-1} \cdot mol^{-1}$), R is the gas constant 8.314 ($J \cdot K^{-1} \cdot mol^{-1}$), and n is the component content (at.%).

The mixed entropy value calculated using Equation (1) is shown in Table 1. The mixed entropy value at each point is greater than the definition of HEA of 12.47 $J \cdot K^{-1} \cdot mol^{-1}$, and the FeCoNiWMoCr HEA coatings were successfully prepared on the surface of Fe. Interestingly, the quantity ratio of Mo and W is relatively low, but the content in the HEA coatings is relatively high. Meanwhile, the quantity ratio of Ni and Cr is relatively high, but the content in the HEA coatings is relatively low. This result is attributed to the use of the isotropic mode in this experimental procedure and the anti-sputtering influence on the substrate surface under vacuum conditions. Under the bombardment of 100 eV Ar^{+}, the sputtering parameters of the Fe, Co, Ni, W, Mo, and Cr elements [23] are provided in Table 2. The sputtering queues of the five elements are relatively low and exhibit good sputtering performance. Ni and Cr elements have higher sputtering rates. They are easily sputtered onto the substrate surface, but are also more susceptible to the back-sputtering effect and being back-sputtered out. Meanwhile, W and Mo have lower sputtering rates and are less affected by the back-sputtering effect. They are more easily deposited onto the surface of Fe. The atomic radii of the Cr and Ni do not differ considerably from the atomic radius of the substrate Fe, and thus, they are more easily diffused into the substrate. Meanwhile, the atomic radii of the Mo and W elements differ considerably from the atomic radius of the substrate Fe, and thus, they are relatively difficult to diffuse into the interior of the substrate.

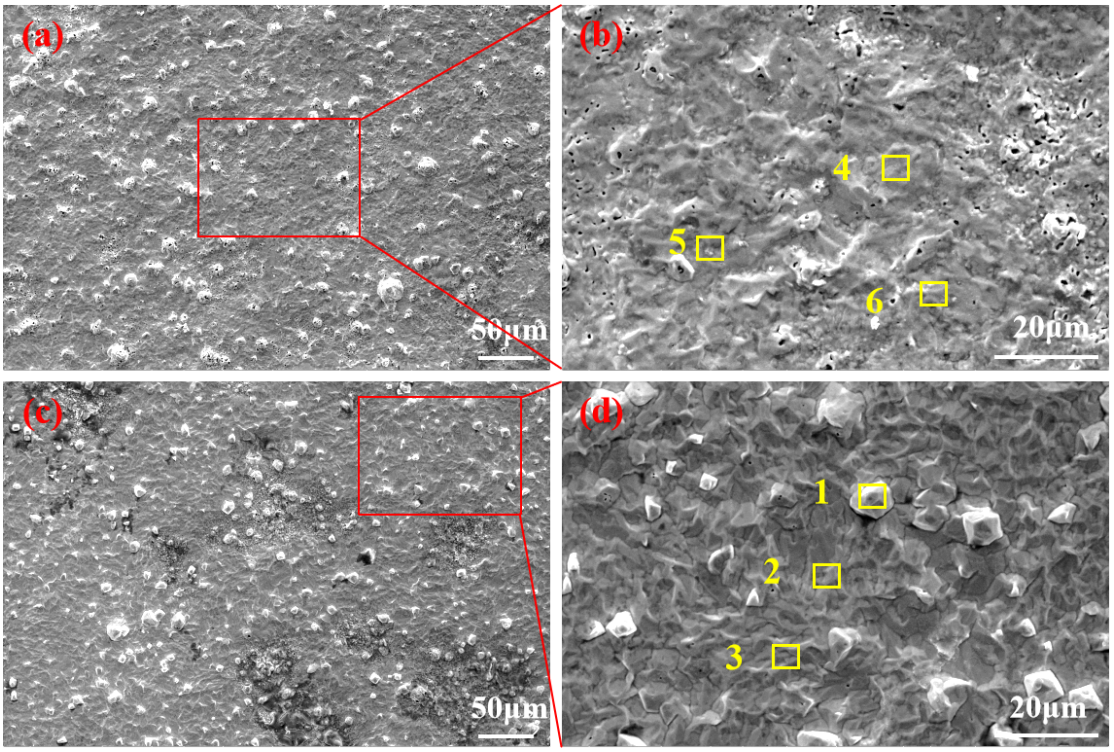

Fig.2: Surface morphology of FeCoNiWMoCr HEA coatings before and after aging treatment, (a)C1, (b)C2, (c) Partial magnification of (a), (d) Partial magnification of (b).

Table 1: EDS at the marker points of FeCoNiWMoCr HEA coatings before and after aging treatment and the calculated mixed entropy values.

Elements	Fe	Co	Ni	W	Mo	Cr	$\triangle S_{mix}$
1	20.68	9.44	6.97	33.79	20.64	8.48	13.55
2	24.64	9.35	7.34	32.19	18.2	8.29	13.71
3	22.8	8.78	7.22	32	21.19	8.05	13.64
average	22.71	9.19	7.18	32.66	20.01	8.27	13.63
4	21.72	9.26	7.05	32.56	19.60	8.35	13.56
5	23.65	8.98	7.37	32.08	20.76	8.32	13.70
6	24.39	9.15	7.19	32.38	21.03	8.15	13.71
average	23.25	9.13	7.20	32.34	20.46	8.27	13.66

Table 2: Sputtering threshold and sputtering rate of the Fe, Co, Ni, W, Mo, and Cr element under 100 eV Ar+ bombardment.

Elements	Fe	Co	Ni	W	Mo	Cr
Sputtering threshold/eV	20	25	21	33	24	22
Sputtering rate	0.2	0.15	0.28	0.068	0.13	0.3

3.2 Cross-section appearance and element distribution of FeCoNiWMoCr HEA coatings

The cross-sectional morphology of FeCoNiWMoCr HEA coatings before and after aging treatment is shown in Fig. 3(a) and Fig. 3(b). Evidently, the deposition layer of the specimens before and after the

aging treatment is continuous and uniform. The thickness is approximately the same, i.e., all the specimens are 4–6 μm. The cross section of C2 is more dense. The source structure design used in this subject fully utilizes the hollow cathode effect between the targets and the tip discharge effect of the long strip-shaped target, considerably enhancing the sputtering volume of the source target elements. Both designs ensure sufficient sputtering deposition volume for easier deposited layer formation, while the aging treatment promotes further diffusion of each element, resulting in a denser coating.

The cross-sectional EDS face scan pattern of FeCoNiWMoCr HEA coatings before and after aging treatment is shown in Fig. 3(c) and Fig. 3(d). The EDS line scanning of the cross section of FeCoNiWMoCr HEA coatings before and after aging treatment is shown in Fig. 3(e) and Fig. 3(f). The contents of Co, Ni, and Cr are relatively high in the diffusion layer and relatively low in the deposit layer. Meanwhile, the opposite is true for W and Mo. The contents of W and Mo are relatively high in the deposit layer and relatively low in the diffusion layer. The content difference of each element in the sediment layer of C1 is large, and the content difference of each element in the diffusion layer is small, and the whole is not uniform. All the elements in the deposition layer and diffusion layer of C2 reach the state of uniform distribution, with an overall gradient distribution.

The results are because, each element has a different atomic radius, and its difficulty level in entering the diffusion layer is also different. The atomic radius of Fe, Co, Ni, W, Mo, and Cr [24] are provided in Table 3. The atomic radii of Co, Ni and Cr are not very different from the atomic radius of Fe, and thus, the resistance to diffusion into the substrate of these elements is relatively small. Meanwhile, the atomic radius of W and Mo are larger, and their resistance to diffusion into the substrate is relatively large. Therefore, these elements are easier to enrich in the deposition layer. The results are consistent with the results of Table 1. The aging treatment promotes the rediffusion of each element in the HEA coating, such that each element in the diffusion layer further diffuses into the substrate, increasing element content in the substrate. Consequently, all the elements reach a state of uniform distribution and gradient distribution.

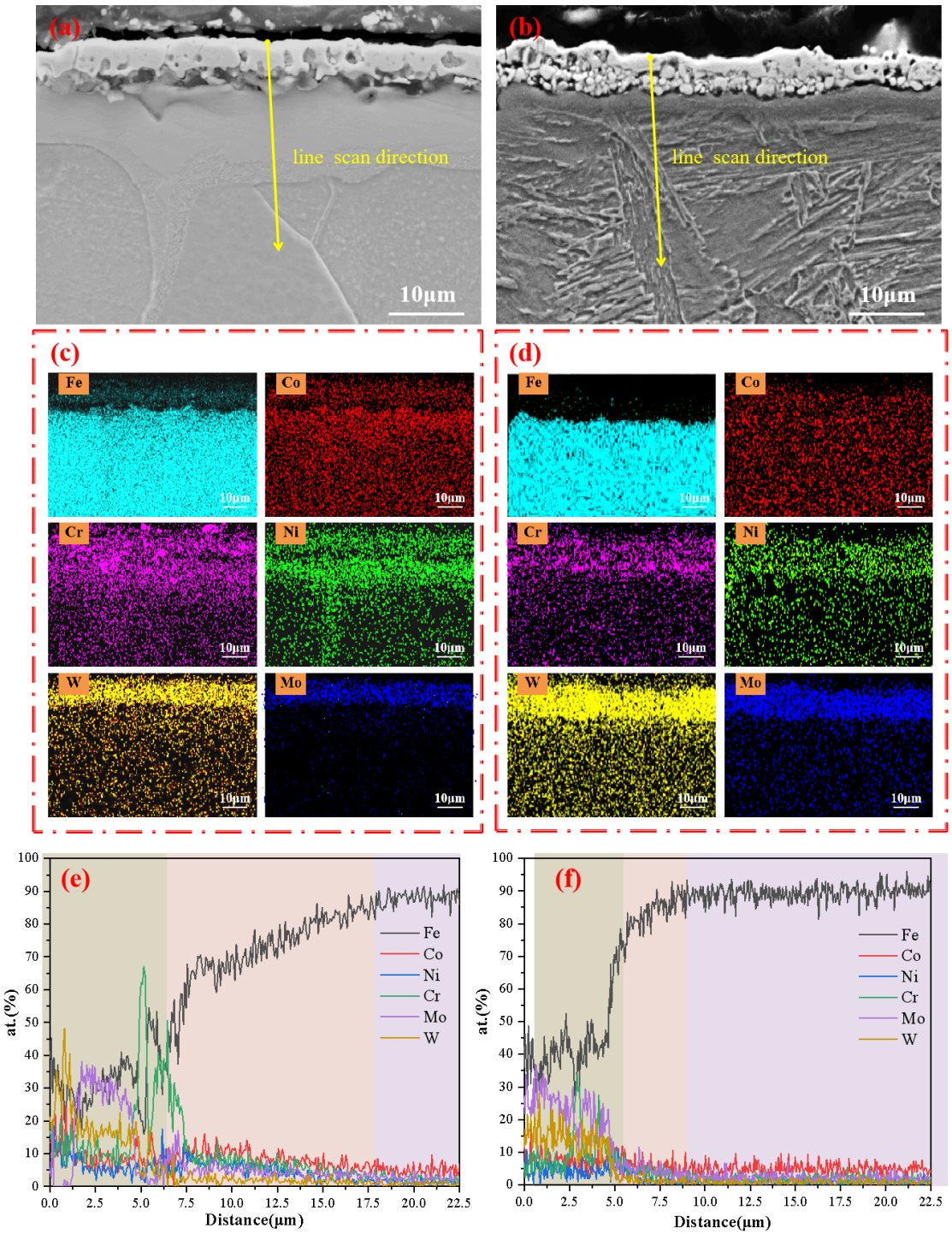

Fig.3: Cross-sectional morphology and EDS of FeCoNiWMoCr HEA coatings before and after aging treatment, (a) Cross-sectional morphology of C1, (b) Cross-sectional morphology of C2, (c) EDS face scan pattern of C1, (d) EDS face scan pattern of C2, (e) EDS Line scanning of C1, (f) EDS Line scanning of C2.

Table 3: Atomic radius of Fe, Cr, Ni, W, Mo, and Co element (Å).

Elements	Fe	Co	Ni	W	Mo	Cr
Atomic radius	1.27	1.27	1.24	1.41	1.40	1.26

3.3 Phase of FeCoNiWMoCr HEA coatings

The XRD of FeCoNiWMoCr HEA coatings before and after aging treatment is shown in Fig. 4. The coatings consist of the σ, face-centered cubic (fcc), and hexagonal closed-packed (hcp) phases. The difference between the atomic radii of Co and W in the HEA coatings is large; therefore, Mo and Co are more easily enriched, forming the Co_7W_6 phase (σ phase). The phase structure before and after aging treatment has not changed considerably.

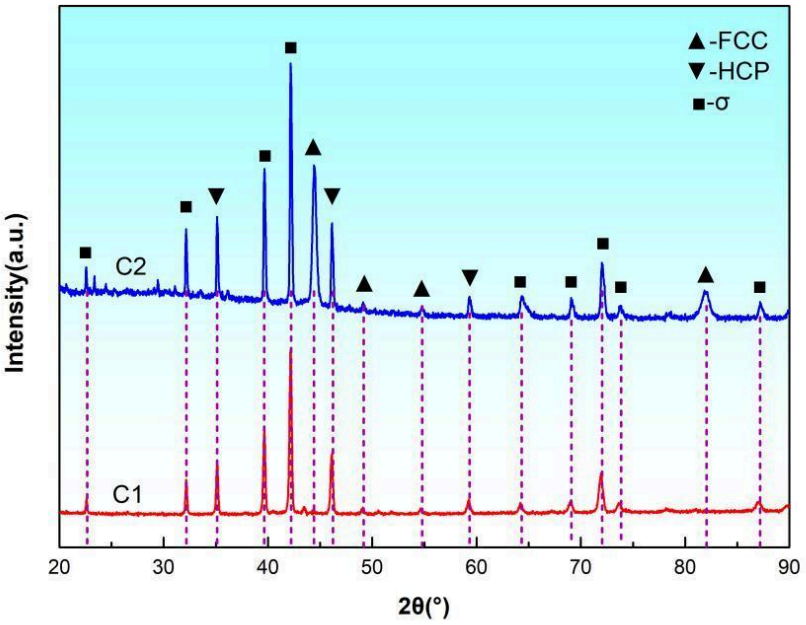

Fig.4: XRD of FeCoNiWMoCr HEA coatings before and after aging treatment.

3.4 Bonding strength of FeCoNiWMoCr HEA coatings

The acoustic emission curves and scratch morphology of FeCoNiWMoCr HEA coatings before and after aging treatment are shown in Fig. 5. It can be seen that the binding force of C1 is 42.5N and that of C2 is 51.4N. The surface morphology of the corresponding scratches shows no large area of spalling near the scratches, indicating that FeCoNiWMoCr HEA coatings achieve good toughness and its bonding with the substrate is good.

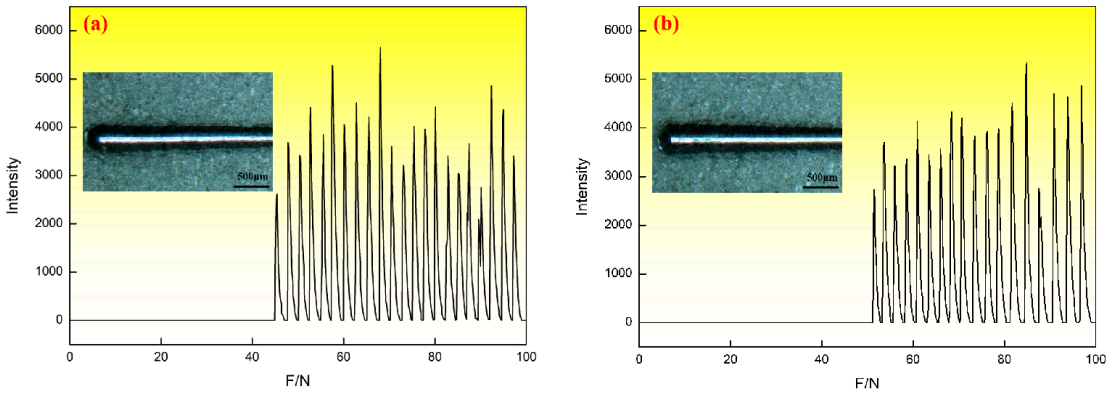

Fig.5: Acoustic emission curves and scratch morphology of FeCoNiWMoCr HEA coatings, (a) C1, (b) C2.

3.5 Microhardness and friction wear properties of FeCoNiWMoCr HEA coatings

The microhardness and wear properties of substrate Fe and FeCoNiWMoCr HEA coatings before and after aging treatment are shown in Fig. 6. From Fig. 6(b), the microhardness of FeCoNiWMoCr HEA coatings is significantly increased compared with that of substrate Fe. The microhardness of C2 is even higher, increasing from 108 HV of the substrate Fe to 802 HV, i.e., an increase of nearly 7.5 times. Surprisely, the wear of FeCoNiWMoCr HEA coatings is significantly lower compared with that of the substrate Fe, where the wear of C2 is even smaller, i.e., 2×10^{-3} mm^3, which is nearly 6.5 times higher than the 12.93×10^{-3} mm^3 of the substrate. The microhardness of FeCoNiWMoCr HEA coatings is positively correlated with friction wear performance. That is, the higher the microhardness, the better the wear resistance, the higher the microhardness of C2, the better its wear resistance.

From Fig. 6(a), it is clearly shows that the friction coefficients of substrate Fe and FeCoNiWMoCr HEA coatings enter a stable phase after a short break-in phase under friction conditions at room temperature. In the beginning of the friction sub-contact with the surface of the HEA coatings, the friction curve fluctuates more and the friction coefficient becomes unstable. As the friction continues, the friction coefficient gradually stabilizes. In the stabilization phase, the friction curve of C2 fluctuates with the gentlest amplitude. From Fig. 6(c), the wear scar surface of FeCoNiWMoCr HEA coatings is relatively flat, without large grooves, and the protrusion of the edge of the wear scar is not serious. The width and depth of the wear scar of FeCoNiWMoCr HEA coatings before and after aging treatment are clearly smaller than those of the substrate Fe, and the HEA coatings exhibit good abrasion resistance. The wear scar depth of C2 is the shallowest and demonstrates the best wear resistance.

Aging treatment improves the wear resistance of the HEA coating, because many hard and large particles are present on the surface of C1 (as shown in Fig. 1). The phenomenon of local stress concentration is more likely to occur during its friction process, such that the hard and large particles on the surface are destroyed to form hard abrasive chips that will cut the HEA coating. After aging treatment, relatively few large hard particles are present on the surface of the HEA coating. The surface is flatter, roughness is lower, and the cutting effect on the HEA coating is reduced after the formation of abrasive chips. Consequently, wear resistance is better.

The surface wear morphology of substrate Fe and FeCoNiWMoCr HEA coatings before and after aging treatment are shown in Fig. 7. The wear surface of the substrate Fe is distributed with a large amount of parallel furrows and abrasive chips, accompanied by adhesion flaking and delamination. In addition, large number of furrows and flaking pits are formed. The wear surface of FeCoNiWMoCr HEA coatings has a small amount of plow grooves and small particles of abrasive chips accompanied by shallow spalling. Its wear surface does not form evident deep grooves and spalling pits with good wear resistance. After aging treatment, the FeCoNiWMoCr HEA coating has less wear surface furrowing and more adhesive spalling.

The EDS face scans of the surface wear morphology of substrate Fe and FeCoNiWMoCr HEA coatings before and after aging treatment are shown in Fig. 8. The substrate and the HEA coatings in the friction and wear process with the friction sub exhibit different degrees of oxidation due to the heat generated during friction. Consequently, the surface is oxidized, generating a dense oxide film, which acts as a lubricant and protects the surface of the substrate and the HEA coatings, slowing down the wear on the grinding ball and improving wear resistance. The O element is the most enriched in the surface wear morphology of C2, and the formed oxide film is the thickest and exhibits the best wear resistance. In addition, the cooling method of C1 involves cooling down to room temperature with a furnace. By contrast, the cooling method of C2 is water cooling, which is equivalent to quenching treatment, improving its hardness and wear resistance. The friction sub uses Si_3N_4, and thus, the enrichment of Si elements indicates the presence of adhesive wear. The wear and tear mechanisms of substrate Fe and FeCoNiWMoCr HEA coatings is abrasive wear with oxidation wear and adhesive wear.

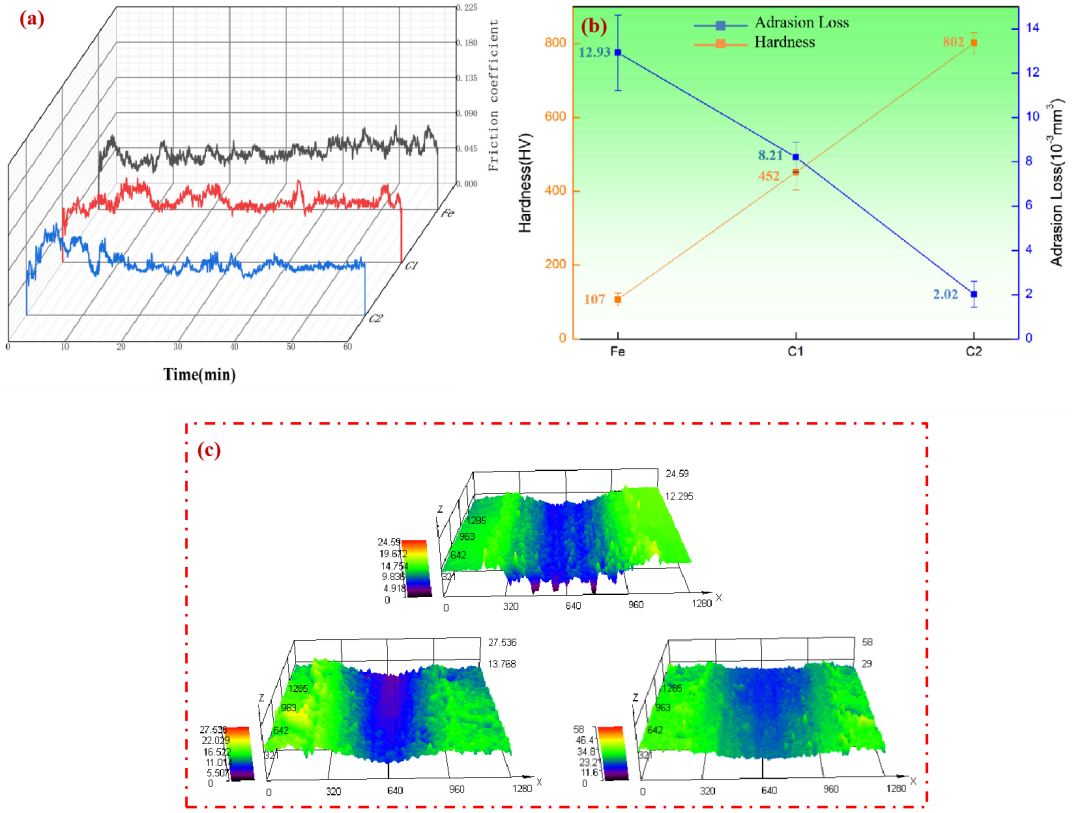

Fig.6: Microhardness and wear properties of substrate Fe and FeCoNiWMoCr HEA coatings before and after aging treatment, (a) Friction coefficient, (b) Microhardness and amount of wear, (c) Measurement of three-dimensional contour.

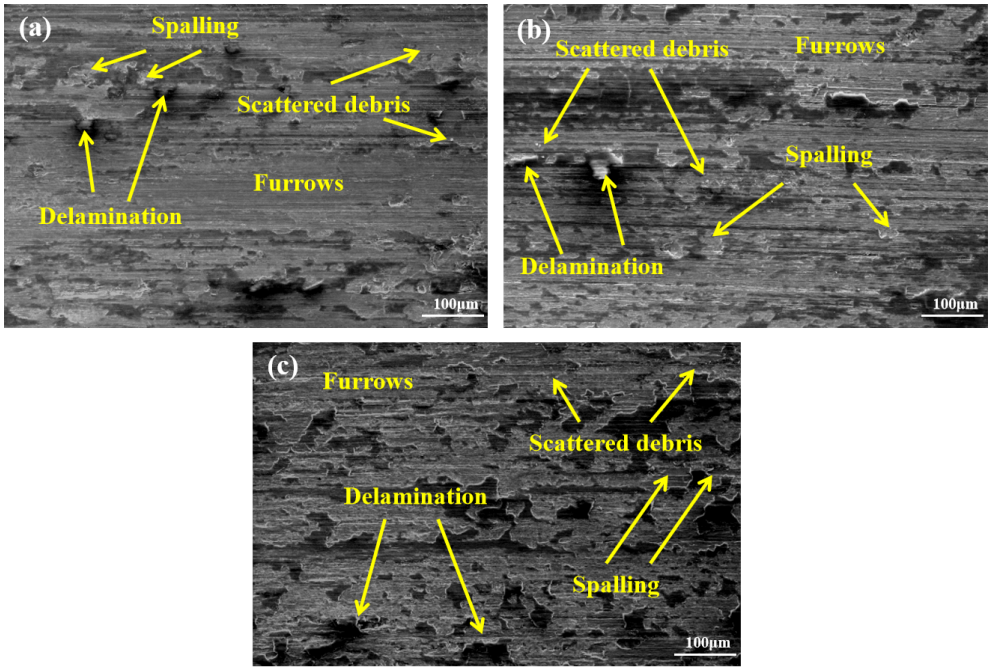

Fig.7: Surface wear morphology of substrate Fe and FeCoNiWMoCr HEA coatings before and after aging treatment, (a) C1, (b) C2, (c) Fe.

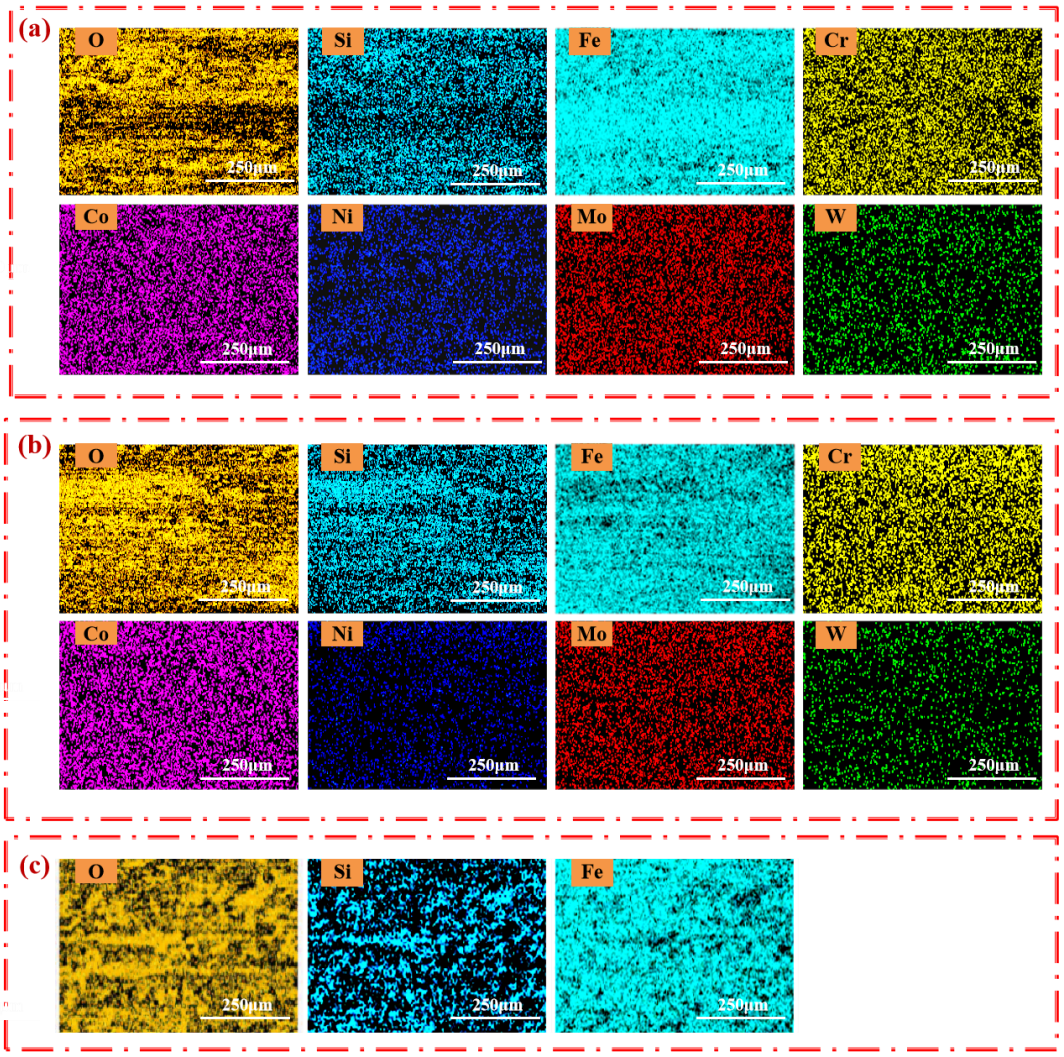

Fig.8: EDS face scans of the surface wear morphology of substrate Fe and FeCoNiWMoCr HEA coatings before and after aging treatment, (a) C1, (b) C2, (c) Fe.

IV. CONCLUSIONS

In this study, a gradient FeCoNiWMoCr HEA coating was successfully prepared on pure Fe substrate via DGPSAT, and then the coating were subjected to aging treatment. The organization, elemental composition, bond strength, microhardness, and wear properties of FeCoNiWMoCr HEA coatings before and after aging treatment were determined. The major findings are as follows.

1. The surface of FeCoNiWMoCr HEA coatings is flat and dense, and the cross section is continuous and uniform. The best quality of the HEA coatings is observed after aging treatment, forming a composite reinforced layer of deposited layer + diffusion layer. FeCoNiWMoCr HEA coatings consist of the σ, fcc, and hcp phases.
2. The bonding strength of FeCoNiWMoCr HEA coatings and the substrate is good, reaching 51.4 N after aging treatment. FeCoNiWMoCr HEA coatings effectively improve hardness, with the microhardness of the HEA coating after aging treatment reaching up to 802 HV, which is nearly 7.5 times higher than the 108 HV of the substrate.
3. FeCoNiWMoCr HEA coatings effectively improve wear resistance. The abrasion resistance of the HEA coating after aging treatment is the best, and its wear amount can be as low as 2×10^{-3} mm^3, which is nearly 6.5 times higher than the $12.93\times10^{-3}mm^3$ of the substrate. The wear and tear

mechanism of FeCoNiWMoCr HEA coatings is abrasive wear with oxidation wear and adhesive wear.

ACKNOWLEDGMENTS

This work was supported by the National Natural Science Foundation of China (52161011); the Natural Science Foundation of Guangxi Province (2023GXNSFDA026046); the Central Guiding Local Science and Technology Development Fund Projects (ZY23055005); the Scientific Research and Technology Development Program of Guilin (20220110-3, 2020010903); the Guangxi Key Laboratory of Information Materials (221024-Z, 221012-K); the Engineering Research Center of Electronic Information Materials and Devices, Ministry of Education (EIMD-AB202009); the Major Research Plan of the National Natural Science Foundation of China (92166112); and Innovation Project of GUET Graduate Education (2020YCXS118, and 2022YCXS200) for the financial support given to this work.

Data Availability

The processed data required to reproduce these findings cannot be shared at this time as the data also forms part of an ongoing study.

REFERENCES

1. Balraj Singh, Gurpreet Singh, Buta Singh Sidhu, In vitro investigation of Nb-Ta alloy coating deposited on CoCr alloy for biomedical implants, Surf. Coat. Technol 377 (2019) 124932.
2. Yan Xu, Yinfeng Wang, Yi Xu, Mingyou Li, Zheng Hu, Microscopic characteristics and properties of Fe-Based amorphous alloy compound reinforced WC-Co-Based coating via plasma spray welding, Processes 9 (2021) 6.
3. Ye Tian, Yifu Shen, Congyang Lu, Xiaomei Feng, Microstructures and oxidation behavior of Al-CrMnFeCoMoW composite coatings on Ti-6Al-4V alloy substrate via high-energy mechanical alloying method, J. Alloys Compd. 779 (2019) 456-465.
4. Chau Josepg, Lik Hang, Hou, Yen-Yu, Pan, Alfard I-Tsung, Yang, Chih-Chao, PARTICUL SCI TECHNOL 10 (2016) 209-213.
5. Chenglei Wang, Yuan Gao, Rong Wang, Deqiang Wei, Miao Cai, Yaokun Fu, Microstructure of laser-clad Ni60 cladding layers added with different amounts of rare-earth oxides on 6063 Al alloys, J. Alloys Compd. 740 (2018) 1099-1107.
6. Feng Ding, Pingze Zhang, Dongbo Wei, Xiaohu Chen, Shiyuan Wang, Zhangzhong Wang, Yimin Zhu, Isothermal oxidation behavior of Zr-Y coating on γ-TiAl by double glow plasma surface metal alloying Technique, Coatings 8 (2018) 361.
7. Naiming Lin, Junwen Guo, RuiQiang Huang, Jiaojuan Zou, Bin Tang, Double glow plasma surface alloying antibacterial silver coating on pure titanium, Surf. Rev. Lett 21 (2014) 1450032.
8. Naiming Lin, Luxia Zhang, Jiaojuan Zou, Qiang Liu, Shuo Yuan, Lulu Zhao, Yuan Yu, Zhiqi Liu, Qunfeng Zeng, Xiaoping Liu, Zhihua Wang, Bin Tang, Yuchen Wu, A combined surface treatment of surface texturing-double glow plasma surface titanizing on AISI 316 stainless steel to combat surface damage: Comparative appraisals of corrosion resistance and wear resistance, Appl. Surf. Sci 493 (2019) 747-765.
9. Dongbo Wei, Pingze Zhang, Zhengyun Yao, Jintang Zhou, Xiangfei Wei, Xiaohu Chen, Double glow plasma chromizing of Ti6Al4V alloys: Impact of working time, substrate–target distance, argon pressure and surface temperature of substrate, Vacuum 121 (2015) 81-87.
10. Zheng Ding, Qiang Miao, Wenping Liang, Zhengang Yang, Shiwei Zuo, Performance enhancement in borocarburized low-carbon steel by double glow plasma surface alloying, Coatings 10 (2020) 1205.

11. Shuo Yuan, Naiming Lin, Jiaojuan Zou, Zhiqi Liu, Zhenxia Wang, Linhai Tian, Lin Qin, Hongxia Zhang, Zhihua Wang, Bin Tang, Yucheng Wu, Effect of laser surface texturing (LST) on tribological behavior of double glow plasma surface zirconizing coating on Ti6Al4V alloy, Surf. Coat. Technol 368 (2019) 97-109.
12. Shuo Yuan, Naiming Lin, Qunfeng Zeng, Hongxia Zhang, Xiaoping Liu, Zhihua Wang, Yucheng Wu, Recent developments in research of double glow plasma surface alloying technology: a brief review, J MATER RES TECHNOL 9 (2020) 6859-6882.
13. Xixi Luo, Jing Cao, Guanghui Meng, Fangli Yu, Qiong Jiang, Pingze Zhang, Hu Xie, Double glow plasma surface metallurgy technology fabricated Fe-Al-Cr coatings with excellent corrosion resistance, Coatings 10 (2020) 575.
14. Jun Huang, Siyu Yang, Shiyu Cui, Jilin Xu, Jianping Zhang, Junming Luo, Influence of the electrode distance on microstructure and corrosion resistance of Ni-Cr alloyed layers deposited by double glow plasma surface metallurgy, J WUHAN UNIV TECHNOL 37 (2022) 1204-1215.
15. Zhongkai Qiu, Pingze Zhang, Dongbo Wei, Xiangfe Wei, Xiaohu Chen, A study on tribological behavior of double-glow plasma surface alloying W-Mo coating on gear steel, Surf. Coat. Technol 278 (2015) 92-98.
16. Xiaoping Liu, Yuan Gao, Zhonghou Li, Zhong Xu, Wenhuai Tian, Bin Tang, Cr–Ni–Mo–Co surface alloying layer formed by plasma surface alloying in pure iron, Appl. Surf. Sci 252 (2006) 3894-3902.
17. J. Y. He, H. Wang, Y. Wu, X. J. Liu, H. H. Mao, T. G. Nieh, Z. P. Lu, Precipitation behavior and its effects on tensile properties of FeCoNiCr high-entropy alloys, Intermetallics 79 (2016) 41-52.
18. Y. Tong, K. Jin, H. Bei, J. Y. P. Ko, D. C. Pagan, Y. Zhang, F. X. Zhang, Local lattice distortion in NiCoCr, FeCoNiCr and FeCoNiCrMn concentrated alloys investigated by synchrotron X-ray diffraction, MATER DESIGN 155 (2018) 1-7.
19. Varun Chaudhary, Visha Soni, Bharat Gwalani, R. V. Ramanujan, Rajarshi Banerjee, Influence of non-magnetic Cu on enhancing the low temperature magnetic properties and curie temperature of FeCoNiCrCu(x) high entropy alloys, SCRIPTA MATER 182 (2020) 99-103.
20. Linzhi Que, Guofu Lian, Mingpu Yao, Hua Lu, Microstructure and properties of AlCoCrFeNiTi high-entropy alloy coatings prepared by laser cladding based on the response surface methodology, Int. J. Adv. Manuf. Technol. 123 (2022) 1307-1321.
21. Y. K. Mu, Y. D. Jia, L. Xu, Y. F. Jia, X. H. Tan, J. Yi, G. Wang, P. K. Liaw, Nano oxides reinforced high-entropy alloy coatings synthesized by atmospheric plasma spraying, Mater. Res. Lett. 7 (2019) 312-319.
22. Michael C. Gao, Jien-Wei Yeh, Peter K. Liaw, Yong Zhang, High-entropy alloys: Fundamentals and applications, 2016.
23. Z. Xu. Plasma Surface Metallurgy, Science Press, 2007.
24. A. Takeuchi, A. Inoue, Classification of bulk metallic glasses by atomic size difference, heat of mixing and period of constituent elements and its application to characterization of the main alloying element, Mater Trans. 46 (2005) 2817-2829.

This page is intentionally left blank

Chemical Diversity of Propolis from Meliponinae: An Ancestral Treasure to be Preserved

Ariane Storch Portal, Caio Mauricio Mendes de Cordova

University of Blumenau

ABSTRACT

Propolis is a mixture made by bees consisting of plant resins and metabolites, salivary enzymes and wax. Some species of bees add soil to this mixture forming geopropolis. This material is used in the defense of the hive as a physical barrier and antimicrobial agent, ensuring the health of the colony. Propolis has been extensively studied and several chemical constituents have been identified, mainly flavonoids, terpenes and phenolics. With the emerging microbial resistance to antibiotics, the interest in the search for active compounds, mainly secondary metabolites of plants, has been increasing significantly. In this paper, we describe the characteristics of the main species of native stingless bees found in South America, especially in Brazil, the ancestral use of propolis produced by them, its chemical composition and its potential for the development of new therapeutic compounds, along with the challenges that the survival of bees face.

Keywords: NA

Classification: FoR Code: 0607

Language: English

Great Britain Journals Press

LJP Copyright ID: 925621
Print ISSN: 2631-8490
Online ISSN: 2631-8504

London Journal of Research in Science: Natural and Formal

Volume 24 | Issue 4 | Compilation 1.0

Chemical Diversity of Propolis from Meliponinae: An Ancestral Treasure to be Preserved

Ariane Storch Portal, Caio Mauricio Mendes de Cordova

ABSTRACT

Propolis is a mixture made by bees consisting of plant resins and metabolites, salivary enzymes and wax. Some species of bees add soil to this mixture forming geopropolis. This material is used in the defense of the hive as a physical barrier and antimicrobial agent, ensuring the health of the colony. Propolis has been extensively studied and several chemical constituents have been identified, mainly flavonoids, terpenes and phenolics. With the emerging microbial resistance to antibiotics, the interest in the search for active compounds, mainly secondary metabolites of plants, has been increasing significantly. In this paper, we describe the characteristics of the main species of native stingless bees found in South America, especially in Brazil, the ancestral use of propolis produced by them, its chemical composition and its potential for the development of new therapeutic compounds, along with the challenges that the survival of bees face.

Author: University of Blumenau, SC, Brazil, Department of Pharmaceutical Sciences, Rua São Paulo 2171, Campus III, CEP 89030-000.

I. INTRODUCTION

Since immemorial times, the therapeutic resources used by humanity came from nature, notably from plants, animals and minerals. The search for pain relief and cure of illnesses through the ingestion of herbs may have been one of the first ways of using natural products (VIEGAS JUNIOR; BOLZANI; BARREIRO, 2006). Plants produce a huge variety of compounds, commonly related to defense mechanisms, including antimicrobial activity. This great diversity of phytochemicals is due, in part, to the evolutionary need to struggle with microorganisms, insects, nematodes and other plants. This defense system effectively prevents infections caused by most plant pathogens (SIMÕES; BENNETT; ROSE, 2009).

Propolis is one of the natural products that has been used by mankind for various therapeutic purposes. It consists of a mixture of resin from plants collected by bees with the wax and saliva of these insects (LAVINAS et al., 2019). Some species of stingless bees mix this resinous material with the soil, forming the so-called geopropolis (LIBERIO et al., 2011). It has great importance for the health of the colony, as it is used in the construction of nests and to seal the hive, preserving the inside temperature and preventing the entry of unwanted visitors. Propolis also acts as a chemical defense against microorganisms, due to its antimicrobial properties (LAVINAS et al., 2019).

In its constitution it can be found about 50% vegetable resins, 30% beeswax, 10% essential oils, 5% pollen and 5% wood and earth waste (MENEZES; 2005). However, the yield of the volatile fraction has usually been reported in the order of 1% (BANKOVA; POPOVA; TRUSHEVA, 2014). The volatile compounds are responsible for the characteristic aroma of propolis and have significant biological activity. Several compounds were identified in their composition, mainly mono and sesquiterpenoids (BANKOVA; CASTRO; MARCUCCI, 2000). Studies have demonstrated the importance of these

London Journal of Research in Science: Natural and Formal

compounds against pathogenic microorganisms, such as Gram-positive and negative bacteria of medical importance (SIMIONATTO et al., 2012; BANKOVA; POPOVA; TRUSHEVA, 2014).

II. IMPORTANCE OF THE PROSPECTION FOR NEW MEDICINES AND THE ROLE OF PROPOLIS

Newman and Cragg (2020) highlighted, in an extensive review, the importance of natural products and structures derived from or related to natural products as a source for new molecules. In the period between January 1981 and September 2019, 126 antibacterial molecules were approved (disregarding prophylactic agents). Of the 126, about 48% (78) are derived from natural products or unaltered natural products. However, since the advent of antibiotics in the 1950s, virtually no antimicrobials have been developed from plant sources. The main natural sources of these agents were bacteria and fungi. With the emergence of resistance to antimicrobials, interest in the search for other sources, mainly secondary metabolites from plants, has increased significantly (SIMÕES; BENNETT; ROSE, 2009; ABREU; MCBAIN; SIMÕES, 2012).

To produce propolis, bees collect the plant resins by selecting the best compounds capable of protecting the nest and ensuring its survival. Considering this natural pre-selection based on the knowledge of these insects, the composition of propolis and its biological activities have aroused the interest of several researchers (BANKOVA et al., 1999a). Despite the great diversity of the bees native to Brazil, most of the studies investigating the composition and activities of propolis are carried out with samples produced by exotic bee species introduced in the country. Studies on its volatile fraction are even more scarce. Knowing that the chemical composition of propolis is quite variable and is related to the species of bee that produces it, seasonality and its geographical location, studies with propolis and geopropolis of native stingless bees provide potential unprecedented results and the discovery of compounds with antimicrobial activity (OLIVEIRA et al., 2009).

2.1 Bee species

Since ancient times, bees have aroused curiosity and human interest. In Greece, they were seen as priestly and chaste animals. The local currency had the image of a bee, symbolizing wealth. The Romans considered them as a representation of territorial defense (SFORCIN et al., 2017). In Christianity they were related to various qualities, above all hope, due to their tireless work, and resurrection, for disappearing in winter and resurfacing in spring (LEXIKON, 1997).

Bees have developed behavioral characteristics, such as the distinction of colors and aromas, that aid in the search for nectar and pollen: their main food sources. These characteristics also benefit the plants, because during foraging, incidentally, they transfer the pollen of the anther of one flower to the stigma of another, performing pollination (TRIPLEHORN; Johnson, 2005).

The order *Hymenoptera* is one of the most diverse groups of species in the class *Insecta*. *Hymenoptera* presents a wide variety of complex habits and behaviors, culminating in the social organization of wasps, ants and the most important pollinating agents: bees (TRIPLEHORN; Johnson, 2005). The bees belong to the superfamily *Apoidea*, which has several families, among them the *Apidae*, which has more advanced social habits and is divided into four subfamilies: the *Apinae* (bees of the genus *Apis*, with about 11 species), the *Meliponinae* (stingless bees, with hundreds of species), the *Bombinae* (bumblebees, with about 250 species) and the *Euglossinae* (orchid bee, with about 175 species) (NOGUEIRA-NETO, 1997).

The subfamily *Meliponinae* is believed to have been the oldest to branch off from less social ancestors and develop high social behavior. A fossil of a female stingless bee about 80 million years old has been

found wrapped in amber. This bee is considered the oldest known species of social bee and has characteristics similar to living species (CRANE, 1999).

2.2 Meliponinae subfamily

The first written records about the meliponines arrived in Europe in the sixteenth century and were made by Spanish and German explorers in Central and South America. These reports and later archaeological studies, particularly in the Mesoamerican region, contributed to the discovery of important data on the traditional search for honey and on the management of meliponines, which was already well structured at least 300 BC. More advanced research occurred only in the nineteenth century, almost two centuries after the beginning of scientific research on bees (HRNCIR et al., 2016).

Meliponines are also known as stingless bees (SB) or indigenous bees because they are traditionally bred by indigenous populations (SILVEIRA et al., 2002). More than 600 species have been described and are found in South America, Central America, southern North America, Africa, Southeast Asia and Northern Oceania. In Brazil more than 200 species can be found, distributed in 29 genera, being *Plebeia, Trigona, Melipona, Scaptotrigona* and *Trigonisca* the ones with the largest number of known species (LAVINAS et al., 2019).

Brazil is home to the largest diversity of SBs in the world. Native species are distributed throughout the Brazilian territory, mainly in the Amazon region. The warm climate and the abundant flora in species that can provide nectar, pollen and resin are favorable conditions for the existence of these bees (VENTURIERI, 2008). They are especially sensitive to low temperatures and depend on the structure of their nests for the thermoregulation of the hive (KLEINERT et al., 2009).

The nests of the meliponines are considered the most elaborate among bees. Some species nest in exposed places, such as on branches, but more often the nests are found in pre-existing cavities in tree trunks or anthills and abandoned termite mounds. They are protected by one or several layers of a casing composed of wax and resin, which assists in maintaining the temperature. The colony is delimited by the bitumen, which consists of a mixture of wax, resin and clay (NOGUEIRA-NETO, 1997; MICHENER, 2000). The upper layer of bitumen is usually compact to avoid infiltration and the lower one is riddled, allowing the flow of water (VILLAS-BÔAS, 2012).

The entrance of the nest presents particular characteristics for each species and can be constituted of geopropolis, clay, cerumen or pure wax (VILLAS-BÔAS, 2018). Some species build quite narrow entrances, which are guarded by a single bee, others build larger entrances that allow the circulation of multiple guards (FONSECA et al., 2017). Camouflage and occlusion of the entrance are strategies that can also be undertaken to prevent invaders (SFORCIN et al., 2017).

Female bees have a well-developed ovipositor (egg-laying organ), which can be modified to form a stinger, which is used as a defense mechanism (TRIPLEHORN; Johnson, 2005). However, female meliponines have a stunted stinger and are therefore unable to use it, and so are known as stingless bees (SFORCIN et al., 2017).

They are considered more docile; however, they are not helpless bees. When they feel threatened by large invaders, such as men, they can curl up in their hair or fur, pinch with their sharp jaws, penetrate holes such as ears and nostrils, or release unpleasant odors. Some species produce formic acid in their mandibular glands, which when released, can cause serious burns (BALLIVIÁN et al., 2008; SFORCIN et al., 2017). The SBs with tamer behavior protect their nests by building them in places of difficult access, including inside anthills or near more defensive bee nests (OLIVEIRA et al., 2013).

These bees have eusocial behavior, that is, they live in well-organized communities, where the queen is responsible for reproductive work and the workers take care of the offspring, the provision of food and the construction and defense of the nests (FONSECA et al., 2017). Food storage is done in pots consisting of cerumen, where pollen and honey are stored separately (VILLAS-BÔAS, 2012).

SBs differ from bees of the genus *Apis* in several aspects. While *Apis* exhibit uniform behaviors and morphology, meliponines are quite diverse. Some species are very small, smaller than fruit flies and others have robust bodies (VELIKOVA et al., 2000; HRNCIR et al., 2016).

The size of the colony is also variable and can house tens to thousands of individuals. The nests may be arranged in clusters or combs. Foraging can be done by groups or solitary bees and is generally characterized by shorter flights, which implies the elaboration of propolis using the plant resources closest to the colony (VELIKOVA et al., 2000; HRNCIR et al., 2016).

The ecological relevance of these insects is undeniable. They act as pollinators of several native and cultivable plants, contributing to the conservation of different biomes and agricultural production, directly impacting the production of fruits and seeds and consequently the economy (BONSUCESSO et al., 2018). The honey produced by ASF is marketed in some regions of Brazil, for its appreciated flavor and medicinal properties. These bees also produce propolis, which has been the subject of studies around the world due to its pharmacological properties (LAVINAS et al., 2019).

2.3 Native bees: sociocultural importance and ethnoknowledge

Indigenous peoples have a close relationship with the meliponines. Before the introduction of the species *Apis mellifera* and the culture of sugar cane in America, the honey of the native bees was used by the indigenous as an indispensable source of energy for the great journeys in the food search. The popular names of many species such as Jataí, Tiúba, Jandaíra, Guarapu and Manduri are part of the sociolinguistic indigenous heritage (VILLAS-BÔAS, 2012).

Indigenous knowledge is closely related to nature. The legacy of these peoples has immeasurable value and has been passed down through the generations. In Mexico the creation of SBs and the use of its products date back to the pre-Columbian period. For the Maya people, one of the most relevant ancient civilizations in history, the SBs played an important role in religious ceremonies, feeding and treating diseases (AYALA et al., 2013).

In Brazil, the Kayapó people use elaborate techniques for the management of swarms, such as platforms that allow the reach of hives in tall trees. In this people, bee specialists are shamans, who possess extensive knowledge about the anatomy and behavior of various SB species. The people use honey and pollen in food, cerumen and resins in the waterproofing of canoes, in addition to being inspired by the social organization of these insects (BALLIVIÁN et al., 2008). For the Pankararé, indigenous people in northeastern Brazil, the creation of 'abeia mansa' (meek bee) is a recreational and medicinal activity. Honey is used in food as an energy source and is extracted in a non-predatory way, ensuring the maintenance of the tree where it was collected and the colony (FONSECA et al., 2017).

The knowledge about the SBs of the Guarani Mbyá people of the Morro da Saudade village, in the city of São Paulo, is transmitted orally through the generations. The teachings are followed and improved by the younger ones and some members of the community are seen as great connoisseurs of the subject. The products from bees are used in handicrafts, religious rituals and medicinal potions, as well as activities related to spiritual and contemplative life (RODRIGUES, 2005). Santos and Antonini (2008) conducted a study on the traditional knowledge about the SBs of the Enawene-Nawe people of the state of Mato Grosso. They were able to conclude that the people were able to identify several

species of SBs not only by morphology but also by the ecological and social characteristics of these insects.

Meliponiculture has also been practiced for generations by other traditional communities such as 'quilombolas' (descendants of black slaves), 'ribeirinhos' (inhabitants of riverbanks), 'sertanejos' (inhabitants of the hinterland), 'caipiras' (countrymen) and 'caiçaras' (traditional fishing communities). The products from the SBs are used for subsistence family consumption and are a source of complementary income. These peoples contribute to the conservation of bees, through the management of species that are practically no longer found in natural habitat, due to the devastation of the native forest. The rational beekeeping of SBs can therefore be a sustainable strategy to promote biodiversity conservation (VILLAS-BÔAS, 2018).

2.4 Introduction of exotic bee species in Brazil

The introduction of the European bee species *Apis mellifera* in Brazil occurred around 1839, brought by the Portuguese to produce wax candles. In 1845 German immigrants brought more bees and settled in the south of the country. Other colonizers have also introduced European bees into different regions (ATHAYDE et al., 2016). In 1956, the biologist and geneticist Dr. Warwick Kerr, at the request of the Brazilian government, brought from Africa some queens of bees to perform crossing by artificial insemination, which would originate a species capable of producing more honey in the tropical climate (BALLIVIÁN et al., 2008; ATHAYDE et al., 2016).

The following year, swarms and their respective queens escaped accidentally and ended up crossing with the European species already inserted in the Brazilian territory, emerging hybrid populations, today called Africanized bees. This incident had an extensive environmental impact since these bees spread to almost the entire American continent (BALLIVIÁN et al., 2008; ATHAYDE et al., 2016).

2.5 Impact of anthropogenic actions on bees

The introduction of exotic species, accidentally or for economic purposes, can cause significant changes in natural environments, such as changes in habitats, hybridization and competition with native species. In addition, the intensive occupation of the environment by man impacts bee populations by eliminating food sources, destroying substrates necessary for the construction of nests and by pesticides (SILVEIRA et al., 2002).

Due to the intense bee die-off, several studies were conducted to evaluate the toxicity of agrochemicals, but most of them were carried out with the species *Apis mellifera*, endemic in several regions of the world. The study conducted by Dorigo et al. (2019) evaluated the effect of the insecticide Dimethoate on the SB species *Melipona scutellaris*, where the average lethal concentration (LC_{50}) was 320 times lower than for *Apis mellifera* larvae, demonstrating the sensitivity of this species to the pesticide and the need to conduct further studies using native bees.

The deforestation of forest areas for urban and agricultural use has also significantly reduced bee populations. The scarcity of resources, competition between species, predation by invaders and inbreeding due to population decrease, can make swarms captive to a small territorial space, or lead them to extinction (SILVEIRA et al., 2002).

Even if the mellipones adapt, Portal et al. (2023) verified that the major volatile compounds in the propolis of native bees in the Itajaí Valley region, in southern Brazil, are compounds found in Pinus and Eucalyptus, indicating that this is the most important plant source in the elaboration of propolis by

those specimens. This 'reforestation' with exotic trees certainly contributes to the difficulty of discovering new molecules with biological activity and potential for the development of new drugs.

As bees contribute to the maintenance of forests through pollination, several species of *Meliponinae* depend on forest environments and are not found in anthropogenic environments, except near forests. This issue is an aggravating factor in Brazil, considering that some species of the genus *Melipona* are translocated to regions distant from their natural occurrence (SILVEIRA et al., 2002).

2.6 Propolis

Propolis is a mixture of substances used by bees in the defense of the hive. Worker bees collect resinous materials from shoots, exudates, and other parts of plants and pack them in their corbicles (part of the posterior tibia used to transport pollen, clay, and resin). These resins are biotransformed by bees with the addition of their salivary enzymes and wax (PRZYBYŁEK; KARPINSKI, 2019; BREYER; BREYER; CELLA, 2016). Physically, propolis has quite variable characteristics. They may have a hard and brittle consistency or be sticky and elastic. The coloration can also vary between cream, yellow, green, light brown or dark brown (SALATINO et al., 2005).

The name propolis is derived from the Greek words *pro*, in defense of, and *polis*, the city, e.g.: "in defense of the city or the hive." In fact, this material has great importance for the health of the colony. Bees use propolis in the sealing and repair of crevices to prevent the entry of invasive insects and maintain the internal temperature (MARCUCCI, 1996; SALATINO et al., 2005). In addition, it is used against microorganisms in the asepsis of the places where the laying of eggs is made. And if the bees cannot remove a dead invader from the hive, they use propolis to embalm it, which prevents decomposition and bacterial proliferation in the nest (MARCUCCI, 1996; SALATINO et al., 2005).

The plant materials used in the composition of propolis are produced by various botanical processes in different parts of the plants. The collection of these materials is a difficult activity to observe and often occurs high in the trees. Among the substances collected, lipophilic compounds from the leaves, mucilages and resins can be highlighted (BANKOVA; CASTRO; MARCUCCI, 2000).

2.7 Historical and popular use of propolis

Propolis has been used in traditional medicine since antiquity. The Egyptians used it to embalm the dead and thus prevent putrefaction. Its properties were also recognized in Greek and Roman medicine by Aristotle, Dioscorides, Pliny and Galen, who employed it in asepsis and wound treatment and as an oral disinfectant. Its use was perpetuated in the Middle Ages in Arab medicine and was recognized by New World civilizations (CASTALDO; CAPASSO, 2002).

In the seventeenth century, propolis was included in the London Pharmacopoeia. Between the seventeenth and twentieth centuries, its use became popular in Europe due to its antibacterial action. It is currently used in various pharmaceutical forms such as extracts, mouthwash, lozenges and formulations for topical use. Also, its employment in the food and cosmetic industries have been benefiting from the propolis properties (CASTALDO; CAPASSO, 2002).

In 1908 the first scientific work on propolis, its chemical properties and composition was indexed in Chemical Abstracts. The first patent appeared decades later in the same index of scientific literature, in 1968, where Romanian propolis was employed in the production of bath lotions. Since then, several studies on propolis have been published, possibly due to its panacea characteristic and its added value (PEREIRA; SEIXAS; NETO, 2002).

Currently, propolis is used for various therapeutic purposes as an antibacterial, antifungal, antiviral, anti-inflammatory agent and to increase the body's natural resistance to infections. Formulations for external use are employed in the treatment of dermatitis and wounds. It is also available in capsules of pure extracts or in combination with other natural products. Throat lozenges and *spray*, mouthwash and hydroalcoholic or glycolic extracts are widely used as a folk remedy (CASTALDO; CAPASSO, 2002).

2.8 Geoprópolis

Some SB species add soil to propolis, giving rise to the so-called geopropolis. Although it is not its main constituent, the presence of earth is a differential in the composition of this product. Its coloration is variable and is related to the plant origin, the soil used in its constitution and the species of bee that produces it. The chemical composition and biological activities of this bee product are still little known (BONSUCESSO et al., 2018).

Fritz Müller, a German naturalist who migrated to Santa Catarina in the mid-nineteenth century, in one of his letters to Charles Darwin, about the habit of various insects, mentioned his observations on the genus *Melipona* and the constitution of propolis. He observed that these bees not only used wax in the construction of the nest structures but added other materials such as resins and soil (MÜLLER, 1874).

III. CHEMICAL COMPOSITION OF GEOPROPOLIS FROM MELIPONINES

In 1998(a), Bankova et al. identified more than 50 compounds present in the Brazilian geopropolis. Among them, the geopropolis of Melipona *compressipes* and *Melipona quadrifasciata anthidioides* collected in the states of Piauí (Northeast) and Paraná (South) respectively. The extracts of these samples were submitted to chemical analysis through GC-MS and a complex chemical composition was observed. The samples showed significant amounts of lactic, phosphoric and long-chain fatty acids, such as stearic and palmitic acid.

Araújo et al. (2015) analyzed the chemical composition of *Melipona fasciculata* geopropolis, collected in Maranhão state (North). The main constituents found were carbohydrates and their derivatives (19.8%), triterpenes (15.9%), hexoses (11.9%), anacardic acid (8.3%), lupeol (7.3%) and alkylresorcinols (5.9 %). Disaccharides, glucuronic acid, salicylic acid and isomers, β-amyrin, inositol, and xylitol, among others, were also found.

In the work of Silva, Muniz and Nunomura (2013) samples of geopropolis of the species *Melipona interrupta* and *Melipona seminigra*, collected in municipalities of Amazonas (Nort), were evaluated for their composition, evidencing the significant presence of phenolic compounds.

Santos et al. (2017) evaluated the composition of the aqueous and hydroalcoholic extracts of *Melipona quadrifasciata*. Rutin, gallic acid, gallocatechin, epicatechin gallate and syringic acid were identified in the aqueous extract. In the hydroalcoholic extract, the main constituents found were quercetin, epigallocatechin, p-hydroxybenzoic acid, epigallocatechin gallate and coumaric acid.

Propolis contains volatile constituents to a lesser extent. This fraction, however, can provide relevant information about the antimicrobial activity and elucidate the classes of compounds present in its composition, contributing to the identification of its botanical origin (TORRES et. al., 2008). Volatile compounds are among the main secondary metabolites present in plants. They perform important functions that ensure survival and adaptation to the environment. Among these functions can be

mentioned attraction of pollinators and seed dispersers, protection through repulsion or intoxication and antibacterial, fungicidal and insecticidal action (BAKKALI et al., 2008).

Volatile oils (VO), also called essential oils (EO) when obtained directly from plants, are a complex mixture of lipophilic substances, consisting mainly of terpenes, fatty acid derivatives, amino acid derivatives and phenylpropanoid compounds. In propolis, terpenes constitute a large part of the volatile compounds (RUFATTO et al., 2017).

Terpenes are classified according to the number of isoprene units (C_5 H $_8$) present in their structure: monoterpenes (C 10 H $_{16}$), sesquiterpenes (C $_{15}$ H 24), diterpenes (C $_{20}$ H 32), triterpenes (C $_{30}$ H 40), tetraterpenes (C 40 H 64) and polyterpenes (DUBEY; BHALLA; LUTHRA, 2003). Monoterpenes make up a large part of the EO and can contribute more than 90% of its total composition. Sesquiterpenes are another important group found in the EOs. Terpenes can be biosynthesized by the classical mevalonate pathway in the cytosol or by the alternative deoxylulose pathway that occurs in plastids (CABALLERO; TRUGO; FINGLAS, 2003).

EOs can be obtained by distillation or pressing of plants or parts thereof. At room temperature, they are liquid and volatile, with a characteristic odor. The density of EOs is generally lower than that of water, but sassafras, cinnamon and clove oils may have higher densities (CABALLERO; TRUGO; FINGLAS, 2003). The composition of an VO can present a major constituent, facilitating chemical correlation with biological activity. However, small amounts of other substances present can act synergistically, contributing to a certain biological action (YUNES; CECHINEL FILHO, 2016). However, the composition of these oils is variable and is directly related to seasonality and the place of collection (OLIVEIRA et al., 2009).

IV. BIOLOGICAL ACTIVITIES OF GEOPROPOLIS COMPOUNDS

Some studies have highlighted the importance of investigating the biological potential of geopropolis, mainly the antibacterial, antifungal, antiviral, antioxidant, anti-inflammatory, antimycoplasmic and antimutagenic properties of SBs geopropolis of the genus *Melipona*.

Dutra et al. (2014) evidenced the antioxidant potential of the hydroalcoholic extract of geopropolis of *M. fasciculata*. The action was correlated with the presence of phenolic compounds such as phenolic acids, gallotannins and ellagitannins. Batista et al. (2016) also suggested that the high concentration of phenolic acids, such as gallic and ellagic acid, was responsible for the antioxidant action of the samples tested.

In the work of Santos et al. (2017) the antibacterial activity of the hydroalcoholic extract of M. *orbignyi* geopropolis was evaluated against the Gram-positive bacterium *S. aureus* (sensitive and methicillin-resistant strains) and Gram-negative *E. coli* (sensitive and cephalosporin-resistant strains) and *P. aeruginosa* (strains sensitive and resistant to amphotericin B). The antibacterial action was attributed to the presence of phenolic compounds, which have some known mechanisms of action, among them the permeabilization of the microbial cytoplasmic membrane.

Valcanaia et al. (2022) investigated the antimicrobial potential of the volatile oil of *Melipona q. quadrifasciata* geopropolis against bacteria with and without cell walls. The antimicrobial action with the lowest minimum inhibitory concentration was against the bacterium without cell wall *Mycoplasma pneumoniae* 129 strain. The volatile oil was fractionated and its subfractions were tested, but these showed no improvement in antibacterial activity. This characteristic had already been observed by Kujumgiev, Tsvetkova and Serkedjieva (1999), who concluded that the isolated compounds from

propolis did not present better results regarding the activities tested, suggesting that the synergy between the compounds favors biological actions.

In the literature, it is possible to find studies that confirmed the antimicrobial activity of the volatile constituents of propolis against several microorganisms. Against Gram-positive bacteria such as *S. aureus*, *Staphylococcus epidermidis*, *Micrococcus glutamicus*, *Bacillus subtilis*, *Bacillus cereus*, *Sarcina lutea*, *Streptococcus pyogenes*, *Streptococcus mutans, Streptococcus faecalis* and Gram-negative bacteria such as *E. coli*, *Enterobacter cloacae*, *Klebsiella pneumoniae* and *P. aeruginosa* (BANKOVA; POPOVA; TRUSHEVA, 2014).

A study conducted in Greece investigated the chemical composition of volatile propolis compounds from different geographic regions. The predominant constituents were terpenoids, especially α-pinene. Other components have also been identified as α-eudesmol, δ-cadinene, α-muurolene, guaiol and trans-β-terpineol. The *in vitro* antimicrobial activity was evaluated against 6 species of bacteria, including *S. aureus*, *P. aeruginosa* and *E. coli*, confirming the antimicrobial potential of the samples tested (MELLIOU; STRATIS; CHINOU, 2007).

In the study by Simionatto et al. (2012), the volatile constituents of propolis samples collected in three municipalities of Rio Grande do Sul, α-pinene and β-pinene were presented as major constituents. The antimicrobial activity was evaluated by the agar diffusion method against *S. aureus*, *P. aeruginosa*, *Klebsiella pneumoniae*, *Bacillus subtilis* and *E. coli* type strains. The antibacterial activity was classified as moderate and the presence of monoterpenes in the samples was attributed to this activity.

Fernandes et al. (2015) evaluated the antimicrobial potential of the volatile oil of *Apis mellifera* propolis collected in Mato Grosso do Sul, Brazil (West). The activity was evaluated by the broth microdilution method against strains of *P. aeruginosa, Klebsiella pneumoniae, Enterococcus faecalis* and *S. aureus*. The volatile oil and two of its isolated constituents - (E)-nerolidol and spathulenol - showed antimicrobial properties.

Oliveira et al. (2009) tested the antimicrobial activity of the volatile oil of *Apis mellifera propolis* collected in Rio de Janeiro. The microorganisms *Staphylococcus aureus, S. epidermides, Streptococcus pyogenes* and *E. coli* were susceptible to the sample tested. The chemical composition presented as major constituents β-caryophyllene (12.7%), acetophenone (12.3%) and β-farnesene (9.2%).

Portal et al. (2023) found that the *M. b. schencki* geopropolis VO with the best minimal inhibition concentration (MIC) was 424±0 μg mL^{-1} against all the mycoplasma strains evaluated. Fractionation of the VO resulted in a reduction of 50% of the MIC. However, its compounds' synergism seems to be essential to this activity. Antibiofilm assays demonstrated 15.25% eradication activity and 13.20% inhibition of biofilm formation after 24h for one subfraction at 2x its MIC as the best results found. This may be one of the essential mechanisms by which geopropolis VOs perform their antimicrobial activity.

V. BACTERIAL RESISTANCE TO ANTIBIOTICS AND THE NEED FOR NEW DRUGS

The increasing microbial drug resistance has been observed worldwide and with increasing mortality, prolonged hospital stays and rising costs, with other sectors of society being impacted beyond healthcare (WHO, 2015).

Between 2011 and 2014, the National Health Safety Network in the U.S. reported high levels of resistance to various antibiotics in Gram-positive bacteria including methicillin-resistant

Staphylococcus aureus, and Gram-negative bacteria such as third-generation cephalosporin-resistant *Escherichia coli* and carbapenem-resistant *Pseudomonas aeruginosa* (WHO; EMP; IAU, 2017).

Data from the European Centre for Disease Prevention and Control from 2015, when compared to US data, showed lower rates of resistance in Gram-positive bacteria and equally worrisome rates among Gram-negative bacteria (WHO; EMP; IAU, 2017).

The U.S. Centers for Disease Control and Prevention estimates that at least 23,000 deaths from resistant infections occur each year in the U.S. In Europe, in the year 2007 alone, 25,000 deaths were attributed to infections by resistant microorganisms (YU et al., 2016).

If this current trend continues, it is estimated that by 2050 there will be 10 million additional deaths due to antimicrobial resistance, surpassing other significant diseases such as cancer and diabetes. In addition, in the same year, microbial resistance is estimated to cumulatively cost $100 trillion worldwide (YU et al., 2016).

Natural products offer an obvious source for the research and development of new pharmacological treatments of infections. Moreover, it is more rational to use the millenary wisdom of bees, that learned to look for the best chemical compounds in nature to produce their propolis for the defense of their hives, in every environment, instead of testing individually each plant species for antimicrobial compounds.

VI. CONCLUSION

Propolis from native stingless bees have an enormous potential to be unveiled, both in its use in the form of herbal medicines and in the discovery of new molecules with potential for drug development. Many species of bees have not even had their propolis chemically characterized. However, it is necessary that their environment be preserved, and that the bees themselves be preserved, so that humankind can benefit from this ancestral treasury.

REFERENCES

1. ABREU, A. C.; MCBAIN, A. J.; SIMÕES, M. Plants as sources of new antimicrobials and resistance-modifying agents. Natural Product Reports, v. 29, n. 9, p. 1007-1021, 2012.
2. ARAÚJO, M. J. A. M. et al. The chemical composition and pharmacological activities of geopropolis produced by *Melipona fasciculata* Smith in Northeast Brazil. Journal of Molecular Pathophysiology, v. 4, n. 1, p. 12-20, 2015.
3. ATHAYDE, S. et al. Engaging indigenous and academic knowledge on bees in the Amazon: implications for environmental management and transdisciplinary research. Journal of Ethnobiology and Ethnomedicine, v. 12, n. 1, 2016.
4. AYALA, R. et al. Mexican Stingless Bees (Hymenoptera: Apidae): Diversity, Distribution, and Indigenous Knowledge. In: VIT, P. et al (ed.). Pot-Honey: a legacy of stingless bees. New York: Springer-verlag, 2013. pp. 135-152.
5. BAKKALI, F. et al. Biological effects of essential oils – A review. Food and Chemical Toxicology, v. 46, n. 2, p. 446-475, 2008.
6. BALLIVIÁN, J. M. P. P. et al (org.). Native stingless bees: Myg pe. St. Leopold: Oikos, 2008. 128 p.
7. BANKOVA, V. et al. Constituints of Brazilian Geopropolis. Zeitschrift für Naturforschung. v. 53, n. 5-6, p. 402-406, 1998a.
8. BANKOVA, V. et al. Phytochemical Evidence for the Plant Origin of Brazilian Propolis from Säo Paulo State. Zeitschrift für Naturforschung. No. 54c, pp. 401-405, 1999.

9. BANKOVA, V.; CASTRO, S.; MARCUCCI, M. Propolis: recent advances in chemistry and plant origin. Apidologie, v. 31, n. 1, p. 3-15, 2000.
10. BANKOVA, V.; POPOVA, M.; TRUSHEVA, B. Propolis volatile compounds: Chemical diversity and biological activity: A review. Chemistry Central Journal, v. 8, n. 1, p. 1 – 8, 2014.
11. BATISTA, M. C. A. et al. Chemical composition and antioxidant activity of geopropolis produced by *Melipona fasciculata* (Meliponinae) in flooded fields and cerrado areas of Maranhão State, northeastern Brazil. Acta Amazônica, v. 46, n. 3, p. 315-322, 2016.
12. BONSUCESSO, J. S. et al. Metals in geopropolis from beehive of *Melipona scutellaris* in urban environments. Science of the Total Environment, v. 634. p.687-694, 2018.
13. BREYER, H. F. E.; BREYER, E. D. H.; CELLA, I. Production and processing of propolis. Florianópolis: EPAGRI, 2016. 21 p.
14. CABALLERO, B.; TRUGO, L.C.; FINGLAS, P.M. Encyclopedia of Food Sciences and Nutrition, 2nd ed.; Elsevier Academic Press: Amsterdam, The Netherlands, 2003.
15. CASTALDO, S.; CAPASSO, F. Propolis, an old remedy used in modern medicine. Phytotherapy, v. 73, 2002.
16. CRANE, E. The World History of Beekeeping and Honey Hunting. New York: Routledge, 1999. 720 p.
17. DORIGO, A. S. et al. *In vitro* larval rearing protocol for the stingless bee species *Melipona scutellaris* for toxicological studies. Plos One, v. 14, n. 3, 2019.
18. DUBEY, V. S.; BHALLA, R.; LUTHRA, R.; An overview of the non-mevalonate pathway for terpenoid biosynthesis in plants. Journal of Biosciences, 28, 637–646, 2003.
19. DUTRA R. P. et al. Phenolic Acids, Hydrolyzable Tannins, and Antioxidant Activity of Geopropolis from the Stingless Bee *Melipona fasciculata* Smith. Journal of Agricultural and Food Chemistry. v. 62, p. 2549-2557, 2014.
20. FERNANDES, F. H. et al. Evaluation of mutagenic and antimicrobial properties of brown propolis essential oil from the Brazilian Cerrado biome. Toxicology Reports, v. 2, p. 1482–1488, 2015.
21. FONSECA, V. L. I. et al (ed.). The bee had jandaíra: in the past, present and in the future. Mossoró: Edufersa, 2017. 254 p.
22. HRNCIR, M. et al. Stingless bees (Meliponini): senses and behavior. Journal of Comparative Physiology A, v. 202, n. 9-10, p. 597-601, 2016.
23. KERR, W. E. Extinction of species: the great biological crisis of the moment and how it affects the meliponines. Proceedings of the V meeting on bees, Ribeirão Preto/SP. p. 4 – 9. 2002.
24. KLEINERT, A. M. P. et al. Social bees: Bombini, Apini, Meliponini. In: PANIZZI, A. R. et al. Bioecology and nutrition of insects: basis for integrated pest management. Brasilia: Embrapa Technological Information, 2009. Ch. 10. pp. 373-426.
25. KUJUMGIEV, A.; TSVETKOVA, I.; SERKEDJIEVA, Y. et al. Antibacterial, antifungal and antiviral activity of propolis of different geographic origin. Journal of Ethnopharmacology, v.64, p.235-40, 1999.
26. LAVINAS, F. C. et al. Brazilian stingless bee propolis and geopropolis: promising sources of biologically active compounds. Brazilian Journal of Pharmacognosy, v. 29, n. 3, p.389-399, 2019.
27. LEXIKON, H. Dictionary of symbols. São Paulo: Cultrix Publishing, 1997. 214 p.
28. LIBERIO, S. A. et al. Antimicrobial activity against oral pathogens and immunomodulatory effects and toxicity of geopropolis produced by the stingless bee *Melipona fasciculata* Smith. Complementary and Alternative Medicine. v. 11, n. 108, 2011.
29. MARCUCCI, M. C. Biological and therapeutic properties of the chemical constituents of propolis. Química Nova, v.19, n.5, p. 529-536, 1996.
30. MELLIOU, E.; STRATIS, E.; CHINOU, I. Volatile constituents of propolis from various regions of Greece – Antimicrobial activity. Food Chemistry, v. 103, n. 1, p. 375-380, 2007.

31. MENEZES, H. Propolis: a review of recent studies of its pharmacological properties. Archives of the Biological Institute, v.72, n.3, p.405-411, 2005.
32. MICHENER, C. D. The bees of the world. Baltimore: The Johns Hopkins University Press, 2000. 913 p.
33. MÜLLER, F. The habits of various insects. Nature, v.10, p. 102-103, 1874.
34. NEWMAN, D. J, CRAGG, G. M. Natural Products as Sources of New Drugs over the Nearly four Decades from 01/1981 to 09/2019. Journal of Natural Products, v. 83, no. 3, pp. 770-803, 2020.
35. NOGUEIRA-NETO, P. Life and Breeding of Stingless Indigenous Bees. São Paulo: Nogueirapis, 1997. 445 p.
36. OLIVEIRA, A. P., et al. Chemical composition and antibacterial activity of Brazilian propolis essential oil. Journal of Venomous Animals and Toxins including Tropical Diseases., Rio de Janeiro, v. 16, n. 1, p. 121-130, 2009.
37. OLIVEIRA, F. F. de et al. Illustrated Guide to the "Stingless" Bees of the Amanã and Mamirauá Reserves, Amazonas, Brazil: (hymenoptera, apidae, meliponini). Tefé: Mamirauá Sustainable Development Institute, 2013. 267 p.
38. PEREIRA, A. D. S.; SEIXAS, F. R. M. S.; NETO, F. R. D. A. Propolis: 100 years of research and its future prospects. New Chemistry, v. 25, p. 321-326, 2002.
39. PORTAL, A. S., SCHIQUET S, PADILHA AMARAL B, MASCARENHAS KREPSKY L, CURBANI L, ANDRADE REBELO R, RAU M, ALTHOFF SL, GUEDES A, MENDES DE CORDOVA CM. Composition, Antibiofilm, and Antibacterial Potential of Volatile Oils from Geopropolis of Different Stingless Bees' Species. Chem Biodivers. 2023 Aug; 20(8): e202300592. doi: 10.1002/cbdv.202300592.
40. PRZYBYŁEK, I.; KARPINSKI, T. M. Antibacterial Properties of Propolis. Molecules, v. 23, n. 24, p. 2047- 2063, 2019.
41. RODRIGUES, A. D. S. Ethnoknowledge about stingless bees: knowledge and practices of the M-byá Guarani Indians in the Atlantic forest. 253 f. Dissertation (Master's Degree) - Course of Ecology of Agrosystems, University of São Paulo, Piracicaba, 2005.
42. RUFATTO, L. C. et al. Red propolis: Chemical composition and pharmacological activity. Asian Pacific Journal of Tropical Biomedicine, v. 7, n. 7, p. 591-598, 2017.
43. SALATINO, A. et al. Origin and Chemical Variation of Brazilian Propolis. Evidence-based Complementary and Alternative Medicine, v. 2, n. 1, p. 33-38, 2005.
44. SANTOS, H. F. D. et al. Chemical Profile and Antioxidant, Anti-Inflammatory, Antimutagenic and Antimicrobial Activities of Geopropolis from the Stingless Bee *Melipona orbignyi*. International Journal of Molecular Sciences, v. 18, n. 5, p. 953-970, 2017.
45. SFORCIN, J. M. et al. Propolis and Geopropolis: a bee inheritance. São Paulo: Unesp Digital, 2017.
46. SILVA, C. I. da et al. Illustrated guide to pollinating bees in Brazil. São Paulo: USP, 2014.
47. SMITH, E. C. C. D.; MUNIZ, M. P.; NUNOMURA, R. D. C. S. Phenolic constituents and antioxidant activity of geopropolis of two species of Amazonian stingless bees. New Chemistry, v.36, n. 5, p. 628-633, 2013.
48. SILVEIRA, F. A. et al. Brazilian bees: systematics and identification. Belo Horizonte: Fernando A. Silveira, 2002. 253 p.
49. SIMIONATTO, E. et al. Chiral analysis of monoterpenes in volatile oils from propolis. Journal of the Chilean Chemical Society, v. 57, p. 1240–1243, 2012.
50. SIMÕES, M.; BENNETT, R. N.; ROSA, E. A. S. Understanding antimicrobial activities of phytochemicals against multidrug resistant bacteria and biofilms. Natural Product Reports, v. 26, n. 6, p. 746-757, 2009.
51. TORRES R. N. S. et al. Volatile constituents of Piauiense propolis. New Chemistry, v. 31, p. 479–485, 2008.

52. TRIPLEHORN, C. A.; JOHNSON, N. F. Borror and De Long's Introduction to the study of insects. 7. ed. Belmont: Thomson Brooks/Cole, 2005. 864 p.
53. VALCANAIA, C. P., Masote JBB, Sommer HF, Schiquet S, Padilha B, Krepsky L, Paganelli CJ, Borges PP, Danielli LJ, Apel MA, Soares KD, Althoff S, Alberton MD, Botelho TKR, Guedes A, Mendes de Cordova CM. Antimicrobial Activity of Volatile Oils from Brazilian Stingless Bees Melipona quadrifasciata quadrifasciata and Tetragonisca angustula Propolis. 2022. Chem Biodivers. 2022 Aug;19(8):e202200369. doi: 10.1002/cbdv.202200369..
54. VELIKOVA, M. et al. Chemical composition and biological activity of propolis from Brazilian meliponinae. Zeitschrift für Naturforschung, v.55, p.785-789, 2000.
55. VENTURIERI, G. C. Creation of Indigenous Stingless Bees. 2. ed. Belém: Embrapa Amazônia Oriental, 2008. 60 p.
56. VIEGAS JUNIOR, C.; BOLZANI, V. S.; BARREIRO, E. J. Natural products and modern medicinal chemistry. New Chemistry, v. 29, n. 2, p. 326-337, 2006.
57. VILLAS-BÔAS, J. Technological Manual: full use of stingless bee products. 2. ed. Federal District: Institute Society, Population and Nature (ISPN), 2018. 212 p.
58. VILLAS-BÔAS, J. Technological Manual: honey from stingless bees. Federal District: Institute of Society, Population and Nature (ISPN), 2012. 96 p.
59. WEBBEE. Information network on Brazilian biodiversity in bees. Available on: <http://www.webbee.org.br/projetos/beelife/mmargin.htm> Access in: 26. Set. 2020
60. WHO. Global action plan on antimicrobial resistance. 2015. Available in: <https://apps.who.int/iris/bitstream/handle/10665/193736/9789241509763_eng.pdf?sequence=1> Access in: 06. May. 2020.
61. WHO/EMP/IAU. Prioritization of pathogens to guide discovery, research and development of new antibiotics for drug-resistant bacterial infections, including tuberculosis. Geneva: World Health Organization, 2017. Available in: <https://www.who.int/medicines/areas/rational_use/PPLreport_2017_09_19.pdf?ua=1> Access in: 06. May. 2020.
62. YU, A. et al. Patient Safety 2030. London, UK: NIHR Imperial Patient Safety Translational Research Centre, 2016. Available at: <https://www.imperial.ac.uk/media/imperial-college/institute-of-global-health-innovation/centre-for-health-policy/Patient-Safety-2030-Report-VFinal.pdf> Accessed: 06 May 2020.
63. YUNES, R. A.; CECHINEL FILHO, V. (org.). Natural Product Chemistry: New Drugs and Modern Pharmacognosy. 5. ed. Itajaí: Univali, 2016. 528 p.